Carbon cycling dynamics in the seasonal sea-ice zone of East Antarctica

by

Nicholas Patrick Roden

BSc (Hons)

Submitted in partial fulfilment of the requirements for the degree of Doctor of Philosophy at the Institute for Marine and Antarctic Studies (IMAS)

November 2016

University of Tasmania

Declaration of originality

This thesis contains no material which has been accepted for a degree or diploma by the University or any other institution, except by way of background information and duly acknowledged in the thesis, and to the best of my knowledge and belief no material previously published or written by another person except where due acknowledgement is made in the text of the thesis, nor does the thesis contain any material that infringes copyright.

Nicholas Patrick Roden

17 November 2016

Authority of access

This thesis may be available for loan and limited copying in accordance with the *Copyright Act 1968.*

Nicholas Patrick Roden

17 November 2016

Statement regarding published work contained in this thesis

The publishers of the papers compromising Chapter 2 and Chapter 3 hold the copyright for that content, and access to the material should be sought from the respective journals. The remaining non-published content of the thesis may be made available for loan and limited copying and communication in accordance with the *Copyright Act 1968.*

Nicholas Patrick Roden

17 November 2016

For Mum and Dad

Table of contents

List of tables

List of figures

Statement of co-authorship

The following people and institutions contributed to the publication of work undertaken as part of this thesis:

Candidate:	*Nicholas P. Roden, Institute for Marine and Antarctic Studies, CSIRO Oceans and Atmosphere and Antarctic Climate and Ecosystems Cooperative Research Centre*
Author 1:	*Bronte Tilbrook, CSIRO Oceans and Atmosphere and Antarctic Climate and Ecosystems Cooperative Research Centre, Supervisor*
Author 2:	*Thomas W. Trull, CSIRO Oceans and Atmosphere and Antarctic Climate and Ecosystems Cooperative Research Centre, Supervisor*
Author 3:	*Patti Virtue, Institute for Marine and Antarctic Studies and Antarctic Climate and Ecosystems Cooperative Research Centre, Supervisor*
Author 4:	*Guy D. Williams, Institute for Marine and Antarctic Studies and Antarctic Climate and Ecosystems Cooperative Research Centre, Supervisor*
Author 5:	*Elizabeth H. Shadwick, Antarctic Climate and Ecosystems Cooperative Research Centre*

Author details and their roles:

Paper 1, Annual cycle of carbonate chemistry and decadal change in coastal Prydz Bay, East Antarctica:

Located in Chapter 3.

Candidate collected and analysed the data and was the primary author. Author 1, Author 2 and Author 5 provided guidance with data analysis and interpretation.

***Paper 2, Carbon cycling dynamics in the seasonal sea-ice zone of East Antarctica*:**

Located in Chapter 2.

Candidate was the primary author. Author 1 and Author 2 provided guidance with data analysis and interpretation. Author 3 and Author 4 assisted with refinement and presentation.

We the undersigned agree with the above stated “proportion of work undertaken” for each of the above published peer-reviewed manuscripts contributing to this thesis:

Signed:

	Doctor Patti Virtue *Supervisor* *Institute for Marine and Antarctic Studies* University of Tasmania	Professor Craig Johnson *Head of School* *Institute for Marine and Antarctic Studies* University of Tasmania
Date:	17 November 2016	17 November 2016

Abstract

The Southern Ocean plays a critical role in the global carbon cycle, accounting for over 40% of the global ocean uptake of anthropogenic carbon dioxide (CO_2). Observations are often localized and widely separated in both space and time, resulting in a heavy dependence on models to characterize carbon fluxes at regional scales in this area. Subsequently, notable discrepancies exist between model and observational results within the seasonal sea-ice zone (SIZ) around Antarctica. Given the important role of atmospheric CO_2 in the climate system and its influence on changing ocean chemistry (ocean acidification), there is a need to accurately attribute the causes of change and develop a regional understanding of the CO_2 sink/source nature of the Southern Ocean.

In this thesis, the carbon cycle in the seasonal sea-ice zone of East Antarctica was investigated across a variety of spatial and temporal scales. In this region a large variability in the drivers and timing of carbon cycling dynamics was observed. Analysis of data from an oceanographic survey carried out during the austral summer (January – March 2006), between 30°-80°E and 60°-69°S, showed the SIZ to be a weak net source of CO_2 to the atmosphere of 0.07 ± 0.13 mol C m^{-2} during the spring/summer ice-free period. Narrow bands of CO_2 uptake were observed near the continental margin and north of the Southern Antarctic Circumpolar Current Front.

Continuous surface measurements of dissolved oxygen and the fugacity of CO_2 (fCO_2) were combined with net community production estimates from oxygen/argon ratios to show that surface heat gain and photosynthesis were responsible for the majority of surface water biogeochemical variability during the survey. On seasonal timescales, winter sea-ice cover acted to reduce the flux of CO_2 to the atmosphere in the study area, followed by biologically driven drawdown of CO_2 as the ice retreated in spring-summer. This highlights the import role that sea-ice formation and retreat has on the biogeochemical dynamics of the region.

The influence of sea-ice formation and retreat was observed in greater detail at a coastal site in Prydz Bay near Davis station (66.5766˚S, 77.9674˚E), where the annual cycles of dissolved CO_2 system parameters were determined using samples collected from May 2010 to February 2011. These observations show the seasonal influence of ice formation and melt, biological production, and sea-air CO_2 flux on changes in

total dissolved inorganic carbon (DIC), pH_{sws} and the saturation state of aragonite (Ω_{ar}). Net community production of 1.8 ± 0.4 mol C m^{-2} in the productive summer months (November-February) caused large seasonal decreases in DIC. The decrease in DIC caused a change in surface water partial pressure of CO_2 from values over-saturated with respect to the atmosphere in the ice-covered winter period, to undersaturated waters in the summer months.

In contrast to the offshore SIZ, the coastal study site was estimated to be an annual net sink for CO_2 of 0.54 ± 0.11 mol C m^{-2} $year^{-1}$. The calculated pH_{sws} and Ω_{ar} values varied seasonally from 7.99 to 8.20 and 1.19 to 1.92, respectively. The observed variability was compared to similar measurements carried out in 1993-95 at the same location, and this revealed that natural variability in carbon cycle dynamics caused changes in pH_{sws} that were nearly twice as large as those expected from changes estimated due to ocean acidification over this time.

In addition to the analysis of carbon cycle dynamics in offshore and coastal East Antarctica, an experiment was designed to assess the impact of ocean acidification on benthic communities near Casey station (66.2818˚S, 110.5276˚E) in East Antarctica from December 2014 to February 2015. Changes in dissolved CO_2 system parameters within this first Antarctic free ocean CO_2 enrichment (antFOCE) experiment showed how the system successfully manipulated seawater carbonate chemistry to maintain a mean pH offset from ambient values of 0.38 ± 0.07 pH units for approximately 6 weeks of the 8-week experimental period.

Diel and seasonal fluctuations in ambient pH were duplicated in experimental chambers, located on the seafloor under sea ice, where the seawater pH was manipulated to match values expected by the end of this century under the Intergovernmental Panel on Climate Change Representative Concentration Pathway 8.5 greenhouse gas concentration trajectory. The mean pH_{sws}, Ω_{ar} and fCO_2 values in the experimental chambers were 7.680 ± 0.085, 0.62 ± 0.15 and 914 ± 160 µatm, respectively. The experiment demonstrates the feasibility of FOCE systems, even under extreme conditions experienced in the Antarctic.

The dynamic nature of the SIZ in general and the observed variability in dissolved CO_2 system parameters in the broader region, demonstrates the need for continued

monitoring of the marine carbon cycle so that regional models can accurately attribute causes of change and predict impacts of future ocean acidification.

Acknowledgements

I would firstly like to thank my supervisors, Patti Virtue, Bronte Tilbrook, Tom Trull and Guy Williams. Their guidance, knowledge and generosity with time has stimulated my interest in the subject matter and made the completion of this thesis possible.

I would like to thank the Australian government for the Australian Postgraduate Award; the CSIRO for the Oceans and Atmosphere top-up scholarship; and Lynchpin – the Ocean Project for interest in this research and additional financial support. Jonny Stark from the Australian Antarctic Division, and Donna Roberts, then Senior Research Fellow, Antarctic Climate and Ecosystems CRC, University of Tasmania, are thanked for their efforts in making the antFOCE project a success.

I would also like to thank the CSIRO's Ocean Carbon Observations team for their friendly support and technical expertise. I would particularly like to thank Erik van Ooijen and Kate Berry.

Finally, to my Mum and Dad, your support and guidance through my university studies, and life in general, is valued and appreciated more than you can ever know. Thank you.

1 Introduction

1.1 The global carbon cycle

The global carbon cycle plays a key role in regulating the Earth's climate by controlling the concentrations of greenhouse gases in the atmosphere. Since the start of the Industrial Revolution (defined as beginning in the year 1750) the atmospheric concentration of these gases, mainly carbon dioxide (CO_2), methane (CH_4) and nitrous oxide (N_2O) have substantially increased (IPCC, 2013). CO_2 in particular has increased from 278 ± 2 ppm (Etheridge et al., 1996) to present values (2016) of ~403 ppm (Dlugokencky & Tans, 2016) throughout the industrial era. This increase is attributed to the burning of fossil fuels and changes to land usage, which in turn affects the radiative properties of the atmosphere (Arrhenius, 1896). The global carbon cycle is characterised by a series of carbon reservoirs and fluxes in the Earth system that exchange carbon over varying timescales. Broadly, the timescales associated with the turnover of carbon in each reservoir, can be divided into two domains, the fast (<10,000 years) and the slow domain (>10,000 years). The fossil fuel extraction from the slow domain, and its subsequent combustion, has resulted in the transfer of a significant amount of carbon from the slow domain into the fast domain. This has resulted in a major human-induced, or anthropogenic, perturbation to the carbon cycle, causing climate change.

The global carbon cycle is dominated by four major carbon reservoirs: the Earth's crust, the atmosphere, the terrestrial biosphere and the ocean. Understanding how carbon is cycled between the various reservoirs is critical to understanding future changes in climate. For example, the total amount of anthropogenic carbon emitted to the atmosphere over the industrial period (to 2011) through fossil fuel combustion, cement manufacturing and land use change is 555 ± 85 Pg C, however the observed atmospheric increase over the same period is 240 ± 10 Pg C (IPCC, 2013). The ocean and the terrestrial biosphere have absorbed the remaining anthropogenic carbon, but there remains considerable uncertainty regarding the relative partitioning of anthropogenic CO_2 between these two reservoirs (Houghton, 2007). Current estimates allocate 155 ± 30 Pg C, or 28% of total anthropogenic CO_2 emissions to the oceanic reservoir (Le Quéré et al., 2015).

Atmospheric CO_2 is exchanged with the surface ocean across the sea-air interface and is transported within the ocean by the biological pump and the combined action of the solubility pump and large scale circulation (Volk & Hoffert, 1985). These transport mechanisms produce a vertical gradient of dissolved inorganic carbon (DIC) within the ocean, whereby the DIC concentration in the deep ocean is more than 10% higher than at the surface (Gruber & Sarmiento, 2002). The solubility pump is driven by the temperature gradient in the ocean and the increased solubility of CO_2 at lower temperatures. The biological pump is further divided into the soft tissue pump and the marine carbonate pump (Volk & Hoffert, 1985). The soft tissue pump refers to the fraction of organic carbon that is exported to, and subsequently remineralized in, the deep ocean from photosynthetic activity in the surface. The marine carbonate pump describes the biogenic formation and dissolution of calcium carbonate ($CaCO_3$) and the net downward transport of both alkalinity and DIC from the surface into the deeper ocean. In the absence of these "pumps", large-scale circulation would mix the DIC and alkalinity uniformly and cause atmospheric CO_2 to almost double its preindustrial concentration (Gruber & Sarmiento, 2002). Therefore future change in climate will depend not only on the intensity of carbon emissions, but also on the efficiency of the pumps that remove CO_2 from the atmosphere to the deep ocean.

1.2 The Southern Ocean

The Southern Ocean is the primary conduit by which anthropogenic CO_2 enters the ocean, accounting for over 40% of the global ocean uptake of anthropogenic CO_2 (Sabine et al., 2004; Khatiwala et al., 2009). This strong uptake is due to the vigorous overturning circulation in these high latitudes, in which water masses are formed and subducted into the ocean interior (Sallée et al., 2012). Circulation within the Southern Ocean is dominated by the eastward flowing Antarctic Circumpolar Current (ACC) (Rintoul et al., 2001), which consists of a number of circumpolar fronts that correspond to different water mass boundaries and eastward flow regimes (Orsi et al., 1995). A series of key zones for carbon cycling are defined by the fronts (Lenton et al., 2013). These zones from north to south are 1) the Subantarctic zone (SAZ) between the Subtropical Front (STF) and the Subantarctic Front (SAF); 2) the polar frontal zone (PFZ), between the SAF and the Polar Front (PF); 3) the Antarctic zone (AZ) between the PF and the Antarctic coast (Figures 1.1 and 1.2).

Westerly winds across the Southern Ocean produce a northward Ekman transport of surface waters, creating a divergence driven upwelling of carbon-rich Circumpolar Deep Water (CDW) near the Southern Boundary (SB) of the ACC (Rintoul et al., 2001). From here, two meridional overturning cells form (Figure 1.1), providing a significant conduit for anthropogenic carbon to enter the deep ocean (Marshall & Speer, 2012). The first cell, consisting of intermediate and mode waters that are transported north to intermediate depths, makes up the largest contribution to the uptake and storage of anthropogenic carbon by the Southern Ocean (McNeil et al., 2001; Sabine et al., 2004; Sallée et al., 2012). A second cell is driven by the formation of Antarctic Bottom Water (AABW), which originates in specific regions on the Antarctic shelf and sinks to abyssal depths due to varying combinations of brine rejection from sea-ice formation and ocean/ice-shelf interactions. In doing so, AABW contributes significantly to the global overturning circulation and sequesters heat and atmospheric gases to the deep ocean (Orsi et al., 1999; Johnson, 2008; Marshall & Speer, 2012).

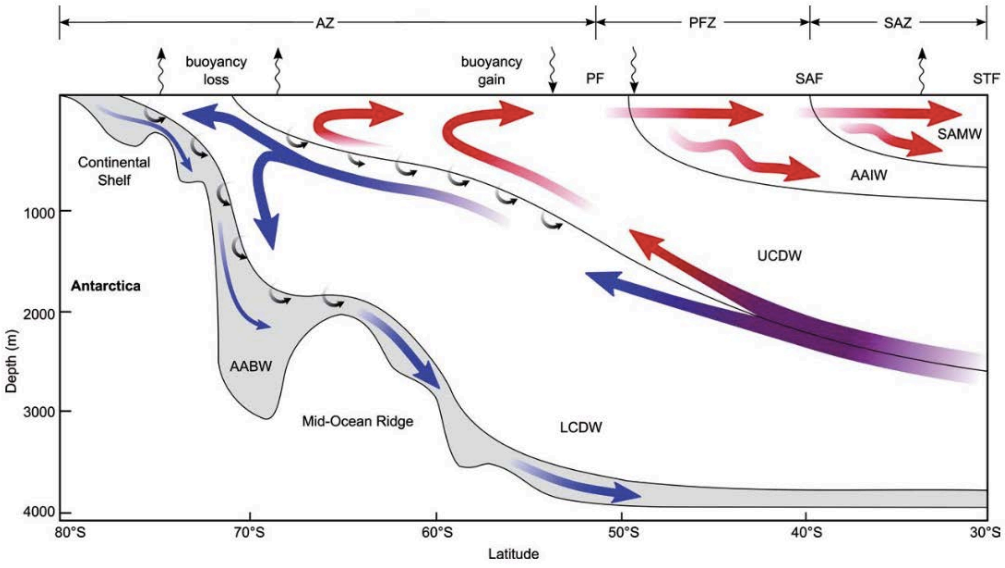

Figure 1.1 Schematic of Southern Ocean circulation showing the divergence driven upwelling of Upper and Lower Circumpolar Deep Water (UCDW and LCDW) and the mean flow of the upper (red arrows) and lower (blue arrows) meridional overturning cells. See text for definitions of Fronts and Zones (Source: Post et al. 2014).

Despite the importance of the Southern Ocean to global biogeochemical cycles, it remains one of the most poorly sampled ocean regions (Lenton et al., 2013) with

observations often localized and widely separated in both space and time. This results in a heavy dependence on models to characterize carbon fluxes at regional scales in this area. Notable discrepancies exist between model and observational results within the seasonal ice zone (SIZ) around Antarctica. Ocean biogeochemical models, for example, indicate a weak annual sink of CO_2 for the area south of 58°S, whereas atmospheric inversions show the area to be a small source (Lenton et al., 2013). These discrepancies are most likely due to sparse observations and incomplete model formulations that do not adequately resolve the large seasonal variability in processes that govern atmosphere-ocean interactions, such as temperature, wind regimes, sea-ice conditions, and biological productivity (Takahashi et al., 2012).

1.3 Ocean acidification

The uptake of anthropogenic CO_2 by the ocean has reduced the amount of CO_2 that would otherwise remain in the atmosphere, thereby minimizing some of the impacts of global warming. This uptake however, changes the chemical balance of seawater through the thermodynamic equilibrium of CO_2 with seawater. The chemical reaction lowers the pH and the dissolved carbonate ion (CO_3^{2-}) concentration of seawater (Feely et al., 2004; Orr et al., 2005), causing ocean acidification. A consequence of declining CO_3^{2-} concentration is a reduction in the saturation state (Ω) of $CaCO_3$, a mineral used in the production of shells and skeletal material of many marine organisms. Laboratory experiments indicate that many marine organisms react adversely to decreases in pH and CO_3^{2-} concentrations that will occur under future atmospheric CO_2 scenarios (Raven et al., 2005).

The Southern Ocean is considered particularly sensitive to changes in carbonate chemistry, due primarily to its low buffer capacity (Sabine et al., 2004), which results in greater ocean acidification per unit CO_2 increase than temperate and tropical waters (Revelle & Suess, 1957). The Southern Ocean is predicted to be one of the first regions to experience widespread undersaturation of aragonite ($\Omega_{ar} < 1$) (McNeil & Matear, 2008), a major biogenic form of $CaCO_3$ in high-latitude Southern Ocean waters (Honjo, 2004; Hunt et al., 2008; Post et al., 2010; Bednaršek et al., 2012). The decline in ocean pH is predicted to have serious consequences for marine ecosystems (Orr et al., 2005), from direct effects on physiology, metabolism, and calcification rates; to indirect effects on food webs, species interactions (Kroeker et al., 2013) and

phytoplankton community composition (Neven et al., 2011; Trimborn et al., 2013). This Southern Ocean sensitivity varies significantly with latitude, with waters close to Antarctica exhibiting lower pH and carbonate saturation states. As a result, important biogeochemical thresholds such as carbonate undersaturation and pH values below Holocene levels, are expected to be crossed earlier than waters further north (Orr et al., 2005; McNeil & Matear, 2008).

1.4 Objectives of this study

The overall objective of this study was to investigate the carbon cycle dynamics of the seasonal sea-ice zone of East Antarctica. The study considered a range of spatial and temporal scales that contribute to the variability of carbon cycling in the region. The task was carried out as three major efforts, which make up the three main chapters of this thesis.

Firstly, a survey of the large-scale characteristics of biogeochemical properties in East Antarctic waters within the SIZ was undertaken. Specifically, the vertical and surface distribution of biogeochemical properties in the seasonally ice covered region of the southwest Indian Ocean sector of East Antarctica (30°-80°E, 60°-69°S) was investigated during austral summer (January – March 2006) during the Baseline Research on Oceanography, Krill and the Environment – West (BROKE-West) survey (Figure 1.2). The physical and biological processes influencing the observed changes in carbonate system parameters and the winter to summer evolution of such properties were determined, and the uptake and storage of anthropogenic carbon in the region was also investigated. This work is presented in Chapter 2, and has recently been published in the Journal of Geophysical Research: Oceans.

Secondly, the full annual cycle of carbon system variations and their relationships to sea ice and water column structure was investigated for a coastal site in East Antarctica using samples collected from May 2010 to February 2011 in Prydz Bay. This is one of the few coastal sites in Antarctica with seasonal data. This work allowed a comparison with observations made nearly twenty years earlier from the same site and were used to assess decadal variability in carbon cycle dynamics. This work is presented in Chapter 3, and was published in 2013 in Marine Chemistry.

Finally, a first effort to examine possible future ramifications of ocean acidification using a free-ocean CO_2 enrichment (FOCE) experiment was undertaken (Chapter 4). This chapter describes manipulation of seawater carbonate chemistry in experimental chambers of the first Antarctic FOCE (antFOCE) experiment. Conducted from December 2014 to February 2015 at a coastal site near Casey station in East Antarctica, the experiment was designed to study the response of benthic communities to ocean acidification. High-resolution monitoring of seawater pH under different sea-ice regimes was also undertaken so that local variability in biogeochemical properties could be determined. This work also provided additional insights into small spatial scale and rapid temporal natural variability in ocean carbon system status in near shore waters with multiyear fast ice cover.

Following these 3 experimental studies, a brief Conclusion chapter summarizes the overall advances of the thesis and identifies important issues for further research.

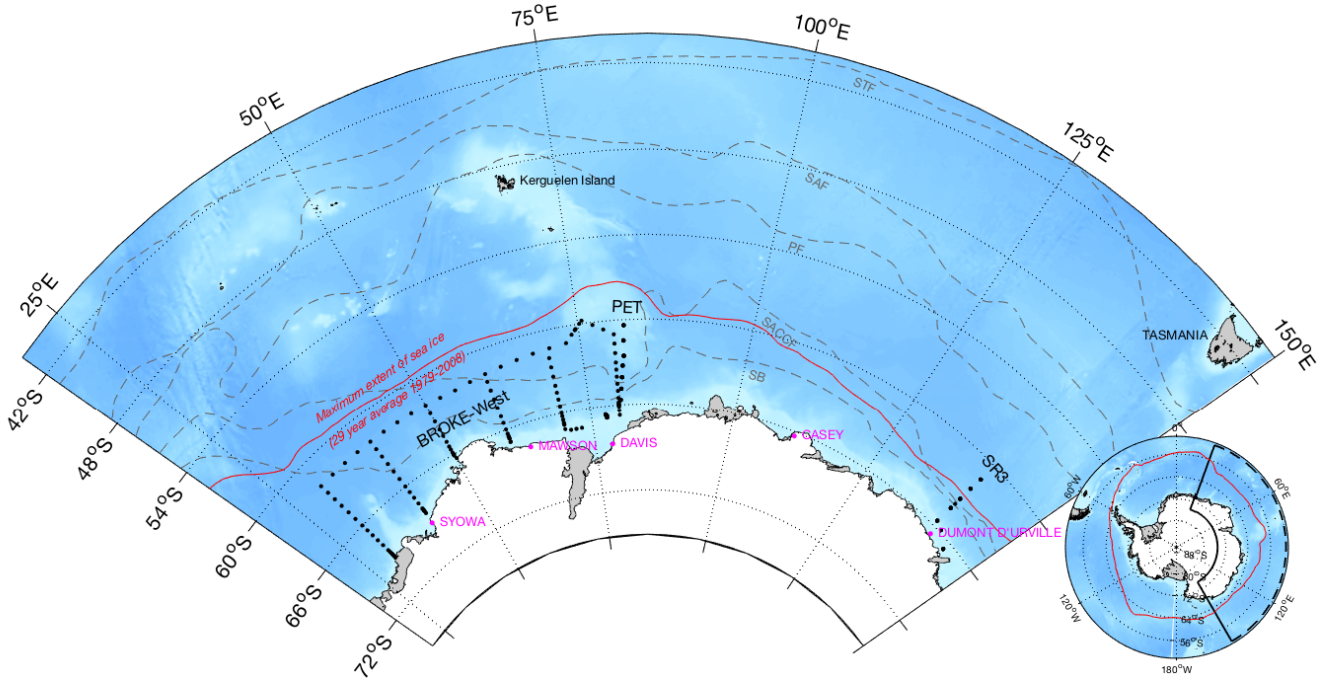

Figure 1.2 The historical location of Southern Ocean fronts and boundaries, including the Subtropical Front (STF), the Subantarctic Front (SAF), the Polar Front (PF), the Southern Antarctic Circumpolar Current Front (SACCF) and the Southern Boundary (SB) of the ACC (Orsi et al., 1995), with the average (1979-2008) maximum extent of sea ice (red line) (Cavalieri et al., 2015) and the location of sample sites used in this thesis, including the Baseline Research on Oceanography, Krill and the Environment – West (BROKE-West; 2006), the Princess Elizabeth Trough (PET; 2005) and the southern end of the 1994 WOCE SR3 transect.

2 Carbon cycling dynamics in the seasonal sea-ice zone of East Antarctica between 30°-80°E

All of the research contained within this chapter has been published as:

Roden, N.P., Tilbrook, B., Trull, T.W., Virtue, P. & Williams, G.D., (2016). Carbon cycling dynamics in the seasonal sea-ice zone of East Antarctica. *Journal of Geophysical Research: Oceans*, 121.

Abstract

The carbon cycle of the seasonally ice covered region of the southwest Indian Ocean sector of East Antarctica (30°-80°E, 60°-69°S) was investigated during austral summer (January – March 2006). Large variability in the drivers and timing of carbon cycling dynamics were observed and indicated that the study site was a weak net source of carbon dioxide (CO_2) to the atmosphere of 0.07 ± 0.13 mol C m^{-2} during the ice-free period, with narrow bands of CO_2 uptake observed near the continental margin and north of the Southern Antarctic Circumpolar Current Front. Continuous surface measurements of dissolved oxygen and the fugacity of CO_2 were combined with net community production estimates from oxygen/argon ratios to show that surface heat gain and photosynthesis were responsible for the majority of observed surface water variability. On seasonal timescales, winter sea-ice cover reduced the flux of CO_2 to the atmosphere in the study area, followed by biologically driven drawdown of CO_2 as the ice retreated in spring-summer highlighting the important role that sea-ice formation and retreat has on the biogeochemical cycling of the region.

2.1 Introduction

The Southern Ocean plays a critical role in the global carbon cycle, accounting for over 40% of the global ocean uptake of anthropogenic carbon dioxide (CO_2) (Sabine et al., 2004; Khatiwala et al., 2009). This area is one of the most poorly sampled ocean regions (Lenton et al., 2013) with observations often localized and widely separated in both space and time, resulting in a heavy dependence on models to characterize carbon fluxes at regional scales in this area. Notable discrepancies exist between model and observational results within the seasonal ice zone (SIZ) around Antarctica. Ocean biogeochemical models, for example, indicate a weak annual sink of CO_2 for the area south of 58°S, whereas atmospheric inversions show the area to be a small source (Lenton et al., 2013). These discrepancies are most likely due to sparse observations and incomplete model formulations that do not adequately resolve the large seasonal variability in processes that govern atmosphere-ocean interactions, such as temperature, wind regimes, sea-ice conditions, and biological productivity (Takahashi et al., 2012).

Given the important role of atmospheric CO_2 in the climate system, there is a need to accurately attribute the causes of change and develop a regional understanding of the CO_2 sink/source nature of the Southern Ocean. For example, Arrigo et al. (2008) modelled CO_2 uptake in the south-western Ross Sea, which equates to 27% of their CO_2 sink estimate for the entire Southern Ocean. While this suggests the shelf regions around Antarctica may be a significant component of the Southern Ocean CO_2 uptake, the quantification of their role in carbon uptake is largely unresolved. Furthermore, future change in the Southern Ocean carbon cycle is likely to be complicated by climate related physical and biological feedbacks associated with changes in sea-ice dynamics (Massom et al., 2013), increased stratification (Smith & Nelson, 1986) and the intensification of winds (Thompson et al., 2011; Meijers, 2014). Recent evidence indicates the efficiency of the Southern Ocean CO_2 sink has increased in the past decade (Landschützer et al., 2015), after weakening in the previous decade (Le Quéré et al., 2007), indicating changes to large-scale ocean dynamics will not only influence future atmospheric CO_2 levels, but may also influence the rate of ocean acidification in this region (Lenton et al., 2009).

The majority of the Southern Ocean is characterized as a high-nutrient, low-chlorophyll (HNLC) zone, which refers to areas of the ocean with low standing stocks of phytoplankton and high macronutrient concentrations. Although modest rates of annual average net primary production occur in the Southern Ocean (Arrigo et al., 2008), intense phytoplankton blooms can occur. The marginal ice zone (MIZ), defined as the outer edge of the summer pack ice, has been recognized as a site of elevated biomass and productivity (Smith & Nelson, 1986). Here, the spring bloom of phytoplankton is initiated during the development of a stable water column formed by the input of low-density water from the receding sea ice.

Whilst sea-ice dynamics and the development of the seasonal mixed layer (SML) are undoubtedly important processes, the timing and the magnitude of primary productivity in the Southern Ocean is also driven by light availability and the supply of micronutrients, particularly iron (de Baar et al., 1995). The various supply mechanisms of iron to the Southern Ocean have been widely discussed in the literature (Sedwick & DiTullio, 1997; Cassar et al., 2007; Boyd & Mackie, 2008; Lannuzel et al., 2014; Schallenberg et al., 2016). Dust deposition, sea-ice melt, and the oceanic supply through sediment interactions and upwelling are considered to be among the most important processes controlling iron availability and thus, influencing the biological productivity of the Southern Ocean.

For January-March 2006, the SIZ off the coast of East Antarctica between 30°-80°E, was the location of a comprehensive marine study. The Baseline Research on Oceanography, Krill and the Environment – West (BROKE-West) survey concentrated on the Commission for the Conservation of Antarctic Marine Living Resources (CCAMLR) statistical division 58.4.2. The statistical divisions of the CCAMLR area, which tend to align with the general ecosystem characteristics of the Southern Ocean, were implemented so that catch, effort and trade statistics in each region could be reported. The BROKE-West survey included 11 meridional oceanographic transects over the Antarctic shelf, slope and rise every 5° of longitude and a zonal section to the north at 62°S (Figure 2.1).

A series of papers from the BROKE-West study covered the large-scale circulation (Meijers et al., 2010), surface oceanography (Williams et al., 2010), remotely sensed climatologies of the region (Schwarz et al., 2010), primary productivity (Westwood et

al., 2010), phytoplankton (Wright et al., 2010), protistan community composition (Davidson et al., 2010) and krill (Jarvis et al., 2010; Kawaguchi et al., 2010; Virtue et al., 2010). This chapter describes the surface and vertical distribution of biogeochemical properties through the region, the physical and biological processes influencing the observed changes and the winter to summer evolution of such properties.

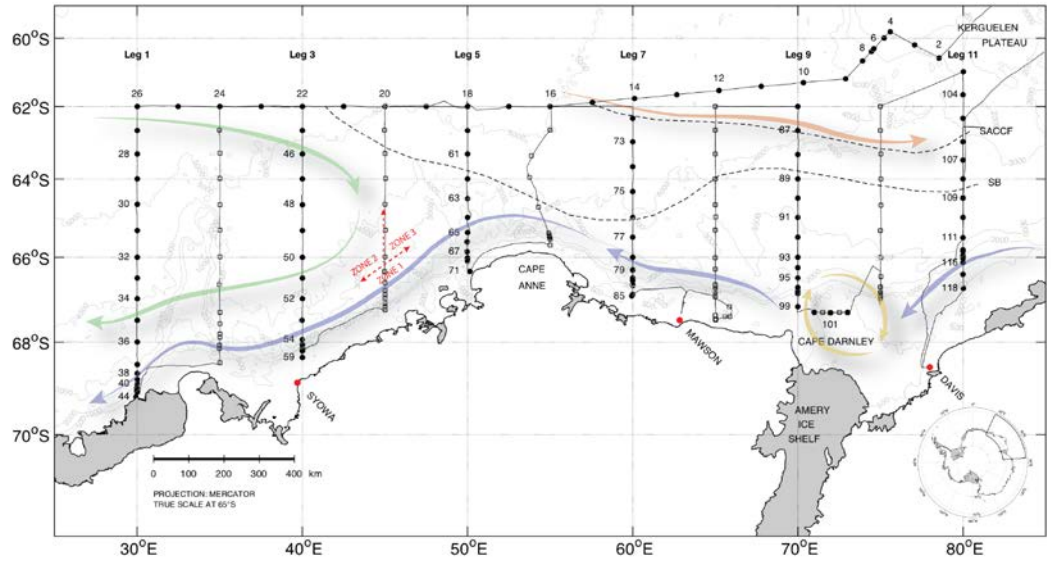

Figure 2.1 Cruise track of the *RV Aurora Australis* during the BROKE-West survey in the South Indian sector of the Southern Ocean. Showing the location of CTD and xCTD stations, marked as black dots and black open squares, respectively. Black dashed lines (labelled) show the location of the Southern Boundary (SB) of Circumpolar Deep Water and the Southern Antarctic Circumpolar Current Front (SACCF). Other large-scale oceanographic features include the main flow in the east of the Weddell Gyre (green arrows), the Antarctic Slope Current (blue arrows), the Prydz Bay Gyre (yellow arrow) (Heywood et al., 1999) and the southern Antarctic Circumpolar Current (red arrow). The intersections of Zones 1, 2 and 3 are delineated with red dashed arrows, for precise boundaries refer to text in Section 2.2.1.1.

2.2 Data and methods

2.2.1 Oceanographic setting of the Antarctic margin between 30°-80°E

2.2.1.1 Large-scale circulation and water mass properties

The study region lies inside the Weddell-Enderby basin, with the Kerguelen Plateau immediately to the northeast and the Princess Elizabeth Trough to the east. The large-scale circulation, water masses and frontal boundaries of the BROKE-West study area (Williams et al., 2010; Meijers et al., 2010), include two partial gyres, three major

fronts and six water masses and several upwelling regimes associated with the Weddell Gyre, the Antarctic Divergence and the Kerguelen Plateau (Foldvik & Gammelsrød, 1988; Park et al., 1998; Sokolov & Rintoul, 2007; Bakker et al., 2008; Williams et al., 2010). We define water masses of the region in Table 2.1 based on the classifications of Whitworth et al. (1998) and Shadwick et al. (2014).

Table 2.1 Bounding neutral density (γ_n), potential temperature (θ) and water depth values that define the major water masses in the BROKE-West region.

	γ_n (kg m^{-3})	**θ (°C)**	**Water Depth**
Antarctic Surface Water (AASW)	<28.03	>-1.925	Above T_{min} base
Circumpolar Deep Water (CDW)		>1.5	Below T_{min} base to 2500 m
Modified CDW (mCDW)		≤1.5	Below T_{min} base to 2500 m
Antarctic Bottom Water (AABW)	>28.27	>-1.925	>2500
Modified Shelf Water (mSW)	>28.27	>-1.85	600 to 2500 m (Slope)
Low Salinity Shelf Water (LSSW)	>28.27	>-1.85	<600 m (Shelf)
Dense Shelf Water (DSW)	>28.27	-1.925 to -1.85	<600 m (Shelf)
Ice Shelf Water (ISW)		≤-1.925	

The region can be divided into three distinctive zones (Schwarz et al., 2010) that were sampled from the surface to the bottom (Figure 2.1), starting with Leg 1 in January and Leg 11 completed in February. Zone 1, is the continental shelf/slope region (depth < 3000 m) to the south of the Antarctic Slope Front, and is characterised by marginal ice cover in December and January, and by the westward flowing Antarctic Slope Current. Zone 2, covers waters to the north of the Antarctic Slope Front and west of ~45°E and corresponds to the SIZ and the eastern limb of the Weddell Gyre, which is an elongated cyclonic gyre. To the east and offshore, Zone 3 contains the SIZ and includes the Prydz Bay Gyre, the Antarctic Circumpolar Current (ACC) and its southern fronts, i.e. the Southern ACC Front (SACCF) and the Southern Boundary (SB) (Orsi et al., 1995). The SACCF and SB are forced southward by the Kerguelen Plateau and flow eastward through the Princess Elizabeth Trough at the eastern end of the study region.

2.2.1.2 Variability of Antarctic surface water properties

The seasonal growth and melt of sea ice has a significant influence on the structure and properties of surface waters in the region, as described by Williams et al. (2010) and summarised here. Heat loss to the atmosphere in winter drives sea-ice formation and convection, mixing the relatively cold surface waters with the warmer underlying CDW. This forms a deep, homogenous winter mixed layer with the sea-ice cap

restricting sea-air gas exchange. The sea ice begins to melt in spring-summer and melt water stratifies the surface water and warms, forming a SML. The properties of the winter mixed layer are still present at depth, recognizable by a temperature minimum, or T_{min}, layer with a seasonal pycnocline separating it from the overlying SML. South of the sea-ice edge, convection continues and a SML is absent or weak, especially over the shelf where mixing can reach the seafloor.

Sea ice covered the BROKE-West study area during the winter prior to the survey and retreated from the north-east to the south-west from November to January (Figures 2.2a, 2.2b and 2.2c). The sea ice was mostly gone from the region by the start of the survey in January, apart from the westernmost legs, and persisted over the continental shelf at the southern end of most transects throughout the study. For waters north of the Antarctic Slope Front, the SML was typically about 40-60 m deep and saltier in the east and shoaled to depths as low as 12 m and freshened in the west. The deeper and saltier waters in the east appear to result from a combination of the transport of ACC waters into this eastern region and greater time since the seasonal retreat of sea ice for wind mixing to deepen the SML (Williams et al., 2010).

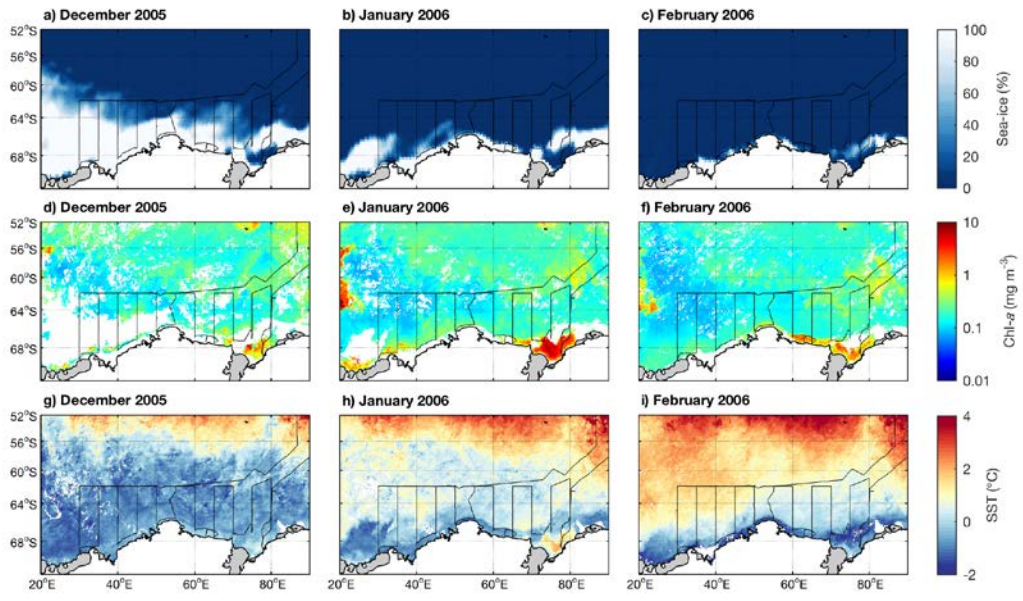

Figure 2.2 Monthly satellite derived concentrations of sea ice (%, a to c), chlorophyll-*a* (mg m^{-3}, d to f) and sea surface temperature (°C, g to i) with the cruise track overlaid in black. Sea-ice data are from Nimbus-7 (25 km) (Cavalieri et al., 2015). Chlorophyll-*a* and sea surface temperature from MODIS-Aqua (9 km).

2.2.2 Biogeochemical measurements

For a comprehensive description of oceanographic field measurements, processing and calibration from BROKE-West, see Rosenberg & Gorton (2006). A total of 118 Conductivity-Temperature-Depth (CTD) casts were conducted aboard the *RV Aurora Australis* using a Sea-Bird SBE 9plus with 22 × 10 litre General Oceanics Niskin bottles mounted onto a Sea-Bird rosette. Eighty expendable CTD (xCTD) probes were also used on meridional transects between the major CTD transects.

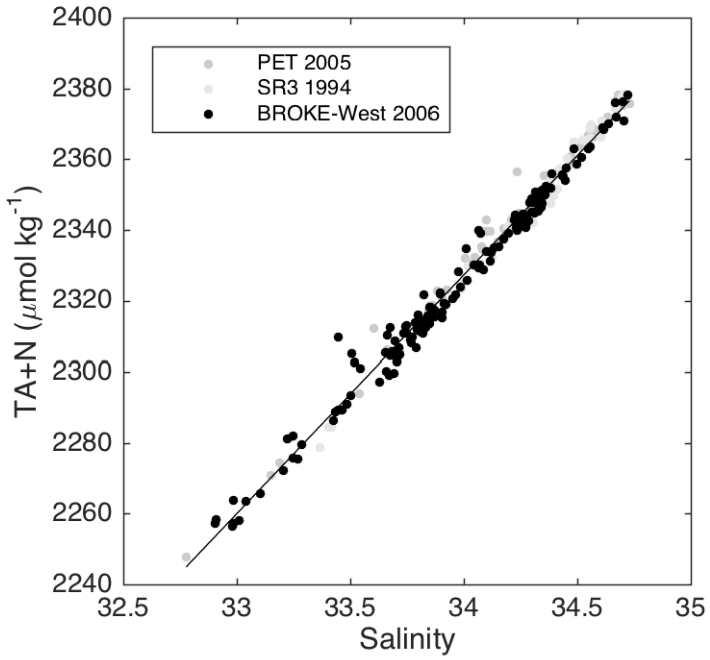

Figure 2.3 The salinity and TA+N relationship of waters south of 60°S and shallower than 500 m from BROKE-West in 2006, the Princess Elizabeth Trough in 2005 (PET) and from the WOCE SR3 transect, measured in 1994 (data available from GLODAP). A linear regression yielded the following equation, $y = (67 \pm 1)x + (36 \pm 18)$ (n = 237, $r^2 = 0.99$, standard error = 4 μmol kg^{-1}).

Seawater samples of 250-mL were collected from the Niskin bottles on CTD casts and were analysed on-board for total dissolved inorganic carbon (DIC) and total alkalinity (TA). For each of these samples, 100-μL of a saturated $HgCl_2$ solution was added to halt biological activity. DIC was determined using a Single Operator Multiparameter Metabolic Analyser following the procedure in Dickson et al. (2007). TA was determined by open-cell potentiometric titration using a 0.1 M hydrochloric acid titrant (Dickson et al., 2007). Routine analysis of Certified Reference Material

(batches 70 and 72) from Scripps Institution of Oceanography were used to verify the measurement accuracy and precision for DIC and TA analyses, which were better than ± 2 μmol kg^{-1}. Samples for dissolved phosphate (HPO_4^{2-}), silicic acid (H_4SiO_4) and nitrate + nitrite ($NO_3^- + NO_2^-$) (hereafter nitrate) were collected and analysed spectrophotometrically (Pasquer et al., 2010) and yielded a measurement accuracy and precision of ± 0.05 μmol kg^{-1}, ± 1.5 μmol kg^{-1} and ± 0.4 μmol kg^{-1}, respectively.

TA was only measured at the surface and on nine full depth CTD casts. These data were combined with data from previous cruises that used the same measurement techniques and a linear regression of salinity versus TA and nitrate (TA+N), known as potential alkalinity, was calculated. This relationship (Figure 2.3) was used to calculate TA at sample sites without alkalinity measurements. Data used to calculate the regression were from samples shallower than 500 m and included measurements from this study, together with those south of 60°S on CO_2/World Ocean Circulation Experiment (WOCE) hydrographic sections of the nearby Princess Elizabeth Trough in 2005, and measurements from the southern end of the 1994 WOCE SR3 transect along 140°E. The sum of TA and nitrate concentrations accounts for changes in TA associated with the uptake or release of dissolved nitrate during photosynthesis or respiration (Brewer & Goldman, 1976):

$$106\ CO_2 + 138\ H_2O + 16\ NO_3^- \rightarrow (CH_2O)_{106}\ (NH_3)_{16} + 16\ OH^- + 138\ O_2 \quad \textbf{Equation 2.1}$$

Once TA+N values were calculated at sample sites, concurrently measured nitrate concentrations were subtracted to give an estimate of TA. The correlation between the parameters in Figure 2.3 (y = (67 ± 1)x + (36 ± 18); n = 237, r^2 = 0.99, standard error = 4 μmol kg^{-1}) indicates net calcification/dissolution of carbonate minerals in the water column was not a significant contributor to the TA variability.

High-resolution surface water measurements of the fugacity of CO_2 (fCO_2) coupled with atmospheric CO_2 measurements, were made by pumping seawater from the ship's intake into a Weiss style spray equilibrator (Pierrot et al., 2009). The accuracy and precision of the measurements is estimated to be better than ± 2 μatm (see Appendix A). The sea-air gradient in fCO_2 (ΔfCO_2) was used to compute sea-air CO_2 flux using the following equation:

$$\mathrm{CO_{2\ flux}} = k \cdot \alpha \cdot \Delta f\mathrm{CO_2} \qquad \textbf{Equation 2.2}$$

where k is the gas transfer velocity (cm hr^{-1}) (Wanninkhof et al., 2013), scaled linearly with sea-ice cover by multiplying k by the fraction of open water, and α is the CO_2 solubility (mol m^{-3} atm^{-1}) (Weiss, 1974). The gas transfer velocity was computed using measured wind speeds from the ship's 10-metre wind anemometer for underway estimates of $\mathrm{CO_{2\ flux}}$ ($\mathrm{CO_2}_{\mathrm{flux}}^{\mathrm{uw}}$). A positive sea-air $\mathrm{CO_{2\ flux}}$ value implies a net transfer from the ocean to the atmosphere.

A calculation of the sea-air flux of CO_2 since ice retreated ($\mathrm{CO_2}_{\mathrm{flux}}^{\mathrm{ice-free}}$) was also made at each CTD station using wind speed history, sea-ice concentration and estimates of the seasonal development of ΔfCO_2 values. The number of ice-free days at each station were estimated from the day of sampling to when sea-ice concentrations obtained from the National Snow and Ice Data Centre (Cavalieri et al., 2015) first fell below 15% (Schwarz et al., 2010) (Figure 2.4). The reduction from complete ice cover to 15% occurs rapidly and the time of emergence of 15% cover is considered a good marker of when surface waters become open and can exchange gas across the sea-air boundary. The wind speed history at each CTD site was taken from daily mean cross-calibrated multiplatform (CCMP) winds (Atlas et al., 2011).

The sea-air gradient, ΔfCO_2, in Equation 2.2 was estimated for each ice-free day prior to sampling at CTD sites. Atmospheric fCO_2 was calculated after Weiss (1974) using the mean atmospheric mole fraction of CO_2 (XCO_2) measured in the study region and sea-level pressure values from the NCEP-DOE Reanalysis 2 data product interpolated in time. Ice-free surface water fCO_2 values were estimated from linearly interpolated surface water properties from the day of sampling to the first ice-free day, assuming that surface conditions at ice-free day 0 resembled the properties observed in the T_{min} layer. It is possible that primary production may have reduced surface water fCO_2 values before ice concentrations fell below 15% (Gibson & Trull, 1999; Roden et al., 2013) and could lead to an overestimate of the sea-air flux.

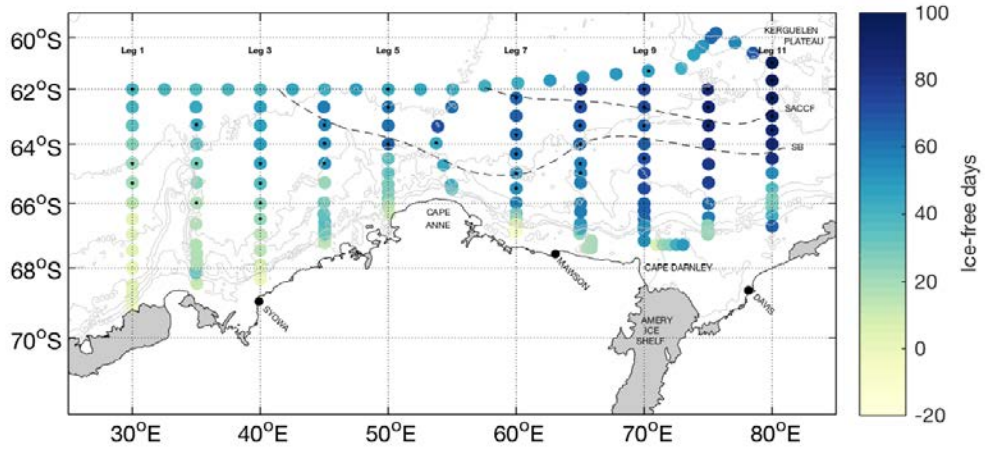

Figure 2.4 The number of ice-free days at each CTD and xCTD station prior to sampling. Negative numbers indicate areas that became ice-free after sampling had occurred.

The saturation state of aragonite (Ω_{ar}) (Mucci, 1983), fCO_2 and pH on the seawater scale (pH_{sws}) were calculated from DIC, TA, phosphate and silicic acid data using the standard set of carbonate system equations with the CO2SYS program (van Heuven et al., 2011) and the dissociation constants of Roy et al. (1993). For further information on the marine CO_2 system, the reader is referred to Zeebe & Wolf-Gladrow (2005). Errors associated with measured input parameters were incorporated into a Monte Carlo simulation to estimate uncertainties for Ω_{ar}, fCO_2 and pH_{sws} of ± 0.03, ± 14 µatm and ± 0.01 respectively (see Roden et al., 2013). To estimate the concentration of anthropogenic CO_2 (C_{ant}) in the study area we used the composite tracer TrOCA, which utilizes measurements of potential temperature, DIC, TA and O_2 to estimate the anthropogenic component of DIC (Touratier & Goyet, 2004; Touratier et al., 2007). Propagating the uncertainties associated with these measured input parameters, we estimate an uncertainty of ± 5 µmol kg^{-1} for C_{ant} estimates. The TrOCA method is not suitable for surface waters that experience large seasonal variability, which precludes estimates of C_{ant} for Antarctic Surface Water (AASW). The same method may also lead to some overestimate of C_{ant} in deep and bottom waters (Pardo et al., 2014).

2.2.3 Net community production

Values of net community production (NCP), defined as the difference between net primary production and heterotrophic respiration, were obtained for each CTD profile by calculating the seasonal carbon and nitrate deficits from the surface to the T_{min}

layer (Le Corre & Minas, 1983; Jennings et al., 1984) (see Appendix D). This approach assumes no vertical or lateral mixing takes place in either the SML or with the underlying winter mixed-layer during the winter to summer period when the SML shoals. Continuous underway shipboard measurements of oxygen/argon (O_2/Ar) ratios (Cassar et al., 2007) using membrane inlet mass spectrometry (MIMS) (Kaiser et al., 2005) were also utilised for NCP estimates (Appendix D). The use of O_2/Ar ratios in the oceanic mixed layer provides a method to constrain biological processes (ΔO_2^{bio}) because oxygen and argon share similar physical solubility properties, but only oxygen is biologically consumed and produced. Additional measurements of underway surface oxygen concentration were made using an oxygen optode (accuracy of ± 2 μmol kg^{-1}; Appendix A). The optode data were then combined with ΔO_2^{bio} (Appendix E), to partition total oxygen saturation (ΔO_2^{total}) into biological (the sum of photosynthesis and respiration) and physical (ΔO_2^{phys}) drivers (temperature changes, bubble injection, mixing) (Cassar et al., 2011) using:

$$\Delta O_2^{phys} = \Delta O_2^{total} - \Delta O_2^{bio} \quad \textbf{Equation 2.3}$$

While the MIMS technique provides an alternative estimate of NCP, the calculation of ΔO_2^{bio} using this method is complicated in high latitude waters due to a number of processes including ice melt, temperature change, and the entrainment of oxygen undersaturated waters into the SML that can lead to underestimates of ΔO_2^{bio} (e.g. Castro-Morales et al., 2013; Cassar et al., 2014; Eveleth et al., 2014). Although these complications do provide challenges to interpretation of the O_2/Ar signals in our study region, the method does provide an alternative estimate of NCP and addresses different time scales (days to weeks) compared to the seasonal estimates based on carbon and nitrate deficits.

2.3 Results

2.3.1 Vertical sections of biogeochemical properties

The mean property values for the water masses of the BROKE-West region are listed in Table 2.2. AASW, AABW, mCDW and mSW were observed on all major CTD legs, CDW was not observed on Leg 1 and LSSW, DSW and ISW were only observed at the southern end of Leg 9. Here, we focus on the distribution of carbonate

system parameters along sections in Legs 3 and 11 to illustrate the most important features exhibited in the study region with results from other legs illustrated in Appendix F. The highest values of DIC and fCO_2 were at depth with Ω_{ar} and pH_{sws} values increasing toward the surface. AASW was the predominant water mass in the mostly ice-covered shelf waters at the southern end of Leg 3 (Figure 2.5). These AASW waters had the lowest observed DIC and calculated fCO_2 values of 2039 μmol kg^{-1} and 173 μatm, respectively, corresponding to Ω_{ar} and pH_{sws} values of 2.30 and 8.33, respectively. Further offshore, between 64°S and 66°S, water higher in DIC and fCO_2 shoals to around 100 m due to the upwelling of Warm Deep Water (WDW), a type of mCDW associated with the Weddell Gyre, as noted previously by Williams et al. (2010).

Table 2.2 Mean values of characteristic properties in each water mass in the BROKE-West region.

	AASW	**CDW**	**mCDW**	**AABW**	**mSW**	**LSSW**	**DSW**	**ISW**
γ_n (kg m^{-3})	27.75	28.00	28.19	28.34	28.29	28.34	28.51	28.23
θ (°C)	-1.01	1.74	0.48	-0.35	-0.11	-1.77	-1.89	-1.99
Salinity	34.21	34.69	34.68	34.66	34.67	34.49	34.56	34.46
O_2 (μmol kg^{-1})	275	174	193	208	204	278	280	283
DIC (μmol kg^{-1})	2187	2255	2251	2255	2257	2232	2237	2228
TA (μmol kg^{-1})	2291	2340	2340	2351	2350			
fCO_2 (μatm)	376	564	517	487	508	418	414	409
pH_{sws}	8.04	7.87	7.88	7.77	7.83	7.99	7.98	8.00
Ω_{ar}	1.33	1.04	0.96	0.50	0.72	1.15	1.09	1.17
NO_3^- (μmol kg^{-1})	28.03	32.08	31.59	31.85	31.67	30.17	30.15	29.81
PO_4^{2-} (μmol kg^{-1})	1.72	2.02	2.00	2.05	2.01	1.90	1.91	1.89
Si (μmol kg^{-1})	56.5	84.5	99.3	129.4	117.2	66.6	66.8	62.4
C_{ant} (μmol kg^{-1})		16	22	25	25	50	53	51

Leg 11 (Figure 2.6) in the eastern part of the study area, along with Leg 9 (Figure 2.15), are located in a different physical oceanographic regime when compared to the western CTD legs (Meijers et al., 2010). Both of these eastern sections encompass the SB and the SACCF with intrusions of the ACC, which Meijers et al. (2010) identified by a rapid deepening of the 28.03 kg m^{-3} density surface north of ~64°S. At the northern end of Leg 11, CDW protrudes over the southern edge of the Kerguelen Plateau and has the highest subsurface fCO_2 value of 659 μatm (station 103, depth 198 m). This coincides with a pocket of aragonite undersaturation ($\Omega_{ar} < 1$), a state where the dissolution of aragonite becomes thermodynamically favourable. Whilst the average depth of the aragonite saturation horizon ($\Omega_{ar} = 1$) across all sections is 711 ± 134 m (1 s.d.; n = 38), pockets of aragonite undersaturation at depths as shallow

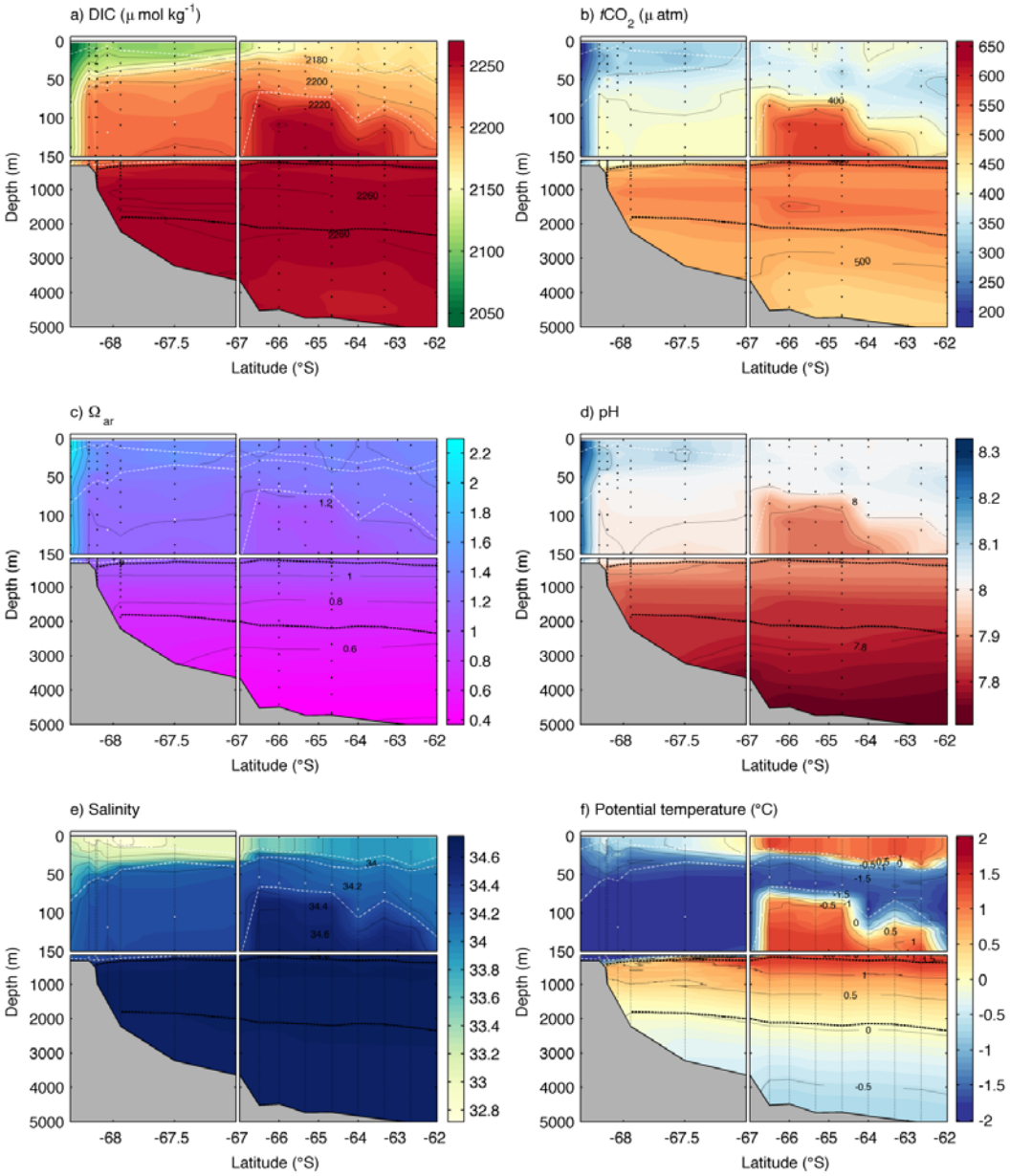

Figure 2.5 Leg 3, a) DIC (μmol kg^{-1}), b) fCO_2 (μatm), c) saturation state of aragonite (Ω_{ar}), d) pH_{sws}, e) salinity and f) potential temperature (°C). The black dashed lines, on this and other similar plots, represent the 28.03 kg m^{-3} (upper) and the 28.27 kg m^{-3} (lower) neutral density surfaces that partly delineate major water masses in the study region. The black dots show the bottle and CTD locations. The white dots show the location of the T_{min} value and the white lines show the base of the seasonal mixed layer (upper), seasonal pycnocline (middle) and T_{min} layer (lower). The marginal ice zone is indicated by a white rectangle at the surface towards the southern end of each leg. Scale changes are indicated by the breaks in the axis.

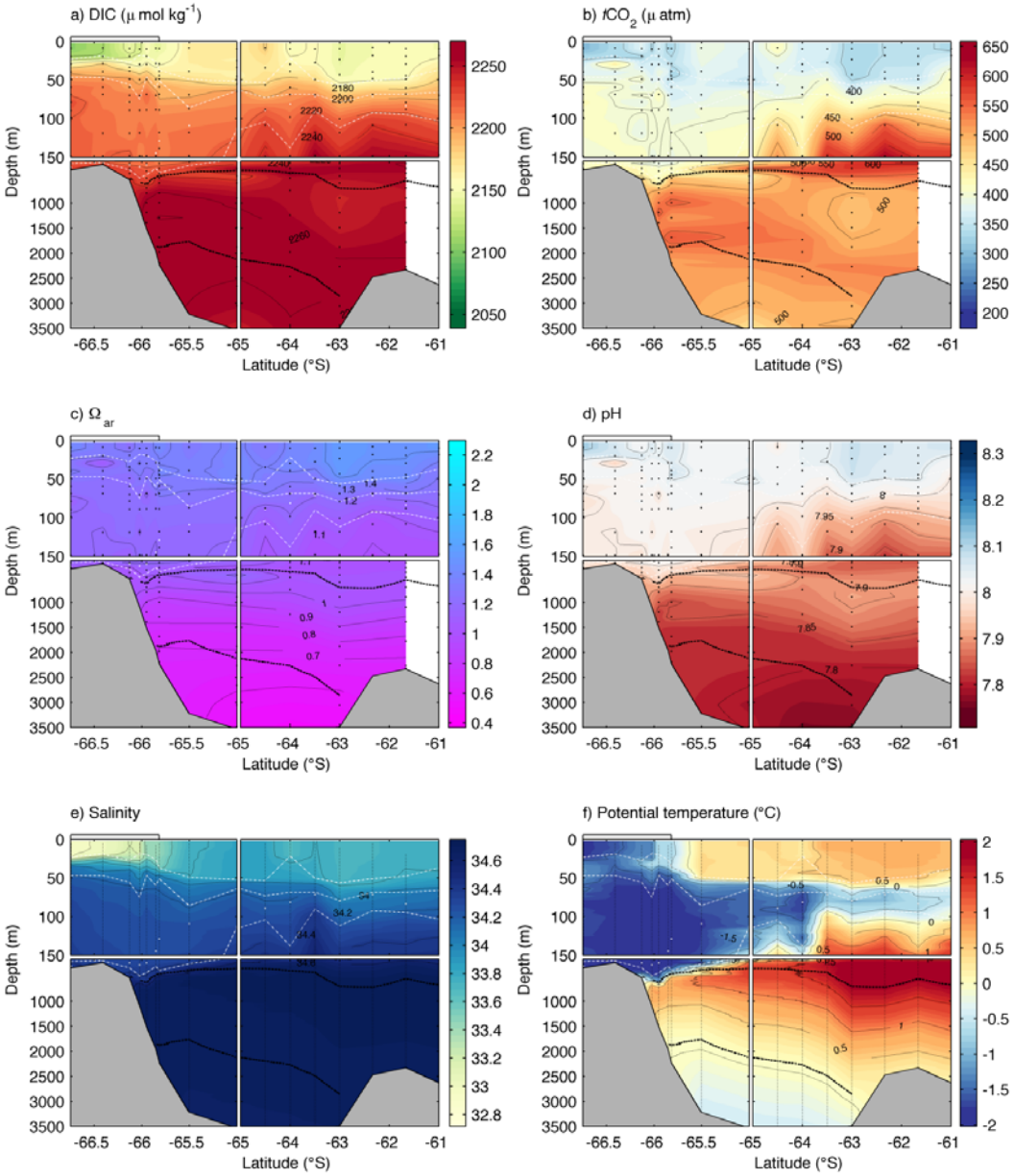

Figure 2.6 Leg 11, a) DIC (μmol kg^{-1}), b) fCO_2 (μatm), c) saturation state of aragonite (Ω_{ar}), d) pH_{sws}, e) salinity and f) potential temperature (°C).

as 198 m occur near the base of the T_{min} layer towards the northern ends of Legs 7 and 11 (Ω_{ar} = 0.94 and 0.99, respectively). The undersaturation coincides with stations that Williams et al. (2010) identified as locations of upwelling of relatively warm, O_2-depleted, nutrient- and carbon-rich mCDW/CDW into the surface layer (black dots on Figures 2.7, 2.8, 2.9 and 2.11b).

The distribution of biogeochemical properties in each of the deeper water masses showed little variation from east to west. Meijers et al. (2010) identified a decreasing temperature and salinity trend in sections from east to west, but no significant trends were observed in the CO_2 system properties for the same sections. The calculated mean fCO_2 of AABW varied between 500 ± 10 µatm (1 s.d.; n = 10) in Leg 9 to 481 ± 13 µatm (1 s.d.; n = 30) in Leg 1. The calculated AABW C_{ant} concentration was 25 ± 3 µmol kg^{-1} (1 s.d.; n = 127) across all sections (Figure 2.10). The water masses observed over the shelf (excluding AASW) were the most enriched in C_{ant}, with DSW being the highest at 53 ± 3 µmol kg^{-1} (1 s.d.; n = 3), although these shelf waters were only observed at the southern end of Leg 9.

2.3.2 Distribution of sea-air CO_2 flux and oxygen saturation

The measured underway sea-surface values of fCO_2 varied between 187 and 411 µatm with the lowest values observed over the Antarctic shelf and slope in Zone 1 (Table 2.3) and north of the SACCF. The higher values were observed over a broad region that encompassed the eastern limb of the Weddell Gyre in Zone 2 and in a narrow band stretching further to the east and to the north of the Antarctic Slope Front. These broad features are visible in the underway measurements of ΔfCO_2, whereby negative values imply surface water conditions that are undersaturated with respect to the atmosphere (Figure 2.7a). The sea-air $CO_{2\ flux}$ (Figure 2.7b) shows a similar pattern to that of ΔfCO_2. However, the sea-air flux estimates are determined by a combination of the magnitude and sign of ΔfCO_2, the strength of the winds and sea-ice cover in the area. This is apparent near Mawson station (67.6027°S, 62.8738°E) where fCO_2 undersaturated waters, minimal sea-ice cover, and strong wind speeds of up to 30 m s^{-1} resulted in a maximum flux estimate of -221 mmol C m^{-2} day^{-1}.

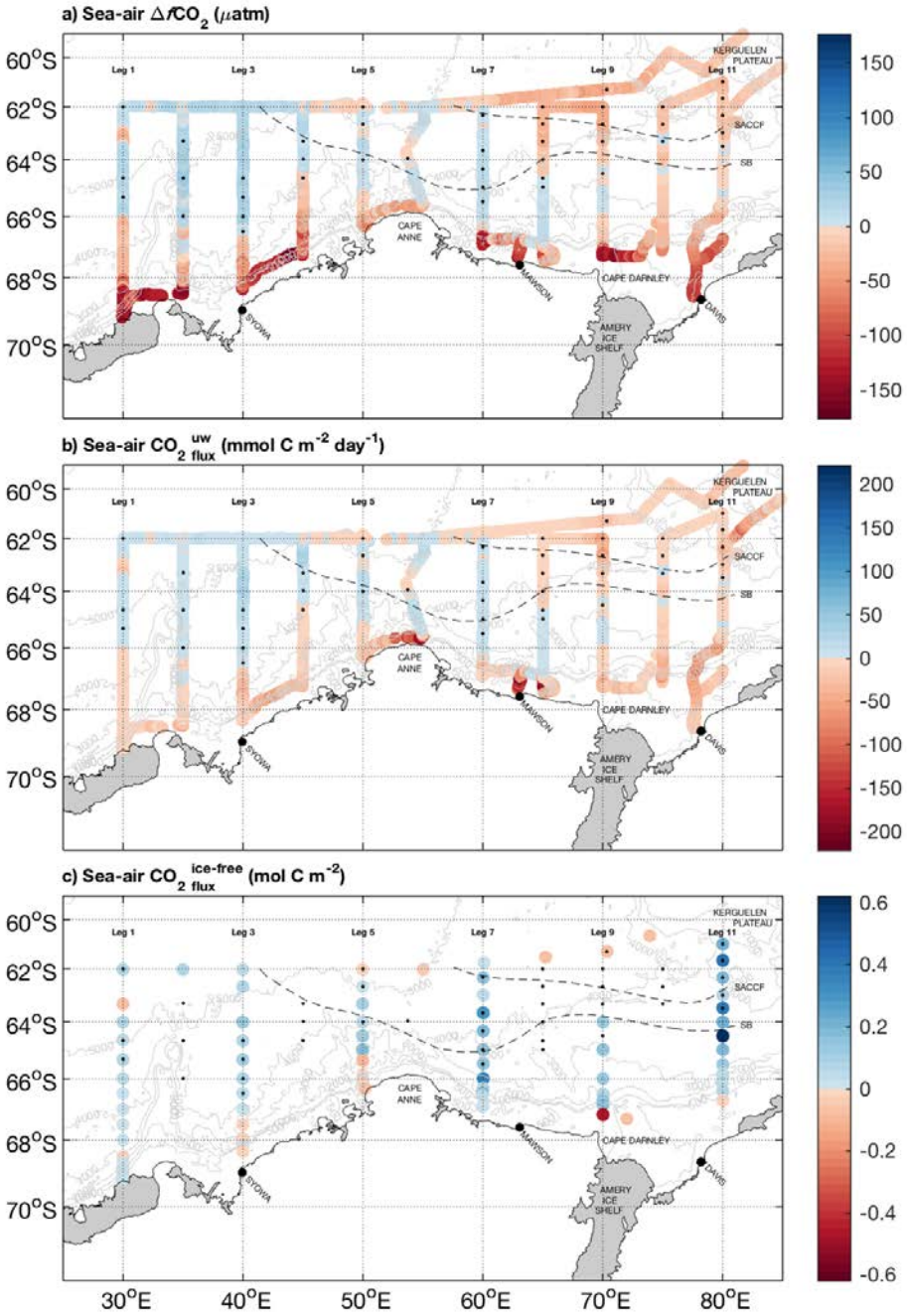

Figure 2.7 Underway surface measurements of, a) sea-air Δ*f*CO_2 (µatm), b) sea-air $\mathbf{CO_{2_{flux}}^{uw}}$ (mmol C m^{-2} day^{-1}) and c) sea-air $\mathbf{CO_{2_{flux}}^{ice-free}}$ (mol C m^{-2}) estimates calculated from daily average CCMP wind speeds during each ice-free day prior to the ship's arrival on station. Positive sea-air flux values imply a net transfer from the ocean to the atmosphere. The small black dots, on this and other similar plots, represent the locations of surface layer upwelling zones as determined by positive anomalies of potential temperature at 100 m (Williams et al., 2010).

The mean $CO_{2\,flux}^{uw}$ across the whole survey, based on the underway measurements, was -8 ± 21 mmol C m^{-2} day^{-1} (1 s.d.; n = 59375). In comparison, the sea-air $CO_{2\,flux}^{ice-free}$ (Figure 2.7c) estimated for the ice-free period prior to sampling, varied from -0.48 and 0.62 mol C m^{-2}. Although our measurements are not made over a full year, the $CO_{2\,flux}^{ice-free}$ units are given in mol C m^{-2} to allow a comparison in Section 2.4.1 with other yearly estimates of $CO_{2\,flux}$. The mean $CO_{2\,flux}^{ice-free}$ for the study area was 0.07 ± 0.13 mol C m^{-2} (1 s.d.; n = 85), indicating that the study area was a weak net source of CO_2 to atmosphere.

Table 2.3 Mean surface value properties (± 1 s.d.) in Zones 1 (continental shelf/slope), Zone 2 (offshore west of ~45°E) and Zone 3 (offshore east of ~45°E).

	Zone 1	**Zone 2**	**Zone 3**
Temperature (°C)	-0.69 ± 0.63	0.67 ± 0.80	0.62 ± 0.30
fCO_2 (µatm)	300 ± 50	365 ± 20	348 ± 14
Ice-free days	28 ± 31	23 ± 16	56 ± 19
$CO_{2\,flux}^{ice-free}$ (mol C m^{-2})	0.03 ± 0.13	0.04 ± 0.04	0.14 ± 0.16
$CO_{2\,flux}^{uw}$ (mmol C m^{-2} day^{-1})	-20 ± 28	3 ± 8	-6 ± 15
NCP_C (mol C m^{-2})	1.7 ± 1.2	0.8 ± 0.5	1.1 ± 0.6
NCP_N (mol C m^{-2})	2.1 ± 1.1	0.9 ± 0.6	0.9 ± 0.4
NCP_O (mmol C m^{-2} day^{-1})	5 ± 17	-1 ± 7	0 ± 10
F_e (mmol C m^{-2} day^{-1})	0.005 ± 0.005	0.006 ± 0.005	0.03 ± 0.02
F_v (mmol C m^{-2} day^{-1})	0.6 ± 0.1	0.44 ± 0.04	0.52 ± 0.07
ΔO_2^{total} (%)	3 ± 5	2 ± 2	2 ± 2
ΔO_2^{bio} (%)	2 ± 4	-1 ± 2	0 ± 1
ΔO_2^{phys} (%)	0 ± 3	1 ± 3	2 ± 2
C/N utilization ratio*	5.5 ± 2.3	5.9 ± 2.0	8.1 ± 3.1
C/Si utilization ratio*	2.5 ± 1.8	2.3 ± 1.2	1.5 ± 0.5
Si/N utilization ratio	3.0 ± 1.5	3.0 ± 1.1	5.7 ± 2.1

*Estimates corrected for sea-air CO_2 flux.

Surface water O_2 concentrations (ΔO_2^{total}) were supersaturated throughout most of the study area (Figure 2.8a). The greatest values of 22% supersaturation were observed over the shelf in the western part of the survey region. O_2 undersaturation was observed in small pockets on most transects, with the most significant regions of undersaturation observed in the MIZ on Leg 1 in the west, and a broad region of undersaturation just north of the shelf on Leg 8. The associated biological (ΔO_2^{bio}) and physical (ΔO_2^{phys}) changes from O_2/Ar data are shown in Figure 2.8b and Figure 2.8c. Eveleth et al. (2014) suggested using their Equation 5 to calculate ΔAr to assess the physical oxygen changes. Comparison with the method used in Equation 2.3 of this thesis, which assumes $[Ar]/[Ar]_{sat} = 1$ (Equation 2.12), shows the two methods agree

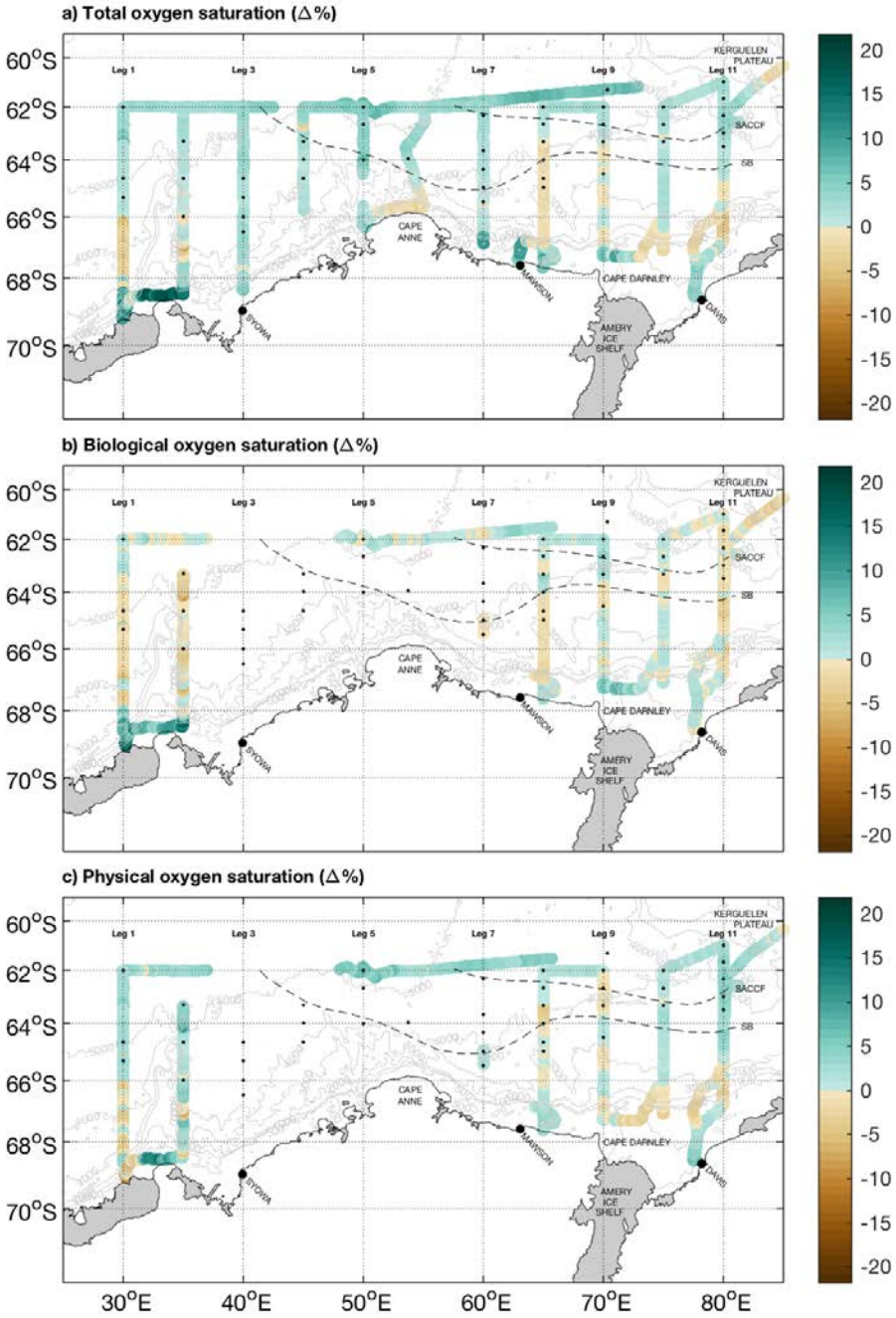

Figure 2.8 Distribution of, a) total change in surface oxygen saturation (Δ%), b) biological change in oxygen saturation (Δ%) and c) physical change in oxygen saturation (Δ%) from underway measurements.

within 0.17 ± 0.14% for the entire duration of the study and indicates the Ar concentration was close to saturation values. The greatest difference observed was 1% in the MIZ in the far south of Leg 1, perhaps due to cooling of ice-melt that can lower Ar concentrations.

The high values of biological undersaturation (Figure 2.8b) need not have been due to respiration in the SML and instead may reflect supply of low O_2 waters from below that can lead to measured values of O_2/Ar being less than the O_2/Ar ratio at saturation with the atmosphere (e.g. Cassar et al., 2014). This would lead to underestimates of biological productivity, as discussed later in Section 2.3.3, and therefore overestimate the contribution of ΔO_2^{phys} to the ΔO_2^{total} supersaturation observed throughout most of the study. However, $\Delta O_2^{phys}$was typically within ± 3% with small pockets of undersaturation approaching 10% in ice-covered waters at the southern end of Leg 1.

2.3.3 Net community production

Seasonally integrated estimates of NCP, throughout the ice-free period prior to sampling, from both carbon (NCP_C) and nitrate (NCP_N) (Pasquer et al., 2010) depletion profiles show distinct regions of biological productivity (Figures 2.9a and 2.9b). NCP estimates as high as 6.4 and 6.0 mol C m^{-2} for carbon and nitrate, respectively, were observed near the Japanese research station, Syowa (69.00°S, 39.35°E), and over the shelf near Cape Darnley, Prydz Bay (70°E). Although the Kerguelen Plateau and the Antarctic shelf and slope featured the highest rates of biological productivity, the majority of the survey area exhibited much lower values with a mean NCP_C of 1.3 ± 0.9 mol C m^{-2} (1 s.d.; n = 81) and NCP_N of 1.4 ± 0.9 mol C m^{-2} (1 s.d.; n = 108).

The daily estimates of NCP from the underway O_2/Ar system (NCP_O) showed more variability than the seasonally integrated estimates described above (Figure 2.9c). There was some agreement in terms of the shelf being more productive (maximum NCP_O of 62 mmol C m^{-2} day^{-1}), although the NCP_O estimates also revealed broad regions of negative NCP values. The lowest of these values (-46 mmol C m^{-2} day^{-1}) was observed in the northeast sector of the study region and coincided with a senescent phytoplankton bloom (K. Westwood, personal communication 2015) visible in Figure 2.2f as a modest concentration of chlorophyll-*a* averaged over the

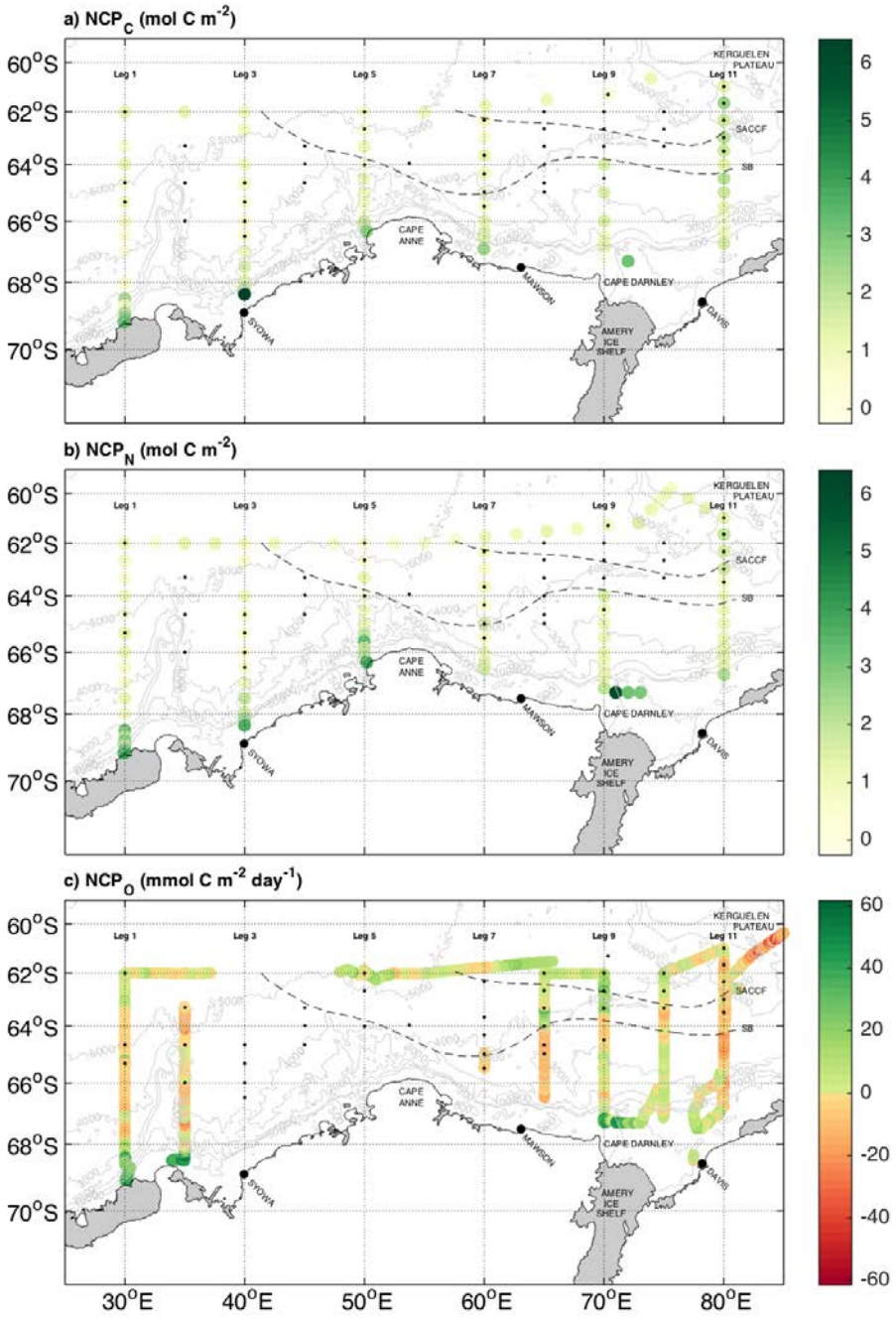

Figure 2.9 Net community production (NCP) estimates based on seasonally integrated a) carbon (mol C m^{-2}) and b) nitrate (mol C m^{-2}) deficits and c) underway O_2/Ar values (mmol C m^{-2} day^{-1}).

month of February. Whilst this may indicate a broad area of biological respiration (net heterotrophy), the upwelling of O_2 depleted water into the mixed layer could also influence these values, leading to underestimates of biological productivity in some areas and therefore incorrectly signal net heterotrophy in others. Other vertical processes, such as entrainment (F_e) and diffusion (F_v), have been accounted for in the O_2 mixed layer budget. The influence of entrainment was found, on average, to increase NCP_O estimates by ~1%. This was due to the general shoaling of the mixed layer depth during the winter to summer transition, which would result in no change to the O_2 mixed layer budget. The influence of diffusion however, was found to be more significant, with NCP_O estimates increasing by up to ~40% (Table 2.3).

2.4 Discussion

2.4.1 CO_2 uptake and storage

Biological activity over the shelf and slope during the summer resulted in surface fCO_2 values as much as 48% undersaturated with respect to the atmosphere, which produced uptake of CO_2 from the atmosphere in this region (Figures 2.7a and 2.7b). Underway measurements can bias net season flux estimates due to limited sampling in space and time. In order to assess the potential for bias, $CO_{2\,\mathrm{flux}}^{\mathrm{ice-free}}$ was also estimated for the period between sea-ice melt and when sampling occurred (Figure 2.7c). The pre-melt under ice conditions indicate most wintertime surface mixed-layer fCO_2 values were supersaturated with respect to the atmosphere (Figure 2.11a), consistent with other under-ice observations from within the study area and the Weddell Gyre (Bakker et al., 1997, 2008; Bellerby et al., 2004). These $CO_{2\,\mathrm{flux}}^{\mathrm{ice-free}}$ estimates suggest that the study area as a whole was a net source of CO_2 to the atmosphere, albeit with uncertain significance. This uncertainty relates to the assumptions associated with the onset and development of biological productivity, the 20% error associated with the gas transfer velocity (Wanninkhof, 2014) and the effectiveness of sea ice as a barrier to sea-air gas exchange (Loose et al., 2009).

Although the $CO_{2\,\mathrm{flux}}^{\mathrm{ice-free}}$ estimates suggested that the survey region was a net source of CO_2 to the atmosphere, areas of CO_2 uptake were observed, which was most enhanced over the shelf near Cape Darnley (-0.48 mol C m^{-2}). This is less than the uptake estimated for the Ross Sea by Arrigo et al. (2008) (-1.7 to -4.2 mol C m^{-2} $year^{-}$

[1]), but is comparable to the uptake of -0.5 mol C m^{-2} $year^{-1}$ measured at a nearby coastal location in Prydz Bay (Roden et al., 2013), and is of similar magnitude to the uptake measured in the west Antarctic Peninsula (Legge et al., 2015) and the Scotia Sea (Jones et al., 2015). Further offshore in Zone 2, both $CO_{2_{flux}}^{uw}$ and $CO_{2_{flux}}^{ice-free}$ estimates show that the eastern limb of the Weddell Gyre was a net CO_2 source to the atmosphere. This area had a recent retreat of sea ice (Table 2.3 and Figure 2.4) and the net source here may be more indicative of under-ice conditions, before biologically-induced reductions in fCO_2 could occur, as previously observed in this region (Bakker et al., 2008; Brown et al., 2015). The various controls of surface water biogeochemical dynamics in the study area will be discussed later in Section 2.4.2.

The high CO_2 uptake observed at the southern end of Leg 9 coincided with the highest concentrations of C_{ant}, which were observed in the underlying shelf waters (Table 2.2). The C_{ant} concentration of these shelf waters was similar to the TrOCA based C_{ant} value of 44 μmol kg^{-1} estimated by Shadwick et al. (2014) for DSW in the Mertz Polynya region of East Antarctica. Whilst DSW was only observed in one location in the BROKE-West study region, its presence is significant as it is a precursor for the formation of AABW, which originates in specific regions around Antarctica and sinks to abyssal depths due to varying combinations of brine rejection from sea-ice formation and ocean/ice-shelf interactions. In doing so, it contributes significantly to the global overturning circulation and sequesters heat and atmospheric gases to the deep ocean (Orsi et al., 1999; Johnson, 2008; Marshall & Speer, 2012). No areas of AABW production were identified during the summertime BROKE-West study (Williams et al., 2010). However, a significant site of AABW production was recently discovered in the Cape Darnley/Prydz Bay region near the southern end of Leg 9 (Ohshima et al., 2013; Williams et al., 2016). The westward flow of AABW that is observed high on the continental slope between Legs 5 and 7, as noted previously by Meijers et al. (2010), could therefore represent recently formed AABW from the Cape Darnley region that is moving downslope and deflected westward (Gill, 1973).

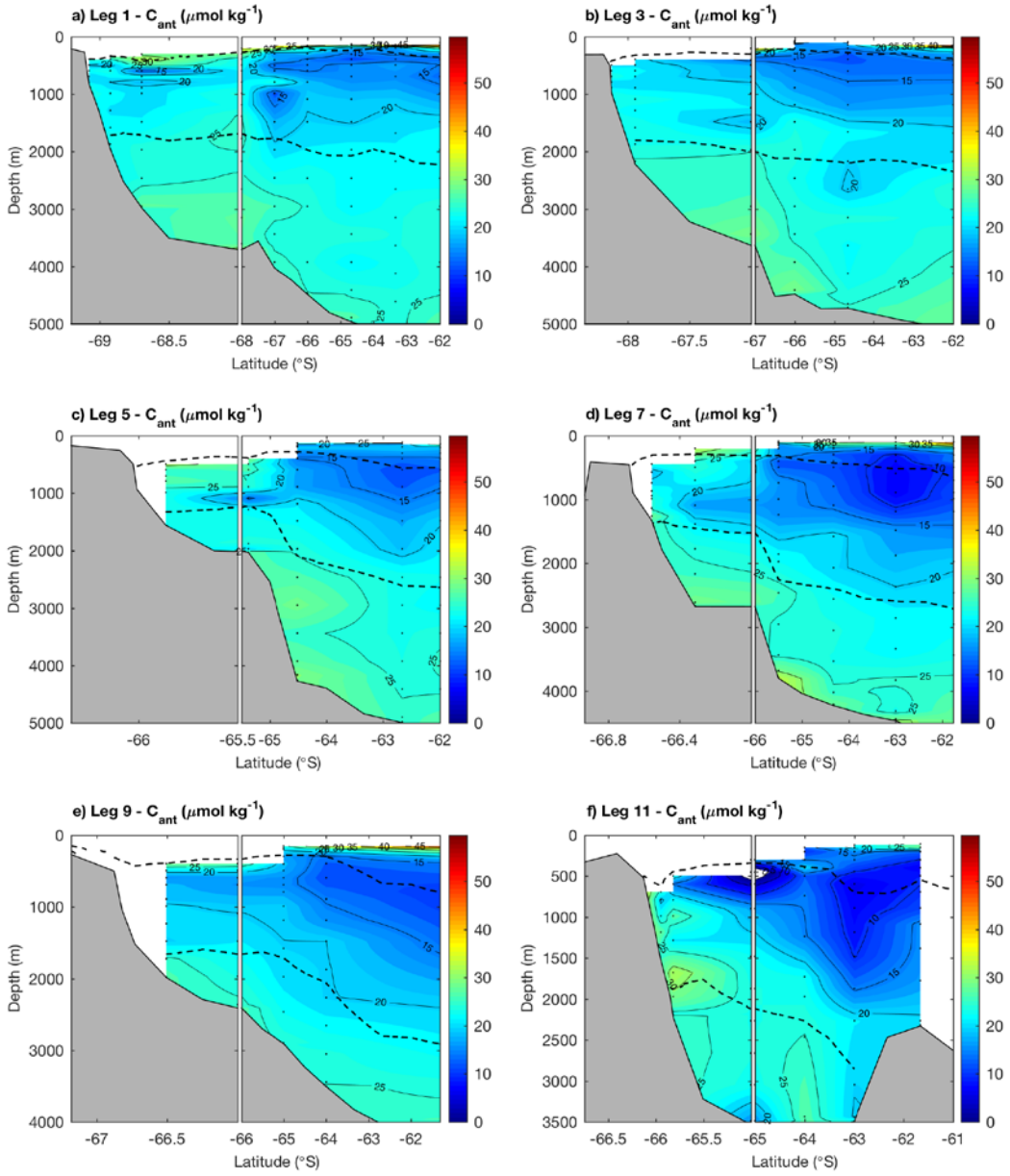

Figure 2.10 Anthropogenic carbon estimates (μmol kg^{-1}) for all sections, excluding surface water classified as AASW.

The higher temperature, salinity and fCO_2 and lower oxygen values of AABW to the east of Cape Darnley, relative to the west, indicates a greater elapsed time since formation and hence greater mixing with the warmer and more saline overlying mCDW and CDW (Meijers et al., 2010). Given the formation of AABW at Cape Darnley and its subsequent transport west, we might also expect to see higher C_{ant}

concentrations in the western CTD legs, although no significant trend in AABW C_{ant} concentration was observed. Furthermore, the high values of C_{ant} in AABW may in part reflect the tendency towards over-estimation of C_{ant} in deep waters by the TrOCA method (Pardo et al., 2014). Nonetheless, it is likely that high C_{ant} values observed in the shelf waters of the Cape Darnley region contribute anthropogenic CO_2 to AABW.

The complex role of high-latitude Southern Ocean waters in the global climate system makes its future response to projected climate forcing extremely difficult to model (Meijers, 2014). As such, predicting the future uptake and storage of CO_2 in the SIZ of East Antarctica is beyond the scope of this thesis. Particularly as change and variability in East Antarctic sea-ice seasonality comprises mixed signals on regional to local scales (Massom et al., 2013; Hobbs et al., 2016). In contrast, the west Antarctic Peninsula has experienced a rapid reduction in sea-ice cover in recent years (Stammerjohn et al., 2008; Li et al., 2014), although as yet, no significant long-term trends in carbonate system parameters have been detected as a result (Hauri et al., 2015). Sea ice can influence sea-air CO_2 exchange by acting as a physical barrier to sea-air gas exchange itself (Semiletov et al., 2004; Zemmelink et al., 2006; Miller et al., 2011; Nomura et al., 2013) and by controlling mixed layer development and the subsequent availability of light and nutrients (Venables et al., 2013). This was observed by Geibert et al. (2010) in the eastern boundary of the Weddell Gyre who found that the cumulative melting of both sea ice and icebergs provided a steady source of iron that sustained biological productivity and therefore influenced the sea-air gradient in CO_2.

The present synergy between winter sea-ice cover and summer biological productivity, particularly over the shelf, acts to reduce the flux of CO_2 from deep waters to the atmosphere in the BROKE-West study region. This seasonal synergy has been previously described in Arctic waters as a rectification process (i.e. one that emphasizes uptake by biological processes in summer and minimizes outgassing by physical processes in winter) (Yager et al., 1995). To examine how this seasonal ice cover might influence the uptake of CO_2 by the surface waters in the BROKE-West region, we compared the *n*DIC concentration measured in the T_{min} layer by Ishii et al. (1998) during the austral summer of 1992/1993 with values measured in this study. Values from the T_{min} layer are used as a reference level and to minimize the potential to bias the results due to the seasonal drawdown of carbon in spring and summer.

Using a Revelle factor (Revelle & Suess, 1957) of 16.4 and an atmospheric growth rate in fCO_2 of ~1.9 µatm yr^{-1}, the expected increase in DIC of surface waters in the region would be 0.66 µmol kg^{-1} $year^{-1}$, or 8.52 µmol kg^{-1} from 1993 to 2006. Our average *n*DIC concentration from the T_{min} layer for the entire survey area was 2206 ± 8 µmol kg^{-1} (1 s.d.; n = 87) compared to the 1992/1993 value of 2197 ± 4 µmol kg^{-1} (1 s.d.; n = 14), which represents an increase in DIC of 9 µmol kg^{-1}. Variations in biological productivity or increased upwelling during this time could also be responsible for the increase in *n*DIC, however a comparison of the mean *n*N values between our study and 1992/1993 showed no significant change ($nN_{1992/1993}$ = 28.7 ± 0.7 µmol kg^{-1} (1 s.d.; n = 14); nN_{2006} = 29.5 ± 1 µmol kg^{-1} (1 s.d.; n = 108)), which suggests that surface waters in the SIZ of the BROKE-West region are tracking the atmospheric increase in fCO_2. A similar trend was observed by van Heuven et al. (2014) in the western Weddell Sea, suggesting that sea-ice cover in these locations, does not constitute a major impediment for sea-air CO_2 equilibration on annual time scales.

2.4.2 Surface water biogeochemical cycling

Concurrent measurements of dissolved O_2 and carbon parameters can help constrain understanding of controls on surface ocean carbon dynamics (Bender et al., 2000; Álvarez et al., 2002). For example, a detection of fCO_2 undersaturation and O_2 supersaturation, with respect to the atmosphere, would imply photosynthesis as a controlling mechanism, whereas fCO_2 supersaturation and O_2 undersaturation would indicate a source of net respiration or mixing with deeper waters below the SML. Carrillo et al. (2004) utilised this approach in the west Antarctic Peninsula by segregating measurements of O_2 and fCO_2 into one of four classifications. This was done based on the saturation state of each gas relative to the atmosphere, which allowed each classification to represent changes in gas concentration that were dominated by either physical or biological processes.

The incorporation of NCP values from underway O_2/Ar measurements provides further insights into the processes influencing the O_2 and fCO_2 distributions (Figure 2.11a). Each classification, or quadrant, partitions the underway-surface observations into changes driven predominantly by 1) photosynthesis, 2) warming, 3) net respiration/deep mixing and 4) cooling, with the highest NCP_O values being

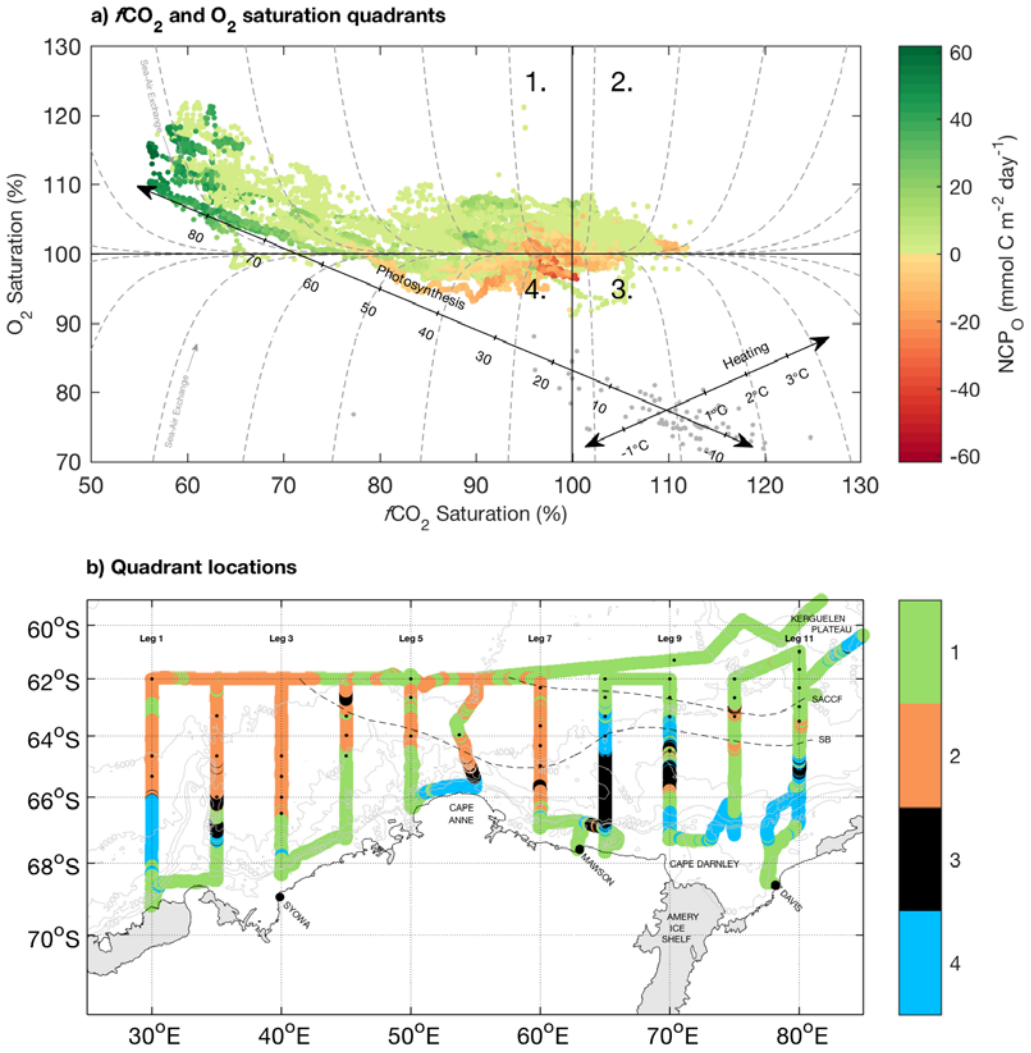

Figure 2.11 a) Percentage saturation of fCO_2 versus the percentage saturation of O_2, coloured with underway surface estimates of NCP (mmol C m^{-2} day^{-1}) from O_2/Ar ratios. Vertical and horizontal lines represent 100% saturation of fCO_2 and O_2. Based on these relationships the figure is separated into quadrants, whereby each quadrant represents changes dominated by 1) photosynthesis, 2) warming, 3) respiration or upwelling and 4) cooling. The process vectors centred on the mean wintertime saturation state for each gas (grey dots; taken from the T_{min} layer) represent the production of O_2 and consumption of CO_2 at a theoretical photosynthetic quotient of -0.7 with overlaid NCP (mmol C m^{-2} day^{-1}) values based on an average MLD and ice-free day period of 40 m and 37 days, respectively. The second process vector represents changes in saturation caused by 1°C of warming/cooling ($\Delta O_{2\ sat}$ = 2.64% $°C^{-1}$ and $\Delta fCO_{2\ sat}$ = 4.23% $°C^{-1}$). The dashed lines represent the O_2 and fCO_2 saturation values based on a model of sea-air exchange (see Carrillo et al. (2004)). b) Shows the spatial distribution of the quadrants.

associated with photosynthesis. Deviations from these theoretical relationships, illustrated by the process vectors in Figure 2.11a, may result from the different sea-air exchange rates for O_2 and fCO_2 (see model of sea-air exchange in Figure 2.11a) with timescales that range from days to weeks for O_2 and months for fCO_2 (Broecker & Peng, 1982), or from the formation and dissolution of calcium carbonate (Dieckmann

et al., 2008). Plotting the spatial distribution of each data point based on its quadrant classification (Figure 2.11b) reveals distinct regions where these biological and physical processes appear to dominate.

Two processes in particular, warming and photosynthesis, can explain much of the observed variability in O_2 and fCO_2 saturation during the BROKE-West study, accounting for 31% and 49% of the observed values, respectively. Those waters that were dominated by surface warming, resulting in decreased gas solubility, are associated with the relatively warmer waters of the Weddell Gyre in the northwest sector of the study area (Figures 2.2h and 2.2i), which agrees with the findings of Nomura et al. (2014) who found a similar temperature control on surface fCO_2 values in this region. The variability driven by photosynthesis occurs over the shelf and slope with a second region observed offshore, north of the SACCF.

Regions where photosynthesis appears to be the dominant mode of O_2 and fCO_2 variability, i.e. quadrant 1, also show elevated satellite chlorophyll-*a* concentrations, which often indicate intense phytoplankton blooms, particularly near the sea-ice edge and within Prydz Bay (Figures 2.2e and 2.2f). Surface data associated with quadrant 3, which only accounted for 5% of the observations, may indicate areas of localised upwelling or net respiration from biological activity. For example, the broad quadrant 3 classification observed in Leg 8 correlates well with both the biological O_2 undersaturation observed in Figure 2.8b and the positive 100 m temperature anomalies, indicative of upwelling, at two of the xCTD stations (Williams et al., 2010). Data associated with quadrant 4 (cooling) accounts for 15% of the observations and correlates well with areas of marginal sea ice (Figures 2.2b and 2.2c), which suggests that an increase in gas solubility driven by cold sea-ice melt water may cause the observed variability in these areas.

The distribution of surface water biogeochemical properties show distinct regional characteristics, which generally agree with the zones outlined by Schwarz et al. (2010). Table 2.3 summarises the mean values of selected parameters based on this classification scheme. However, when NCP is considered over seasonally integrated time-scales (Figures 2.9a and 2.9b), only two distinct regions are apparent. These observations reveal that the majority of the study area experienced relatively low

biological productivity at the time of sampling, with the exception of waters over the continental shelf and moderate productivity near the Kerguelen Plateau.

Although iron was not directly measured during the study, there are various lines of evidence to suggest that biological activity was limited by its supply to the surface mixed layer. These include phytoplankton species composition and chlorophyll degradation products measured by Wright et al. (2010) and the utilization ratios of macronutrients (Table 2.3), whose individual concentrations were never below limiting levels (Westwood et al., 2010). Wright et al. (2010) further postulated that grazing on the phytoplankton bloom and export of faecal pellets stripped the upper water column of iron, creating a southward migrating iron gradient that followed the retreat of the melting sea ice, thus limiting phytoplankton growth in the upper water column. Our seasonally integrated estimates of NCP do not resolve this pattern of biological activity, however our results suggest that the supply of iron over the shelf, through a variety of mechanisms, may have been sufficient to sustain high levels of biological activity throughout most of the summer period.

2.5 Conclusion

In this study of the biogeochemical dynamics in the seasonal sea-ice zone of East Antarctica, distinct regions of biological activity and sea-air CO_2 flux were found. Estimates of the CO_2 flux since the retreat of sea ice prior to the survey suggest that the entire study area is a weak net source of CO_2 to the atmosphere. Waters over the shelf and north of the SACCF, were generally sites of oceanic CO_2 uptake. This uptake, particularly over the shelf/slope, was driven by strong biological productivity as observed in NCP estimates that were as high as 6.4 mol C m^{-2}. Although micronutrients were not measured, it is likely that this strong biological productivity was sustained through its supply. The largest CO_2 uptake was observed near Cape Darnley and the magnitude of the CO_2 sink is commensurate with other coastal and shelf based estimates of CO_2 uptake, both in East Antarctica and along the west Antarctic Peninsula. Further offshore, in the western sector of the study area, the warmer waters of the Weddell Gyre dominated surface water biogeochemical dynamics, reducing gas solubility and causing a broad region of CO_2 outgassing.

Wintertime under-ice estimates of fCO_2 indicate that the majority of the surface waters in the BROKE-West study region were supersaturated with respect to the atmosphere. The seasonal synergy between winter sea-ice cover and biological productivity during the summer however, act to reduce the flux of CO_2 to the atmosphere, highlighting the important role that sea ice plays in the biogeochemical dynamics of the region. Because the observed changes to the East Antarctic sea ice are complex and are comprised of mixed signals on regional to local scales, making predictions about the future CO_2 source/sink nature of the SIZ is difficult. This is highlighted by the large variability in the drivers and timing of carbon cycling dynamics in this region. As such, the future CO_2 uptake or outgassing in the study area will most likely depend on the response of the solubility and biological pumps to: 1) changes in sea-ice seasonality and 2) the enhanced ventilation of carbon- and nutrient-rich deep water driven by strengthening winds over the Southern Ocean.

Acknowledgments

NR was supported by an Australian Postgraduate Award and a CSIRO Oceans and Atmosphere scholarship. The collection and analyses of samples for this chapter were supported by the Antarctic Climate and Ecosystem Co-operative Research Centre, the Australian Climate Change Research Program, and the Australian Scientific Assessment Committee Project 1302, awarded to BT. The authors would like to thank Kristina Paterson, Ty Hibberd, Mark Pretty and Kate Berry for carbon sampling and analysis as well as the officers and crew aboard the *RV Aurora Australis* for their professionalism and efforts. Professors Michael Bender and Nicolas Cassar, who helped establish O_2/Ar measurements on the ship, provided O_2/Ar ratio measurements on discrete samples used to calibrate the MIMS. The authors would also like to thank Doctor Elizabeth Jones and one anonymous reviewer for their thoughtful comments.
Data availability: Underway carbon data are available from the Surface Ocean CO_2 Atlas at http://www.socat.info. CTD data are available from the Australian Antarctic Data Centre at http://data.aad.gov.au/aadc/metadata/metadata_redirect.cfm?md=/AMD/AU/BROKE-West_CTD_au0603. Data from the Princess Elizabeth Trough and WOCE SR3 transect available from the GLODAPv2 database at: http://cdiac.ornl.gov/oceans/GLODAPv2. MODIS-Aqua data obtained from the NASA Goddard Space Flight Center, Ocean Ecology Laboratory, Ocean Processing

Group http://oceandata.sci.gsfc.nasa.gov/MODIS-Aqua/Mapped/Monthly/9km. NCEP-DOE Reanalysis 2 data provided by the NOAA/OAR/ESRL PSD available from: http://www.esrl.noaa.gov/psd/data/gridded/data.ncep.reanalysis2.html.

Appendix A: Underway measurements

Surface measurements of fCO_2 were made every minute, by pumping seawater from the ship's intake located approximately 8 meters below sea level. A non-dispersive infrared gas analyzer (LI-COR, LI-6252) was used to measure the CO_2 mole fraction (XCO_2), which was calibrated every 6 hours with a set of four standard gases: CO_2-free air, and three concentrations of CO_2-in-air (298.80, 337.17 and 372.05 ppm). The gas standards were provided by the Commonwealth Scientific and Industrial Research Organisation (CSIRO), Melbourne, Australia and were calibrated on the World Meteorological Organisation WMO-X95 mole fraction scale. Atmospheric XCO_2 (dry) was measured after the standards by pumping clean outside air from an intake on the ship's forward mast. The equilibrator temperature measurements were made with a platinum resistance thermometer calibrated to an accuracy of 0.01°C at a National Association of Testing Authorities laboratory at CSIRO, Hobart. Sea surface salinity was measured using a Sea-Bird SBE 45 thermosalinograph along with sea surface temperature, which was measured from a remote temperature sensor (SBE 38 thermistor: accuracy ± 0.003°C) located near the ship's underway seawater intake. The XCO_2 data were corrected to in-situ water temperature and 100% humidity by using the equations of Weiss (1974) and Copin-Montegut (1988).

The accuracy and precision of the underway fCO_2 measurements are better than ± 2 μatm based on field comparisons (Körtzinger et al., 2000) and crossover analyses using the SOCAT database (Bakker et al., 2014). The accuracy of the measurements was also checked with the mean atmospheric XCO_2 concentration measured during the study of 376.96 ± 0.29 ppm (1 s.d.; n = 849) in good agreement with the mean XCO_2 value from the NOAA ESRL Carbon Cycle Cooperative Global Air Sampling Network (Dlugokencky et al., 2015) of 377.48 ± 0.29 ppm, which is an averaged and smoothed product for the same time and region.

Measurements of underway surface oxygen concentration ($[O_2]$) were made using an oxygen optode (Aanderaa, model 4835, serial number: 241) that was calibrated against discrete concurrent measurements of oxygen concentration using modified Winkler titrations (Culberson et al., 1991). The optode calibration coefficients were calculated using a linear regression of sea surface temperature and the observed offset in oxygen concentration ($\Delta[O_2]_{winkler-optode}$) ($y$ = (-1.8 ± 0.3)x + (19.8 ± 0.4); n = 50,

$r^2 = 0.38$, standard error = 2 μmol kg^{-1}). The oxygen concentration at saturation ($[O_2]_{sat}$) was determined from atmospheric pressure, seawater temperature and salinity measurements (García & Gordon, 1992; 1993).

Appendix B: Dissociation constants

The performance of the various dissociation constants used to calculate carbonate system parameters were examined by comparing measured fCO_2 values, from the ship's underway intake, with the mean calculated fCO_2 values from discrete concurrent measurements of DIC, TA and nutrients (Table 2.4). The dissociation constants generally over-predicted fCO_2 values in the study area, with the dissociation constants of Cai and Wang (1998), Roy et al. (1993]) and Mehrbach et al. (1973) refit by Dickson and Millero (1987), providing the best agreement with measured values. Although the constants of Cai and Wang (1998), on average, produced the smallest difference between calculated and measured fCO_2 values, the difference between these three dissociation constants was statistically insignificant. For this study, we used the dissociation constants of Roy et al. (1993) to calculate carbonate system parameters for consistency with previous studies from within the SIZ of the Southern Ocean (Bates et al., 1998; Gibson & Trull, 1999; Sweeney et al., 2000; Roden et al., 2013) and due to the low temperatures that the constants were determined at.

Table 2.4 The mean difference between calculated and measured fCO_2 ($\Delta fCO_{2\ (calc - meas)}$) using different dissociation constants of carbonic acid, determined in a range of temperature, salinity and seawater types.

Dissociation Constants	**Temp Range (°C)**	**Salinity Range**	**Seawater Type**	**Mean $\Delta fCO_{2\ (calc - meas)}$ (µatm) (1 s.d.; n = 75)**
Roy et al. (1993)	0-45	5-45	Artificial seawater	9 ± 13
Goyet & Poisson (1989)	-1-40	10-50	Artificial seawater	10 ± 13
Hansson (1973) refit by Dickson & Millero (1987)	2-35	20-40	Artificial seawater	33 ± 13
Hansson (1973), Mehrbach et al. (1973) refit by Dickson & Millero (1987)	2-35	20-40	Artificial seawater	9 ± 12
Hansson and Mehrbach refit by Dickson & Millero (1987)	2-35	20-40	Artificial seawater	16 ± 13
GEOSECS (Mehrbach et al., 1973)	2-35	19-43	Seawater	23 ± 12
Peng et al. (1987)	2-35	19-43	Seawater	36 ± 13
Cai & Wang (1998)	2-35	0-49	Seawater and artificial seawater	6 ± 12
Lueker et al. (2000)	2-35	19-43	Seawater	12 ± 12
Mojica Prieto & Millero (2002)	0-45	5-42	Seawater	18 ± 13
Millero et al. (2002)	-1.6-35	34-37	Field measurements	14 ± 12
Millero et al. (2006)	0-50	1-50	Seawater	17 ± 12
Millero (2010)	0-50	1-50	Seawater	19 ± 12

Appendix C: Salinity normalization

Nitrate and DIC data (X) were normalized (*n*X) to a mean salinity of 34.208 (the mean salinity in the T_{min} layer), to account for changes in concentrations due to the effects of ice melt and formation. The normalization assumes that as sea ice forms, the brines that originate from salt rejection increase TA, DIC, nutrients and salinity in proportion to each other. Therefore, if the brines exchange with the underlying seawater, the normalized values will not change. Processes that could cause a net change in nitrate or DIC compared to salinity within the brines and potentially influence the normalized values in the underlying water include precipitation of the hydrated $CaCO_3$ mineral, ikaite (Dieckmann et al., 2008), sea-air gas exchange, and biological production/respiration.

$$n\mathrm{X} = \mathrm{X} \cdot \frac{34.208}{\mathrm{Salinity}} \qquad \textbf{Equation 2.4}$$

Appendix D: Net community production

Values of NCP were obtained for each CTD profile by linearly interpolating *n*DIC values between each bottle, based on 2-metre depth intervals (*dz*), and then calculating seasonal carbon deficits using the following equation (Rubin et al., 1998):

$$\mathrm{NCP_C} = \int_0^{z^*} ([nDIC]_{winter} - [nDIC]_{summer})\, dz + \mathrm{CO_2}_{flux}^{ice-free} \quad \textbf{Equation 2.5}$$

where $[nDIC]_{winter}$ indicates the concentration of *n*DIC in the T_{min} layer, which is assumed to broadly reflect the preceding wintertime conditions (Le Corre & Minas, 1983; Jennings et al., 1984), and $[nDIC]_{summer}$ represents the summertime concentration of *n*DIC, integrated to the depth of the T_{min} layer (z^*). Assuming that sea ice forms an effective barrier to sea-air gas exchange, the calculated seasonal deficit value was then corrected for sea-air CO_2 exchange by the addition of $\mathrm{CO_2}_{flux}^{ice-free}$ values for the ice-free period prior to sampling.

Estimates of NCP derived from nitrate concentrations were calculated using a similar approach, however the correction for sea-air CO_2 exchange was not required. Nitrate values were converted to carbon by using the Redfield carbon/nitrate ratio of 6.625 (Redfield et al., 1963).

$$\mathrm{NCP_N} = \int_0^{z^*} ([nN]_{winter} - [nN]_{summer})\, dz \cdot 6.625 \quad \textbf{Equation 2.6}$$

A third method of estimating NCP was utilized from continuous underway shipboard measurements of oxygen/argon (O_2/Ar) ratios conducted every 2 minutes by membrane inlet mass spectrometry (MIMS) (Kaiser et al., 2005). NCP was calculated using the equation:

$$\mathrm{NCP_O} \approx k_{O_2} \cdot [O_2]_{sat} \cdot \Delta(O_2/Ar) \quad \textbf{Equation 2.7}$$

where k_{O_2} is the gas exchange velocity of oxygen, computed using the daily average CCMP winds (Atlas et al., 2011) and the formulation of Wanninkhof et al. (2013). The gas exchange velocity was weighted using the method of Reuer et al. (2007) to

account for wind speed history at the collection site using the climatological mixed layer depths (MLD) of Kara et al. (2003). To correct for the difference between climatological and observed MLDs, 15 m were added to the climatological values. O_2/Ar ratio measurements were calibrated with discrete water samples taken from the same seawater outlet as used for the MIMS. $\Delta(O_2/Ar)$ is defined as the biological oxygen supersaturation (e.g. Cassar et al., 2011) calculated using the vertical flux correction of Castro-Morales et al. (2013):

$$\Delta(O_2/Ar) = \left[\frac{([O_2] + F_e + F_v)/[Ar]}{([O_2]/[Ar])_{sat}} - 1\right] \quad \textbf{Equation 2.8}$$

Where F_e (entrainment flux), describes the change of the mixed layer O_2 inventory during mixed layer deepening and F_v is the change in the O_2 mixed layer inventory due to diapycnal eddy diffusion across the base of the mixed layer, calculated using the following equations:

$$F_e = -\frac{1}{2}\frac{(\Delta z_{mix})^2}{\Delta t}\frac{\partial c(O_2)}{\partial z}\bigg|_{oxy} \quad \textbf{Equation 2.9}$$

$$F_v = -K_z\frac{\partial c(O_2)}{\partial z}\bigg|_{oxy} \quad \textbf{Equation 2.10}$$

The Δz_{mix} term in Equation 2.9, is the thickness of the entrained water column for each of the 30 days (Δt) prior to sampling, estimated from the MLD climatology of Kara et al. (2003). The $\partial c(O_2)/\partial z|_{oxy}$ term in both Equations 2.9 and 2.10 is the concentration gradient in the oxycline, estimated by the difference between measured [O_2] in the mixed layer and the mean [O_2] in the T_{min} layer. The value of the eddy diffusivity coefficient (K_z) in Equation 2.10 is 1.0 x 10-5 m^2 s^{-1} (Howard et al., 2004). Estimates of NCP_O were then divided by 1.4 to allow expression in terms of organic carbon production, (or DIC uptake) (Laws, 1991; Bender et al., 1999).

Appendix E: Partitioning of oxygen saturation

The total change in oxygen saturation was calculated using the following equation:

$$\Delta O_2^{\text{total}} = [O_2] - [O_2]_{\text{sat}} \quad \textbf{Equation 2.11}$$

The biological contribution to changes in oxygen saturation was then calculated as follows:

$$\Delta O_2^{\text{bio}} = \frac{[\text{Ar}]}{[\text{Ar}]_{\text{sat}}} \cdot [O_2]_{\text{sat}} \cdot \Delta(O_2/\text{Ar}) \quad \textbf{Equation 2.12}$$

where $[Ar]/[Ar]_{sat}$ is assumed to equal one (Cassar et al., 2011).

Appendix F: Additional sections

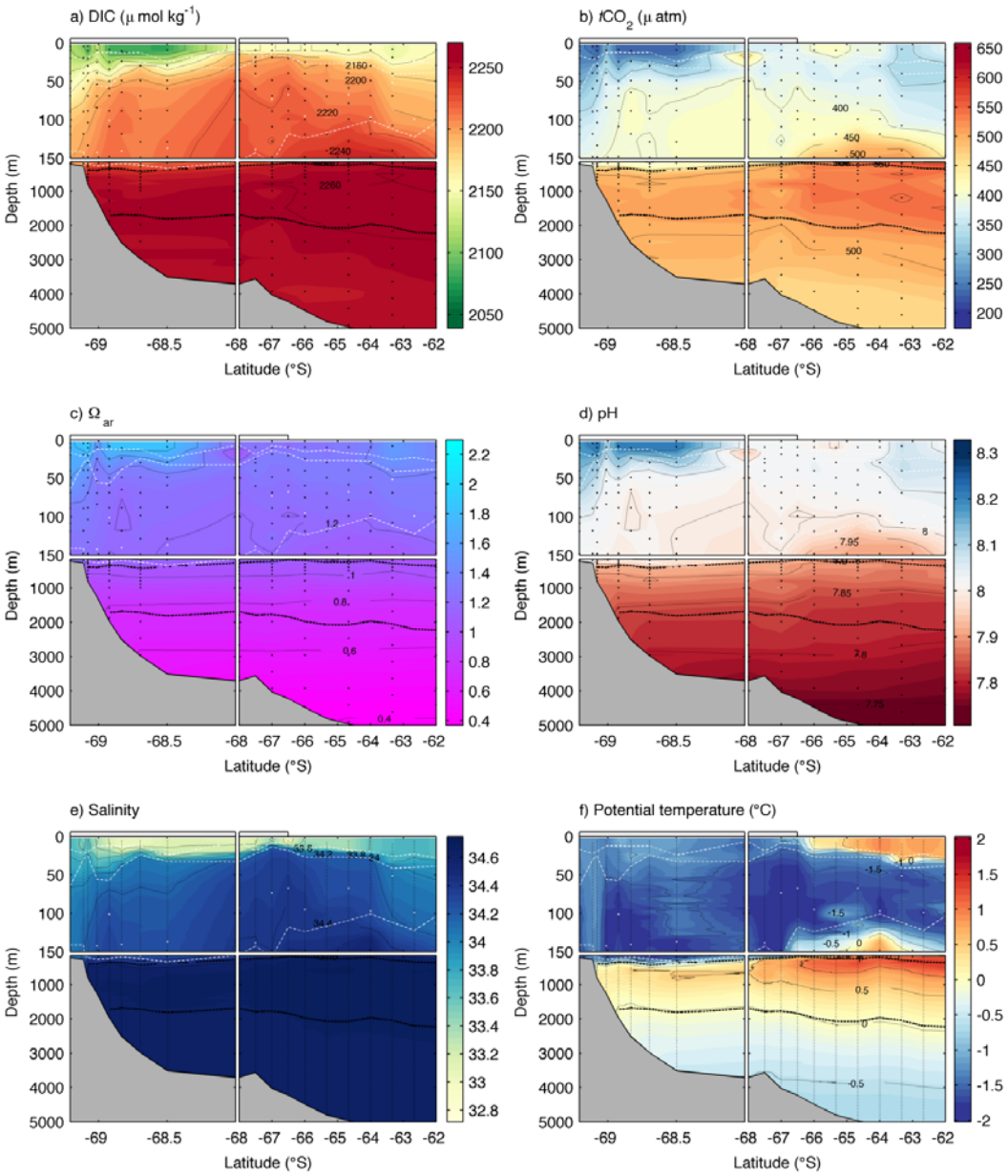

Figure 2.12 Leg 1 at 40°E, a) DIC (μmol kg^{-1}), b) fCO_2 (μatm), c) saturation state of aragonite (Ω_{ar}), and d) pH_{sws}, e) salinity and f) potential temperature (°C). The black dashed lines, on this and other similar plots, represent the 28.03 kg m^{-3} (upper) and the 28.27 kg m^{-3} (lower) neutral density surfaces that partly delineate major water masses in the study region. The black dots show the bottle and CTD locations. The white dots show the location of the T_{min} value and the white lines show the base of the seasonal mixed layer (upper), seasonal pycnocline (middle) and T_{min} layer (lower). The marginal ice zone is indicated by a white rectangle at the surface towards the southern end of each leg. Scale changes are indicated by the breaks in the axis.

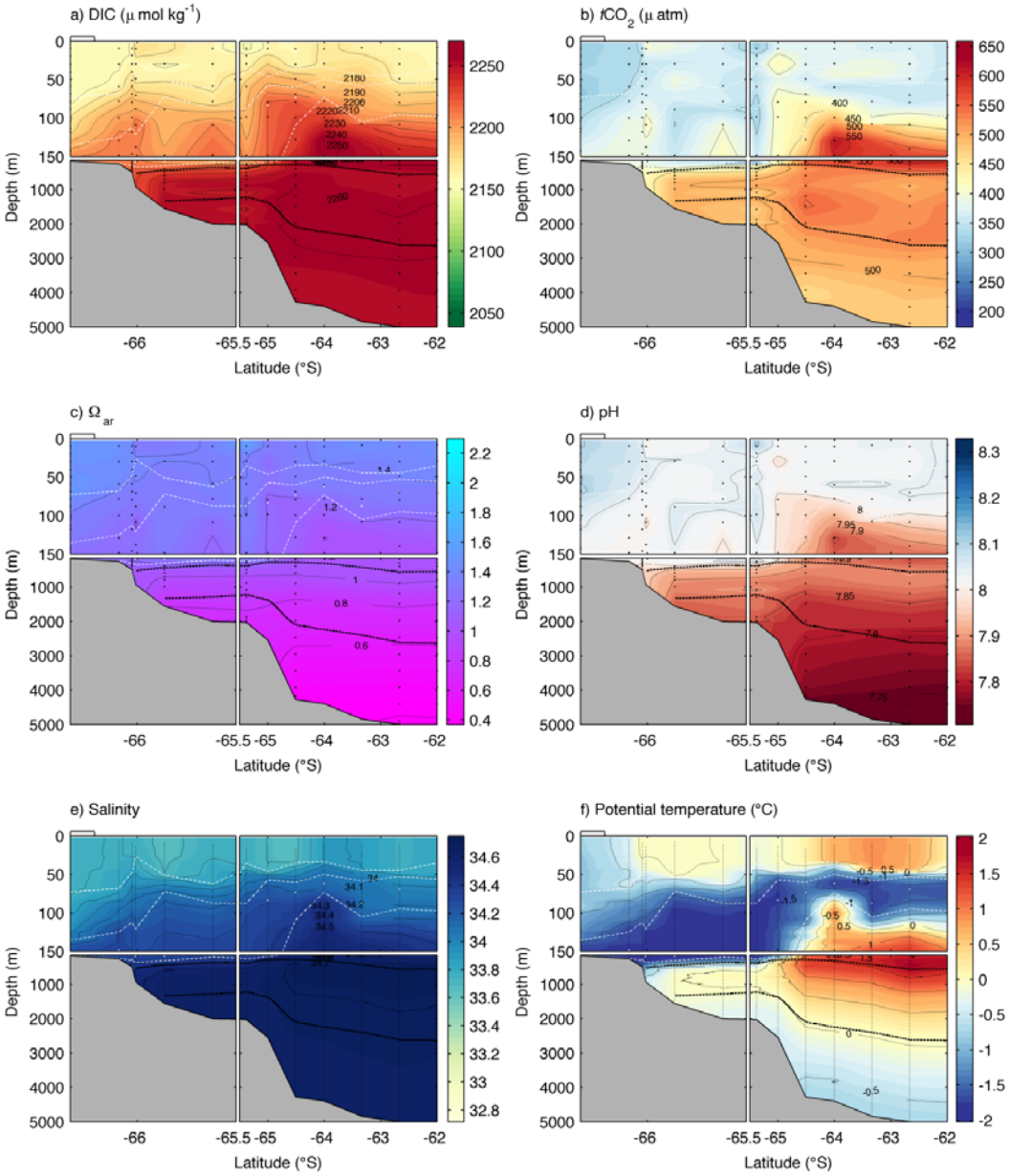

Figure 2.13 Leg 5, a) DIC (µmol kg^{-1}), b) fCO_2 (µatm), c) saturation state of aragonite (Ω_{ar}), d) pH_{sws}, e) salinity and f) potential temperature (°C).

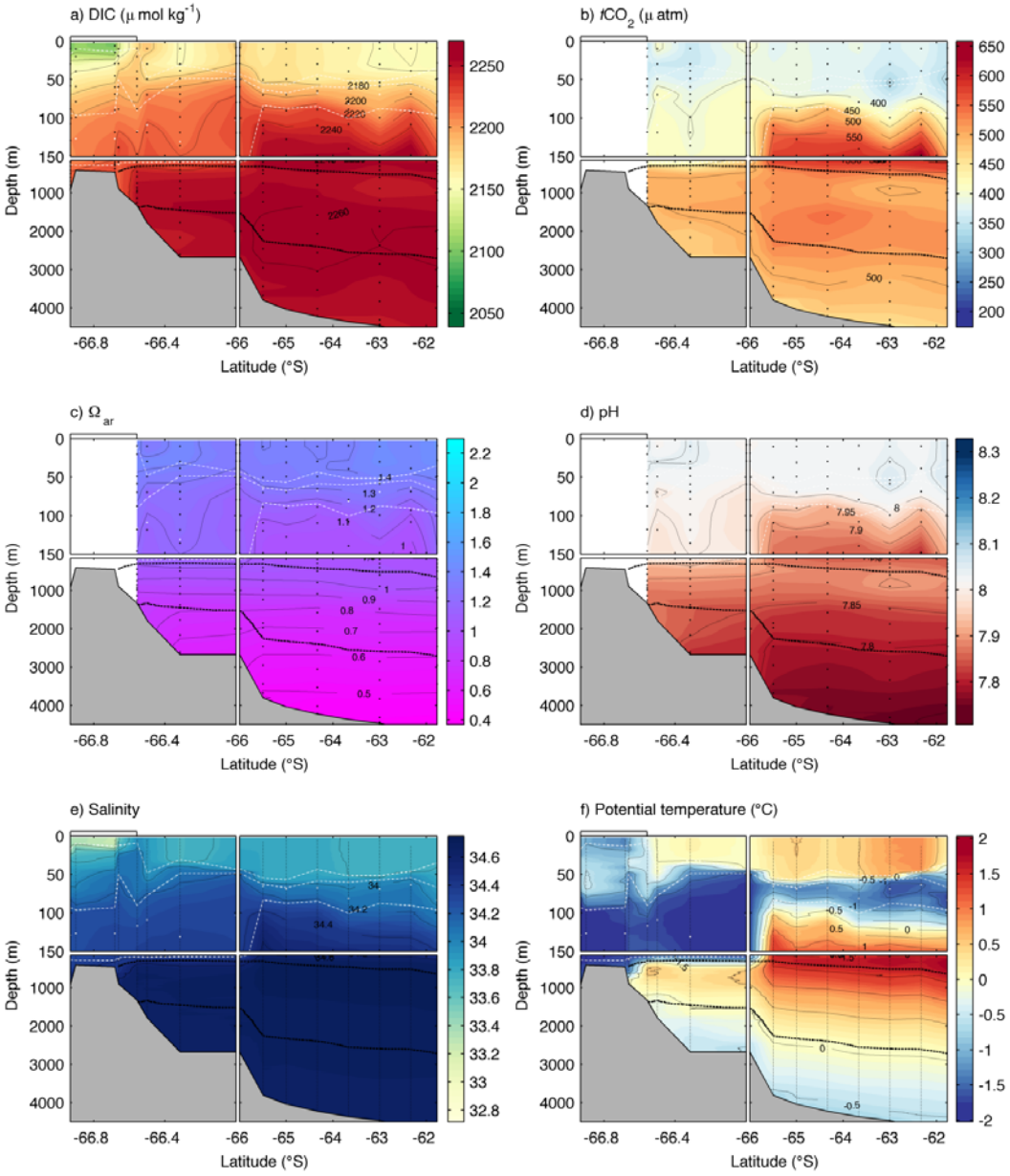

Figure 2.14 Leg 7, a) DIC (µmol kg^{-1}), b) fCO_2 (µatm), c) saturation state of aragonite (Ω_{ar}), d) pH_{sws}, e) salinity and f) potential temperature (°C).

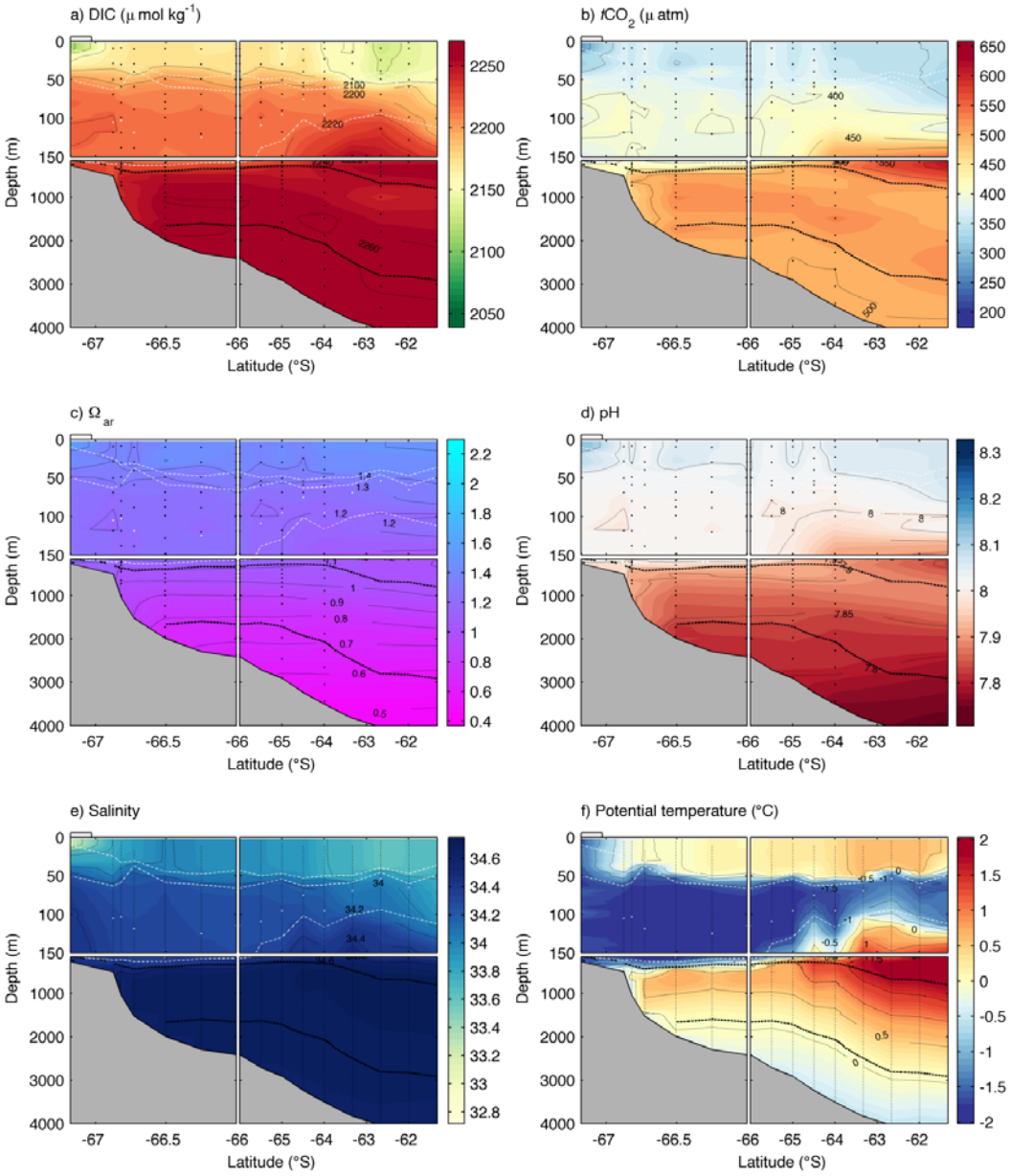

Figure 2.15 Leg 9, a) DIC (µmol kg^{-1}), b) fCO_2 (µatm), c) saturation state of aragonite (Ω_{ar}), d) pH_{sws}, e) salinity and f) potential temperature (°C).

3 Annual cycle of carbonate chemistry and decadal change in coastal Prydz Bay, East Antarctica

All of the research contained within this chapter has been published as:

Roden, N.P., Shadwick, E.H., Tilbrook, B. & Trull, T.W., 2013. Annual cycle of carbonate chemistry and decadal change in coastal Prydz Bay, East Antarctica. *Marine Chemistry*, 155, pp.135–147.

Note: The published CO_2 flux term in this chapter is defined as air-to-sea (rather than sea-to-air) and therefore positive CO_2 flux values indicate oceanic uptake rather than outgassing.

Abstract

The annual cycles of dissolved carbon dioxide (CO_2) system parameters were determined for a coastal site in East Antarctica using samples collected from May 2010 to February 2011 in Prydz Bay. These observations show the seasonal influence of ice formation and melt, biological production, and air-sea CO_2 flux on changes in total dissolved inorganic carbon (DIC), pH_{sws} and the saturation state of aragonite (Ω_{ar}). Net community production of 1.8 ± 0.4 mol C m^{-2} in the productive summer months (November-February) caused large seasonal decreases in DIC. The decrease in DIC caused a change in surface water partial pressure of CO_2 from values over-saturated with respect to the atmosphere in the ice-covered winter period, to undersaturated waters in the summer months. The study site was estimated to be an annual net sink for CO_2 of 0.54 ± 0.11 mol C m^{-2} $year^{-1}$. The calculated pH_{sws} and Ω_{ar} values varied seasonally from 7.99 to 8.20 and 1.19 to 1.92, respectively. The observed variability was compared to similar measurements carried out in 1993-95 at the same location. Natural variability in carbon cycle dynamics caused changes in pH_{sws} that were nearly twice as large as those expected from changes estimated due to the uptake of CO_2 from the atmosphere over this time, assuming that the surface waters tracked increases in atmospheric CO_2. This highlights the difficulties associated with predicting trends in seawater pH and dissolved CO_2 system parameters in dynamic, high latitude, coastal locations with sparse temporal and spatial carbon cycle observations.

3.1 Introduction

The oceanic uptake of anthropogenic carbon dioxide (CO_2) from the atmosphere lowers the pH and the dissolved carbonate ion (CO_3^{2-}) concentration of seawater (Orr et al., 2005; Feely et al., 2004), causing ocean acidification. A consequence of declining CO_3^{2-} concentration is a reduction in the saturation state (Ω) of calcium carbonate ($CaCO_3$), a mineral used in the production of shells and skeletal material of many marine organisms. Laboratory experiments indicate that many marine organisms react adversely to decreases in CO_3^{2-} concentrations and Ω that will occur under future atmospheric CO_2 scenarios (Raven et al., 2005).

The Southern Ocean is considered particularly sensitive to changes in carbonate chemistry, due primarily to its low buffer capacity (Sabine et al., 2004). This region is predicted to be one of the first regions to experience widespread undersaturation of aragonite ($\Omega_{ar} < 1$) (McNeil & Matear, 2008), a major biogenic form of $CaCO_3$ in high-latitude Southern Ocean waters (Honjo, 2004; Hunt et al., 2008; Post et al., 2010; Bednaršek et al., 2012). The role of the coastal ocean in the carbon cycle however, is poorly constrained, particularly in seasonally ice-covered regions (Bates, 2006). Difficulty in understanding the carbon cycle in high-latitude coastal environments stems from a lack of field measurements, particularly in winter, and from strong spatial gradients in carbonate chemistry that occur on many continental shelves (Sweeney et al., 2000; Semiletov et al., 2007; Gao et al., 2008; Takahashi et al., 2009; Shadwick et al., 2011). Furthermore, natural variability may accelerate or dampen changes in the carbonate chemistry associated with ocean acidification (Feely et al., 2008; Borges & Gypens, 2010). Future change in the carbonate chemistry is also likely to be complicated by climate related physical and biological feedbacks in the carbon cycle associated with the loss of sea ice, increased stratification (Smith & Nelson, 1986) and intensification of winds (Borges et al., 2008; Arrigo, G. L. van Dijken, et al., 2008).

The ecological significance of the Antarctic shelf and the disproportionately large fraction of Southern Ocean productivity it supports (Arrigo et al. 1998, 2008) underpins the importance of understanding the exposure of organisms to changing carbonate chemistry. This chapter presents observations on the annual cycle of the inorganic carbon system at a coastal site in Prydz Bay, East Antarctica. Measurements

of physical parameters, as well as the total dissolved inorganic carbon (DIC), total alkalinity (TA) and nutrient concentrations of the seawater were made over a ten-month period in 2010 and 2011. The results show the seasonal influence of sea ice, net community production and air-sea CO_2 flux on the inorganic carbon system at a high-latitude, seasonally ice-covered, coastal location. These data are compared with seasonal observations made at the same site in 1993-95 (Gibson & Trull, 1999), allowing an assessment of decadal change in carbonate chemistry in the seasonal sea-ice zone of East Antarctica.

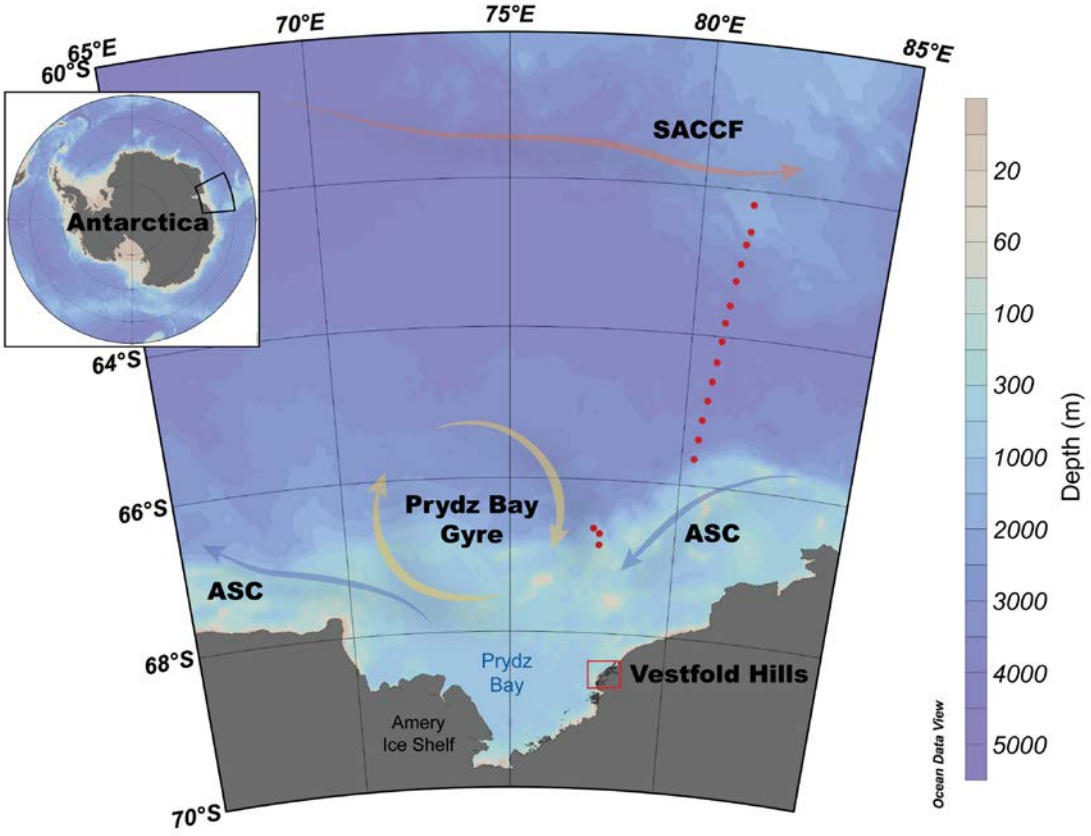

Figure 3.1. Prydz Bay is located in the Indian Ocean sector of East Antarctica. Shown on the map are the approximate frontal location of the Southern Antarctic Circumpolar Current Front (SACCF), the Antarctic Slope Current (ASC) and the Prydz Bay Gyre, derived from the analysis of Smith et al. (1984), Middleton & Humphries, (1989), Nunes Vaz & Lennon, (1996) and Heywood et al. (1999). The red box shows the location of the study site. The red dots show the location of the offshore profiles (Princess Elizabeth Trough, 2005; http://cdiac.ornl.gov/oceans/glodap).

3.2 Data and methods

3.2.1 Oceanographic setting

Prydz Bay is the third largest embayment in the Antarctic continent, and lies in the Indian Ocean sector of East Antarctica (Figure 3.1). The circulation in Prydz Bay is dominated by a large cyclonic gyre, extending from within the Bay to the Antarctic Divergence at about 63°S (Smith et al., 1984; Middleton & Humphries, 1989; Nunes Vaz & Lennon, 1996; Williams et al., 2010). A westward flow along the shelf, that is part of the wind-driven Antarctic slope current (ASC), supplies water to Prydz Bay. A second deeper inflow also occurs across the shelf break. This water is a mixture of recirculated bay waters and warmer upwelled circumpolar deep water (CDW). The main discharge from Prydz Bay occurs via a coastal current to the west.

The three principal water masses on the shelf are Ice Shelf Water, formed by seawater contact at depth with the Amery Ice Shelf, Low Salinity Shelf Water (LSSW) and High Salinity Shelf Water (HSSW). The HSSW and LSSW are typically separated at a salinity of 34.6 (Nunes Vaz & Lennon, 1996). During the relatively ice-free spring/summer periods, HSSW is modified by ice melt and solar warming to form Antarctic Surface Water (ASW) (Nunes Vaz & Lennon, 1996). A complex suite of physical and biological factors drives considerable inter-annual variations in both phytoplankton biomass and speciation in the inshore waters of the region that can influence the dissolved carbon system (Gibson et al., 1997). High levels of biological activity in the region appear to be initiated by sea-ice algae growth in mid-October (Gibson et al., 1999). Dramatic increases in biological production occur in early- to mid-December (Perrin et al., 1987; Davidson & Marchant, 1992; Robinson et al., 1999; Gibson & Trull, 1999) with peak production occurring from December to February, followed by a decline in March when sea ice forms and daylight hours diminish.

3.2.2 Sampling and analytical procedure

Total dissolved inorganic carbon, total alkalinity and nutrient samples were collected every two weeks from May 2010 until February 2011 using a 1.7-L Niskin bottle from three sites offshore from Davis station in the Vestfold Hills, East Antarctica (Figure 3.2, Tables 3.1 and 3.4). Sea-ice formation prevented sampling in March and April. Samples were collected approximately 2 m from the bottom of the water

column at each of the three sites from depths of 20, 30 and 75 m. This chapter will focus on observations made at Site 1, which is the same location as the 1993-95 study. Additional observations from Sites 2 and 3 are used to establish a salinity and TA relationship for the region.

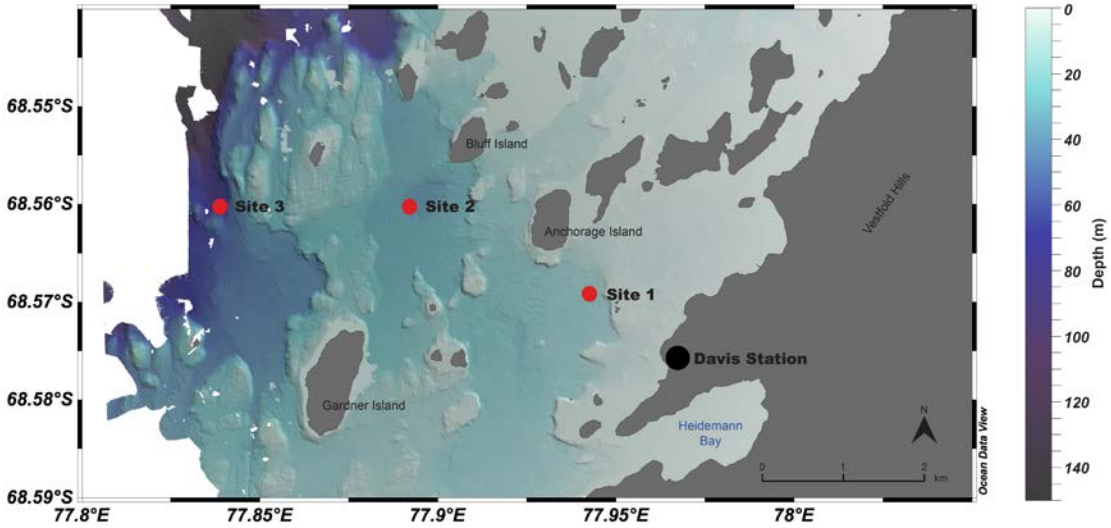

Figure 3.2. The location of the three study sites offshore from the Australian Antarctic research station, Davis, located in the Vestfold Hills of East Antarctica. Bathymetry data courtesy of Geoscience Australia.

Seawater temperature values were measured with a WTW 315i handheld conductivity and temperature meter (accuracy ± 0.5 °C) inserted into the top of the Niskin bottle immediately after retrieval. Samples of 250-mL each for DIC and TA analysis were then drawn from the Niskin bottle, and 100-µL of saturated $HgCl_2$ solution was added to each sample within an hour of sampling to halt biological activity. These samples were tightly sealed in 250-mL Kimax (DIC) and 250-mL Schott Duran (TA) screw cap glass bottles and stored in the dark at ~20 °C for 6-12 months and returned to CSIRO, Australia, for analysis. Tests carried out over a year indicate that the samples can be preserved and stored in excess of 12 months without changing the DIC or TA values by more than the analytical precision of ± 2 µmol kg^{-1} for both parameters (B. Tilbrook, personal communication).

Table 3.1. Location and depth of study sites.

Site	Location		Sampling/water depth
1	68˚34.20 S	77˚56.40 E	20 m
2	68˚33.63 S	77˚53.41 E	30 m
3	68˚33.65 S	77˚50.29 E	75 m

The total DIC in a sample of seawater is defined as (Dickson et al., 2007):

$$\mathrm{DIC} = [\mathrm{CO}_2^*] + [\mathrm{HCO}_3^-] + [\mathrm{CO}_3^{2-}] \qquad \textbf{Equation 3.1}$$

where the square brackets indicate the concentration of the dissolved species. Samples of DIC were analyzed using a Single Operator Multiparameter Metabolic Analyzer following the procedure in Dickson et al. (2007). The TA is defined as the number of moles of hydrogen ion equivalent to the excess of proton acceptors over proton donors in 1 kg of sample (Dickson et al., 2007) and was determined by open-cell potentiometric titration using a 0.1 M hydrochloric acid titrant (Dickson et al., 2007) that had been calibrated by coulometric titration (Dickson & Afghan, 2003). Routine analyses of Certified Reference Material from Scripps Institution of Oceanography were used to verify if the measurement accuracy and precision for DIC and TA analyses were better than ± 2 μmol kg^{-1}. Salinity was measured on the DIC samples using a Seabird SBE4 conductivity sensor with an accuracy of ± 0.05. Analysis of duplicate DIC and TA samples showed ranges of 4 μmol kg^{-1} and 8 μmol kg^{-1}, respectively. Duplicate samples of DIC and TA from the open ocean, that have been stored for similar periods of time as the Prydz Bay samples, typically agree to better than 2 μmol kg^{-1}. The greater difference in the Prydz Bay duplicate samples appears to be related to the difficulties in sampling at near freezing conditions and is small relative to the seasonal variability described below.

Nutrient samples were collected in 15-mL polypropylene tubes and stored in the dark at -20˚C for 10-18 months before analysis at CSIRO, Australia. Samples collected before 2 November 2010 were accidentally defrosted for a 12-day period and refrozen before analyses could be carried out. The inadvertent freeze thaw cycle that the nutrient samples were exposed to may have compromised some of the nutrient samples and will be discussed further in Section 3.3.4. Nutrient concentrations of nitrate + nitrite ($NO_3^- + NO_2^-$) (hereafter nitrate), phosphate (HPO_4^{2-}) and silicic acid

(H_4SiO_4) were determined using standard colorimetric methods (Hansen & Koroleff, 2007), adapted for flow injection analysis on a 5-channel LACHAT Quik-Chem 8000 autoanalyzer. Measurement accuracy for nitrate, phosphate and silicic acid was ± 0.3 μmol kg^{-1}, ± 0.02 μmol kg^{-1} and ± 0.6 μmol kg^{-1} respectively (V. Latham, personal communication). The analysis of duplicate samples affected by the freeze thaw cycle showed ranges of 0.5 μmol kg^{-1}, 0.06 μmol kg^{-1} and 5.7 μmol kg^{-1} respectively, whilst samples that were not affected, showed ranges of 0.3 μmol kg^{-1}, 0.09 μmol kg^{-1} and 1.3 μmol kg^{-1} respectively.

Nutrient, DIC and TA data (X) were normalized (*n*X) to a mean winter salinity (1994 and 2010 combined) of 34.32, to account for changes in concentrations due to the effects of ice melt and formation:

$$n\mathrm{X} = \mathrm{X} \cdot \frac{34.32}{\mathrm{Salinity}} \qquad \textbf{Equation 3.2}$$

The normalization assumes that as sea ice forms, brines that originate from salt rejection increase TA, DIC, nutrients and salinity in proportion to each other. If the brine exchanges with the underlying seawater, the normalized values will not change, irrespective of the ice thickness. Processes that could cause a net change in nutrients, DIC or TA compared to salinity within the brines and potentially influence the normalized values in the underlying water include precipitation of the $CaCO_3$ mineral, ikaite (Dieckmann et al., 2008), air-sea gas exchange, and biological production/respiration.

Delille et al. (2007) attempted to quantify the importance of these processes in Antarctic sea ice. They found that $CaCO_3$ precipitation could account for some variability in TA, although most brine had a constant normalized value similar to the underlying water. Ikaite concentrations in Antarctic ice have typical values of 5 mg L^{-1} of sea ice (Dieckmann et al., 2008). The formation of this much $CaCO_3$ precipitate would cause about a 100 μmol change in TA per liter of ice. If all the brine drains from an average ice thickness of 1 m and mixes into the underlying 20 m deep water column, the net affect will be about a 5 μmol L^{-1} or 4.9 μmol kg^{-1} decrease in the average water column *n*TA, and a 2.4 μmol kg^{-1} decrease for *n*DIC. The near zero intercept for the TA+N versus salinity regression, described below, indicates that

$CaCO_3$ precipitation does not alter the *n*TA values in the seawater underlying the ice to levels greater than the measurement accuracy.

Biological drawdown of DIC and nutrients within the sea-ice brines in spring, as noted by Delille et al. (2007), may cause a decoupling of these parameters with salinity, relative to DIC and nutrient concentrations in the underlying water column. As the ice warms and the brine within the sea ice drains, the signal detected in the underlying water could therefore be a combination of biological activity in the ice or in the water column. Thus the calculated net community production and changes in DIC, discussed later, would still be correct, though would not distinguish between contributions from the sea ice versus the water column.

The saturation state of aragonite (Ω_{ar}), the partial pressure of CO_2 (pCO_2) and pH on the seawater scale (pH_{sws}) were calculated from DIC, TA and nutrient data for both 1993-95 (Gibson & Trull, 1999) and 2010-11 using the standard set of carbonate system equations with the CO2SYS program (van Heuven et al., 2011). The Ω_{ar} is defined as the product of the concentrations of Ca^{2+} and CO_3^{2-} divided by the solubility product for aragonite ($K'_{sp_{ar}}$) (Mucci, 1983). The concentration of Ca^{2+} is estimated from the salinity, and the CO_3^{2-} concentration is calculated from the DIC and TA data:

$$\Omega_{ar} = [Ca^{2+}][CO_3^{2-}]/[K'_{sp_{ar}}] \qquad \textbf{Equation 3.3}$$

The appropriate use of equilibrium constants for different parameter combinations has been widely discussed in the literature (e.g. Johnson et al., 1999; Wanninkhof et al., 1999; Chierici & Fransson, 2009). At water temperatures observed in this study (<0°C), Wanninkhof et al. (1999) and Bates (2006) showed there is only a small difference in calculated carbonate parameters (e.g. pCO_2 < 5 μatm) when different equilibrium constants are used (i.e., Mehrbach et al., 1973 refit by Dickson & Millero, 1987; Goyet & Poisson, 1989; Roy et al., 1993). Furthermore, the equilibrium constants of Goyet & Poisson (1989) and Roy et al. (1993) may be more suitable for polar waters as their determination of dissociation constants was performed at lower temperatures (-1°C or 0°C). For consistency with previous studies from the Antarctic shelf (Bates et al., 1998; Sweeney et al., 2000) we used the equilibrium constants of Roy et al. (1993).

Gibson & Trull (1999) used measured pH at 25°C, DIC and nutrient values to calculate carbonate system parameters. Some pH measurements from their 1993-95 study showed large variations compared to coulometric DIC measurements, which resulted in unrealistic variations in calculated carbonate parameters. Their pH measurements required the samples to be warmed from near freezing temperatures to 25°C for spectrophotometric measurement, during which time some sample alteration may have occurred, and they were unable to determine the accuracy of the pH measurements against seawater standards. We consider the best comparison of carbonate system parameters between this study and that of Gibson & Trull (1999) to be with the directly measured concentrations of DIC, nutrients and salinity. The DIC, nutrient and salinity measurements were made in both studies using the same techniques applied to stored samples returned to Australia for analysis. In order to compare changes between 1994 and 2010, we calculated carbonate system parameters from the measured DIC concentrations and values of TA measured for this study, with TA estimated for Gibson & Trull from a linear regression of salinity, TA and nitrate (TA+N) data (Figure 3.3; $y = (68 \pm 1)x + (7 \pm 21)$, n = 280, $r^2 = 0.98$, standard error = 4 μmol kg^{-1}). The data used to calculate the TA+N/salinity relationship were from measurements made in 2010-11 (this study), and from samples shallower than 500 m that were measured for shelf and offshore waters south of 62°S on CO_2/WOCE hydrographic sections of the nearby Princess Elizabeth Trough in 2005 and at the southern end of the WOCE SR3 transect at 140°E measured in 1994 (http://cdiac.ornl.gov/oceans/glodap). Salinity values from the 1993-95 Gibson & Trull study were used to calculate TA+N values and measured nitrate concentrations were subtracted to estimate the TA for their samples.

3.2.3 Sea-ice thickness measurements

Sea-ice thickness measurements were made near all three sampling sites throughout the study period (P. Heil, personal communication). To determine if changes in salinity at Site 1 were driven by local sea-ice formation, the observed changes in ice thickness were compared to modelled changes in ice thickness based on a salt budget integrated over the 20 m water column at Site 1 (Charrassin et al., 2008). The model utilized mean fast-ice salinity concentrations measured in the region (Worby et al., 1998). The salinity and density of the sea ice was assumed to be 5.3 and 920 kg m^{-3},

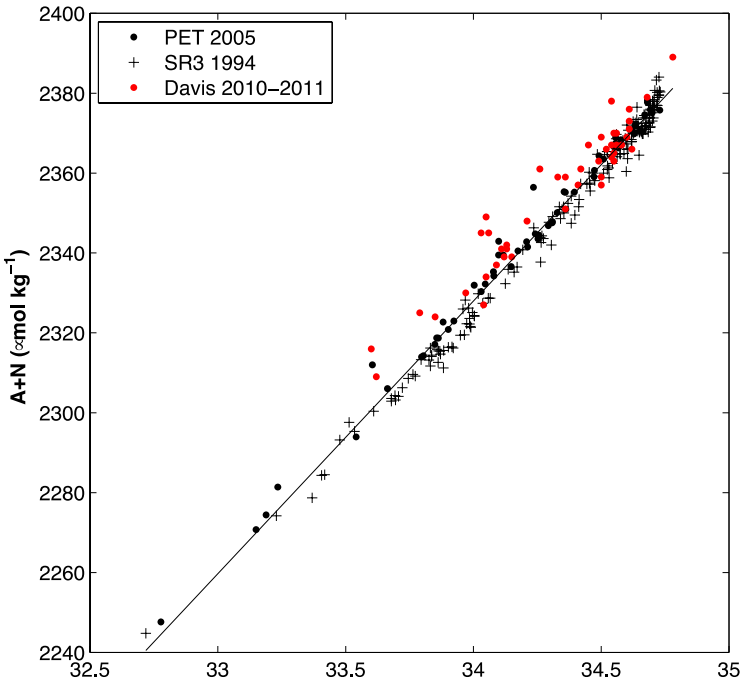

Figure 3.3. The salinity and TA+N relationship of all sampling sites in 2010 (red dots) and from the nearby offshore waters of the Princess Elizabeth Trough (PET, black dots; <500 m depth), measured in 2005, and from the southern end of the WOCE SR3 transect, measured in 1994 (data available from GLODAP: http://cdiac.ornl.gov/oceans/glodap). A linear regression yielded the following equation, $y = (68 \pm 1)x + (7 \pm 21)$ (n = 280, $r^2 = 0.98$, standard error = 4 μmol kg^{-1}).

respectively. The total ice thickness model was initiated from the first measured sea-ice thickness observations in May 2010.

3.2.4 Air-sea CO_2 flux calculations

A positive air-sea CO_2 flux (mol m^{-2} $month^{-1}$) value implies a net transfer from the atmosphere into the ocean and was computed from the air-sea gradient in pCO_2 (ΔpCO_2) in the following equation:

$$CO_{2\ \mathrm{flux}} = k_{\mathrm{av}} \cdot \alpha \cdot \Delta pCO_2 \qquad \textbf{Equation 3.4}$$

where k_{av} (m s^{-1}) is the gas transfer velocity, parameterized as a function of the Schmidt number (Sc) of the gas and the wind speed and α is the CO_2 solubility (mol m^{-3} atm^{-1}). The gas transfer velocity, k_{av}, was computed using average monthly wind speeds recorded by the Australian Bureau of Meteorology's 10-meter wind anemometer at the nearby Davis station field office and using the formulation of Wanninkhof (1992) for long-term winds:

$$k_{\mathrm{av}} = 0.39^2_{\mathrm{av}} \left(\mathrm{Sc}/660\right)^{-0.5} \qquad \textbf{Equation 3.5}$$

The use of long-term average wind speeds, when compared with short-term steady winds, may result in an underestimate of gas transfer velocities by as much as 30% (Wanninkhof, 1992). The in situ CO_2 solubility was computed using seawater temperature and salinity and the equations of Weiss (1974). However, as seawater pCO_2 was computed from DIC and TA concentrations at 20 m, the ΔpCO_2 term may be underestimated in summer due to surface stratification (Gibson & Trull, 1999).

Atmospheric CO_2 values were not directly measured at Davis and are taken from the South Pole station (http://scrippsco2.ucsd.edu/ data/spo.html). A comparison of atmospheric CO_2 concentrations at the South Pole and at Casey station on the Antarctic coast (66˚17S, 110˚31E; Steele et al., 2007) between the years 1997 and 2006 showed very little monthly variation (± 0.44 ppm, 1 s.d.). Indicating the CO_2 concentrations at the South Pole are a good approximation of atmospheric concentrations at the study site. The atmospheric CO_2 concentrations were converted to partial pressures by following the procedure in Dickson et al. (2007) using the mean monthly atmospheric pressure recorded at Davis (www.bom.gov.au/climate/data/stations) and the seawater vapour pressure calculated from the salinity and temperature of the surface waters (Ambrose & Lawrenson, 1972; Millero & Leung, 1976). The computed air-sea CO_2 fluxes were then scaled to account for ice cover by using a multiplier equal to 100 minus the percentage ice coverage. The sea-ice coverage was determined from direct observations at the site (Table 3.2). This method assumes that sea ice provides an effective barrier to air-sea CO_2 gas exchange, and that air-sea CO_2 fluxes are a linear function of sea-ice coverage. Several studies have suggested that sea ice does not fully inhibit air-sea exchange of biogenic gasses (e.g., Semiletov et al., 2004; Loose et al., 2009). At 100% sea-ice coverage, we set the multiplier to 1% for consistency with previous studies (Bates et al., 2006; Mucci et al., 2010; Shadwick et al., 2011).

Table 3.2. Estimation of sea-ice concentration made from observations at the study site.

	May	**Jun**	**Jul**	**Aug**	**Sep**	**Oct**	**Nov**	**Dec**	**Jan**	**Feb**
% ice-cover	100	100	100	100	90	80	80	80	60	0

3.2.5 Controls on total dissolved inorganic carbon

Assuming that their contributions to the property budgets are relatively homogenous regionally, particularly over the shelf (Roden et al., 2016), horizontal advection can be ignored and the temporal changes in DIC are considered to be the sum of the changes due to biological and physical processes and air-sea CO_2 exchange. The contributions of these various processes to the observed monthly changes in DIC were calculated for Site 1 by interpolating single day DIC values between samplings and summing the observed changes for each month. Changes in DIC ($\Delta\mathrm{DIC_{total}}$) are considered to be the sum of the changes due to: 1) freshwater flux from ice formation and melt ($\Delta\mathrm{DIC_{ice}}$), 2) biology ($\Delta\mathrm{DIC_{bio}}$), and 3) air-sea CO_2 flux ($\Delta\mathrm{DIC_{as}}$). Changes in DIC due to $CaCO_3$ formation and dissolution were found to be small, as discussed in Section 3.3.3.

$$\Delta\mathrm{DIC_{total}} = \Delta\mathrm{DIC_{ice}} + \Delta\mathrm{DIC_{bio}} + \Delta\mathrm{DIC_{as}} \quad \textbf{Equation 3.6}$$

The monthly contribution of changes in DIC due to ice formation and melt ($\Delta\mathrm{DIC_{ice}}$) was determined by subtracting the monthly change in salinity normalized DIC (ΔnDIC) from $\Delta\mathrm{DIC_{total}}$:

$$\Delta\mathrm{DIC_{ice}} = \Delta\mathrm{DIC_{total}} - \Delta n\mathrm{DIC} \quad \textbf{Equation 3.7}$$

The change in DIC due to biological processes, or net community production (NCP; NCP = Net Primary Production − Heterotrophic Respiration), was determined using two separate approaches. The first approach estimated the net contribution from biological processes ($\Delta\mathrm{DIC^c_{bio}}$) by calculating the difference between $\Delta\mathrm{DIC_{total}}$ and the sum of the $\Delta\mathrm{DIC_{ice}}$ and $\Delta\mathrm{DIC_{as}}$:

$$\mathrm{NCP_C} = \Delta\mathrm{DIC^c_{bio}} = \Delta\mathrm{DIC_{total}} - \Delta\mathrm{DIC_{ice}} - \Delta\mathrm{DIC_{as}} \quad \textbf{Equation 3.8}$$

The second, independent approach, utilized monthly changes in salinity normalized nitrate (nN) concentrations and a C/N Redfield ratio of 6.6 (Redfield et al., 1963):

$$\mathrm{NCP_N} = \Delta\mathrm{DIC^n_{bio}} = \Delta n\mathrm{N} \cdot 6.6 \quad \textbf{Equation 3.9}$$

3.2.6 Error analysis

The uncertainties in calculated carbonate parameters were estimated by calculating the quadratic sum of the partial uncertainties associated with the input parameters of CO_2 system calculations. A second method of error propagation utilized a Monte Carlo simulation. The inputs for the simulation were generated by a random number generator with a normal distribution, which required the mean and standard deviation of each input variable for carbonate system calculations. The simulation was solved 10,000 times with the standard deviation being used as the magnitude of the error. A comparison of the two methods showed no difference in the estimated uncertainty. Estimates of the uncertainties associated with monthly ΔDIC are listed in Table 3.3. The uncertainty associated with ΔDIC_{total} (σ_{total}) was estimated from the quadratic sum of DIC measurement uncertainty. A 20% uncertainty is associated with ΔDIC_{as} (σ_{as}) term that is largely due to uncertainty in the parameterization of the gas transfer velocity (see Equation 3.5, Naegler et al., 2006; Sweeney et al., 2007; Watson et al., 2009). The uncertainty associated with ΔDIC_{ice} (σ_{ice}) was estimated from the quadratic sum of errors associated with Δ*n*DIC and ΔDIC_{total}. Finally, propagation of the above uncertainties results in an estimate of the errors associated with ΔDIC_{bio} (σ^{c}_{bio}), with the measurement accuracy of nitrate being used to establish the uncertainty of ΔDIC^{n}_{bio} (σ^{n}_{bio}). However, because biological production did not always occur in Redfield ratios, this estimate of σ^{n}_{bio} should be considered a lower limit on the uncertainties associated with changes in DIC due to biological production, as discussed later in Section 3.4.1.

Table 3.3. Estimates of the uncertainties associated with the monthly controls of ΔDIC.

Term	Error (mol m^{-2} $month^{-1}$)
σ_{total}	0.08
σ_{as}	0.09
σ_{ice}	0.2
σ^{c}_{bio}	0.2
σ^{n}_{bio}	0.08

3.3 Results

3.3.1 Physical parameters

For the purposes of this study the seawater temperature values for winter and spring are assumed to be near the seawater freezing point of -1.88 °C, consistent with previous measurements from the study area during this time (Gibson & Trull, 1999). Sea ice started to form and completely cover the region during March. By early-May, when water sampling started, the sea ice was 63–65 cm thick at all sampling sites. Ice thickness increased gradually in the region until a maximum thickness of 167.5 cm was measured at Site 1 in mid-November. Sea-ice thickness then decreased until all ice was blown out from the area on 21 January 2011. The formation and melt of sea ice in the area was largely responsible for changes in salinity (Figure 3.4a). The contribution of evaporation and precipitation (snow) to changes in salinity is

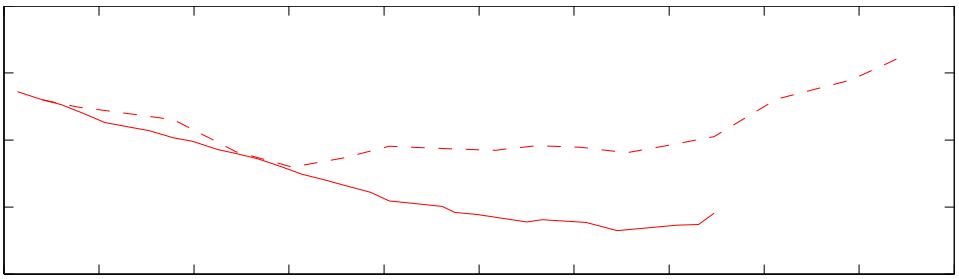

Figure 3.4. a) Measured sea-ice thickness (solid line) and the modeled sea-ice thickness (dashed line) at the study site based on the observed changes in salinity. b) Annual salinity cycle from May 2010 to February 2011 at Site 1, divided into High Salinity Shelf Water (HSSW) and Low Salinity Shelf Water (LSSW) at 34.6. The shaded area represents one standard deviation of measurement accuracy.

negligible due to sea-ice cover and low precipitation rates in the Davis area (www.bom.gov.au). Brine rejection from sea-ice formation increased salinity concentrations to a maximum value of 34.78 in winter, and ice melt during the warmer summer months caused salinity values to decrease to 33.62 in February. The expected sea-ice thickness due to the observed changes in seawater salinity at Site 1 is shown by the dashed line in Figure 3.4a, with the solid line indicating the observed sea-ice thickness. Calculations of sea-ice thickness based on salinity changes agree until early-August. From August to late-September, a decrease in salinity (0.19) caused a departure in the observed and modelled sea-ice thickness. The change in salinity is small relative to the seasonal amplitude and could result from local variations in water column mixing and sea-ice production (Worby et al., 2008).

3.3.2 Total alkalinity

Total alkalinity (TA) can be altered by the formation or dissolution of $CaCO_3$ and changes in salinity through freshwater addition (ice melt) or removal (ice formation). Changes in TA associated with the uptake and release of dissolved nitrate (NO_3^-) during photosynthesis or respiration (Brewer & Goldman, 1976) can be accounted for by summing the concentrations of TA and nitrate (TA+N). Nitrate values, when not available, were linearly interpolated between samples. The TA+N concentrations at the study site show seasonal variability associated with changes in salinity (Figure 3.5a). By normalizing to a constant salinity (*n*TA+*n*N), the seasonal variability is removed (Figure 3.5b), indicating summer melting and winter ice formation can account for all of the TA change within the measurement uncertainties. The measurement uncertainty however, allows for up to a maximum of 12 μmol kg^{-1} change seasonally that could be due to $CaCO_3$ formation and dissolution.

3.3.3 Total dissolved inorganic carbon

The seasonal change in DIC (Figure 3.6a) follows a pattern of lower concentrations for the more productive spring to summer period and higher values in winter. A gradual increase from May to late-July to 2256 μmol kg^{-1} is followed by a decrease in DIC starting in late-spring to a summertime minimum of 2124 μmol kg^{-1} in February. Salinity normalized DIC (*n*DIC) increased by 22 μmol kg^{-1} from May to a mean winter value (Figure 3.6b) of 2224 ± 3 μmol kg^{-1} (1 s.d.; n = 7). This gradual increase

Table 3.4. Measured parameters at Site 1 (20 m) between May 2010 and February 2011. Dates marked with * indicate measurements used to calculate mean winter values.

Date	Salinity	Temp (˚C)	TA (µmol kg^{-1})	DIC (µmol kg^{-1})	Nitrate (µmol kg^{-1})	Phosphate (µmol kg^{-1})	Silicic acid (µmol kg^{-1})
14 May 2010	34.05	-1.9	-	2185	24.0	1.72	46
25 May 2010	34.13	2.1	2316	2206	-	1.85	42
14 June 2010	34.21	-0.9	2323	-	24.6	1.94	48
25 June 2010	34.26	-1.4	2335	2217	25.6	1.97	47
15 July 2010	34.61	-1.9	2349	2233	-	2.01	52
02 August 2010*	34.78	-1.6	2362	2256	-	-	-
18 August 2010*	34.68	-1.3	2351	2248	27.9	2.04	50
02 September 2010*	34.55	-1.7	2337	2239	-	-	-
21 September 2010*	34.58	-1.5	2338	2244	29.2	1.92	52
06 October 2010*	34.60	-1.7	2340	2238	28.8	1.81	57
19 October 2010*	34.55	-1.6	2335	2236	28.7	1.75	57
02 November 2010*	34.56	-1.4	2339	2241	28.3	1.84	57
17 November 2010	34.62	-1.7	2337	2229	28.2	1.91	56
01 December 2010	34.54	-1.8	2340	2225	26.2	1.83	54
15 December 2010	34.45	-1.2	2345	2207	-	-	-
04 January 2011	34.05	-0.5	2318	2148	16.7	1.49	49
28 January 2011	33.85	-0.2	2308	2128	15.8	1.57	51
12 February 2011	33.62	-1.2	2292	2124	16.4	1.50	46

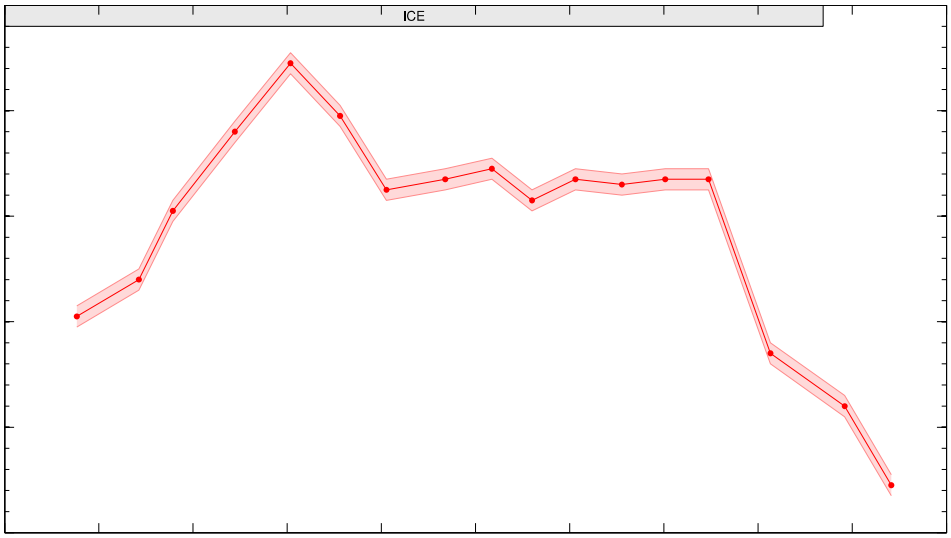

Figure 3.5. Seasonal cycle, from May 2010 to February 2011, of (a) the sum of total alkalinity and nitrate (TA+N) and (b) salinity normalized TA+N (*n*TA+*n*N) at Site 1. The shaded areas represent one standard deviation of measurement accuracy. The gray bar at the top of this and all similar plots represents the presence of sea-ice cover.

from May to July is likely to result from the remineralization of organic matter during the winter. A rapid decrease of *n*DIC of 68 µmol kg^{-1} is observed from early-November (spring) to January. As the effects of freshwater fluxes have been removed from *n*DIC, the 68 µmol kg^{-1} change can be attributed to CO_2 flux and biological activity (NCP). Figure 3.7 shows that the majority of this decrease occurred in the onset of the spring/summer bloom when sea ice still covered much of the study site. Based on the range of *n*TA+*n*N discussed previously, the upper limit of changes in DIC due to $CaCO_3$ formation and dissolution is 6 µmol kg^{-1} (Brewer & Goldman, 1976). Resolving such small changes in DIC however, exceeds the detection limits of this study and any change in DIC due to calcification or dissolution is included in the estimate of NCP. Following a rapid decrease in sea-ice concentrations in January, the air-sea flux of CO_2 caused an increase in DIC. However, a net decrease in DIC is

observed due to the strength of DIC draw down from NCP and ice melt (Figure 3.7, Table 3.5).

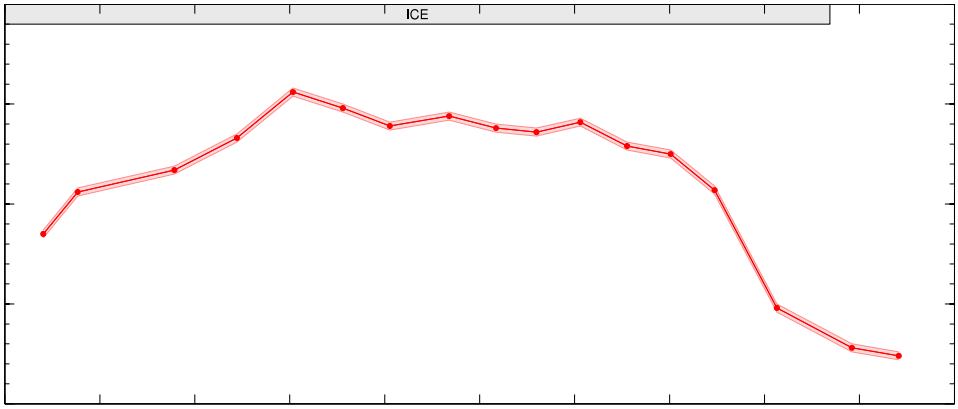

Figure 3.6. Seasonal cycle, from May 2010 to February 2011, of (a) total dissolved inorganic carbon (DIC) and (b) salinity normalized DIC (*n*DIC) at Site 1. The shaded areas represent one standard deviation of measurement accuracy.

3.3.4 Nutrients

The concentrations of salinity normalized macronutrients, phosphate and nitrate, exhibited similar seasonal cycles throughout the study (Figure 3.8a and Figure 3.8b). Concentrations gradually increased throughout the winter to maximum values of phosphate and nitrate in August (2.02 µmol kg^{-1}) and September (29.0 µmol kg^{-1}), respectively. The lowest concentrations of nitrate (16.0 µmol kg^{-1}) and phosphate (1.50 µmol kg^{-1}) coincided with periods of minimum DIC in summer.

The seasonal cycle of salinity normalized silicic acid (Figure 3.8c), showed a minimum in May (42.6 µmol kg^{-1}). The occurrence of minimum silicic acid values this late in autumn is unexpected, as minimum values typically coincide with

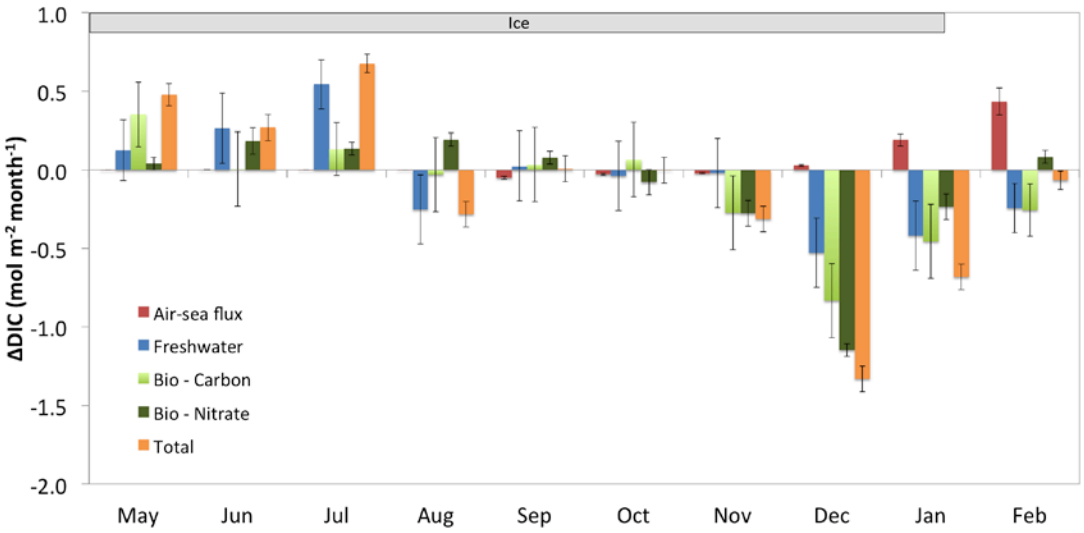

Figure 3.7. Controls on monthly changes in DIC at Site 1 from May 2010 to February 2011. Negative values indicate a decrease in DIC. Error bars represent one standard deviation of propagated uncertainties.

maximum biological productivity in the summer months (Perrin et al., 1987; Davidson & Marchant, 1992; Gibson & Trull, 1999; Robinson et al., 1999). This may be related to the frequency of the sampling not capturing minimum values during the summer or alternatively, it could reflect issues involving the inadvertent freeze-thaw cycle that nutrient samples were exposed to. However, samples collected immediately before and after the inadvertent thawing (late-October versus early-November) show similar silicic acid concentrations, suggesting that any compromising of the samples

Table 3.5. Controls on DIC at Site 1 for a given month from May 2010 to February 2011. Rates of change are in mol m^{-2} $month^{-1}$.

Month	**ΔDIC_{total}**	**ΔDIC_{as}**	**ΔDIC_{ice}**	**ΔDIC^{c}_{bio}**	**ΔDIC^{n}_{bio}**
May	0.48	0.00	0.13	0.35	0.04
June	0.26	0.00	0.26	0.00	0.18
July	0.67	0.00	0.54	0.13	0.14
August	-0.28	0.00	-0.25	-0.03	0.19
September	0.01	-0.05	0.03	0.03	0.08
October	0.00	-0.03	-0.04	0.07	-0.08
November	-0.31	-0.02	-0.02	-0.27	-0.28
December	-1.33	0.03	-0.53	-0.83	-1.15
January	-0.68	0.19	-0.42	-0.45	-0.24
February	-0.06	0.42	-0.24	-0.24	0.08

must have been the result of prolonged storage times (greater than one year) or polymerized silicate (Dore et al., 1996) in some samples rather than the freeze-thaw event itself.

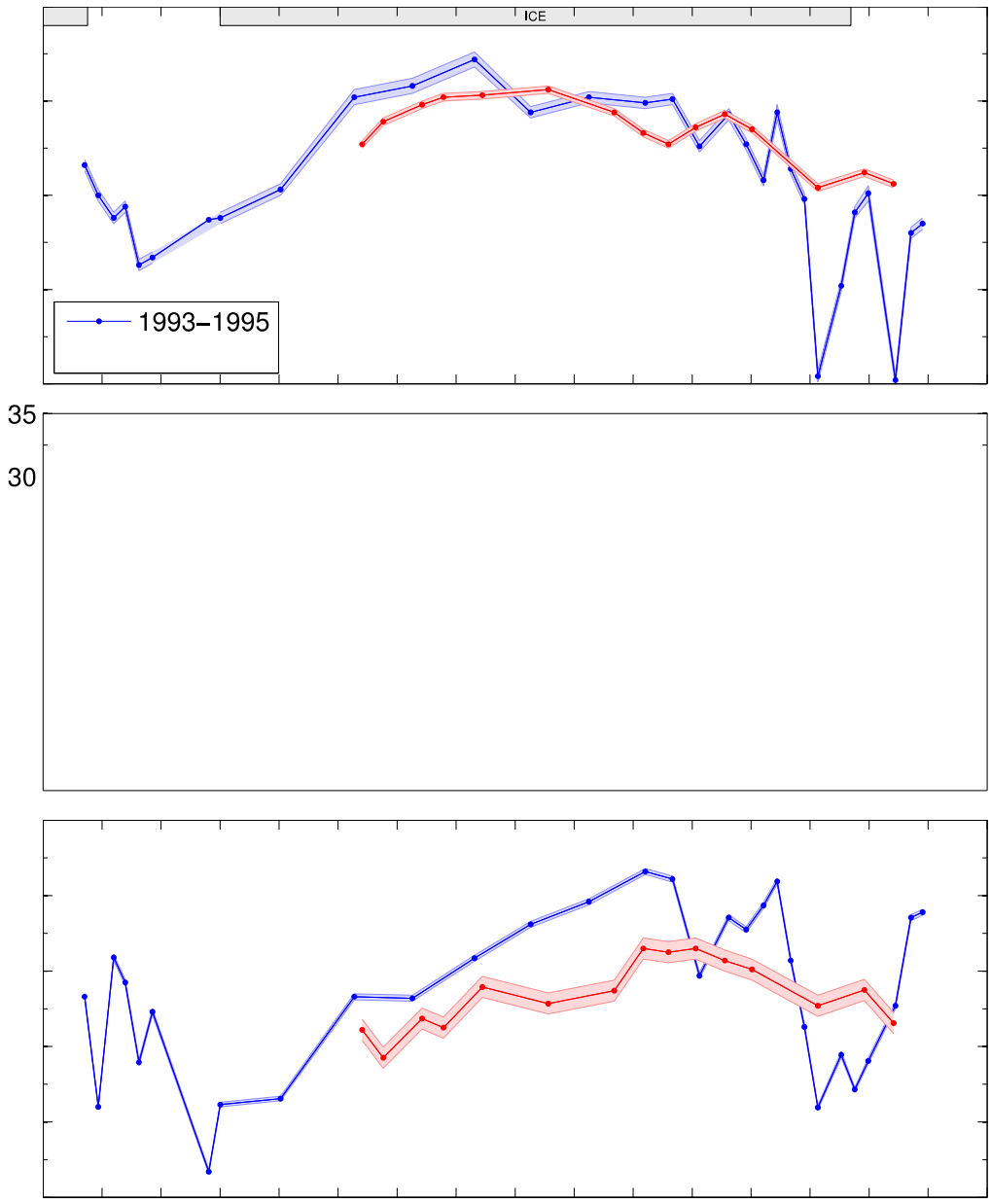

Figure 3.8. Annual cycle from May 2010 to February 2011 (red line) and December 1993 and February 1995 (blue line) (Gibson & Trull, 1999) of salinity normalized (S = 34.32) dissolved inorganic nutrients (a) phosphate, (b) nitrate and (c) silicic acid at Site 1. The shaded areas represent one standard deviation of measurement accuracy.

Monthly nutrient utilization ratios (Table 3.6) were derived from the deficit between the lowest salinity normalized nutrient concentrations in each month versus the highest values observed in winter. The N/P utilization ratios were close to Redfield (106C:16N:1P) in December, but were higher throughout the remaining summer months and lower in November. The Si/N utilization ratio was greater than 1 in November, but below 1 for the summer months, indicating that either the phytoplankton composition was diverse or that diatom growth in this coastal environment was not limited by iron availability (Brzezinski, 1985; Hutchins & Bruland, 1998; Takeda, 1998; Sambrotto et al., 2003).

Table 3.6. The utilization ratios of nutrients during the biologically productive months of December-February, relative to maximum nutrient concentrations in November.

Month	N:P	Si:N
November	5.1	1.6
December	14.3	0.9
January	25.1	0.6
February	24.8	0.8

3.3.5 Calculated carbonate parameters

The seasonal cycle of Ω_{ar} at Site 1 (Figure 3.9b) varied between 1.19 and 1.92, with the variations caused largely by seasonal changes in CO_3^{2-} concentration driven by biological processes. Changes in temperature and salinity also have a small effect on Ω_{ar}. For example a temperature increase of 1°C causes an increase in Ω of <1%. The Ω_{ar} was nearly constant over the winter months with a mean value of 1.24 ± 0.03 (1 s.d.; n = 7), and from November the values increased to a maximum of 1.92 in January. The seasonal cycle of pH_{sws}, calculated at in-situ temperature (Figure 3.9a), showed a similar trend to that of Ω_{ar} and mirrored the cycle of DIC. Minimum values of 7.99 were calculated for September with a maximum of 8.20 in January.

The calculated pCO_2 (Figure 3.9c) was over-saturated with respect to the atmosphere in late-winter and spring, with a maximum value of 433 μatm in September. Minimum values of 252 μatm were calculated over summer, with the shift to undersaturated and ice-free waters resulting in CO_2 uptake. The estimates of air-sea flux were scaled to account for ice-cover in the study area (Figure 3.7). Assuming a net air-sea CO_2 flux of zero for the ice-covered months of March and April, when no

sampling was undertaken, we estimate that the study site was a net sink for CO_2, with a net annual air-sea CO_2 uptake of 0.54 ± 0.11 mol C m^{-2} $year^{-1}$.

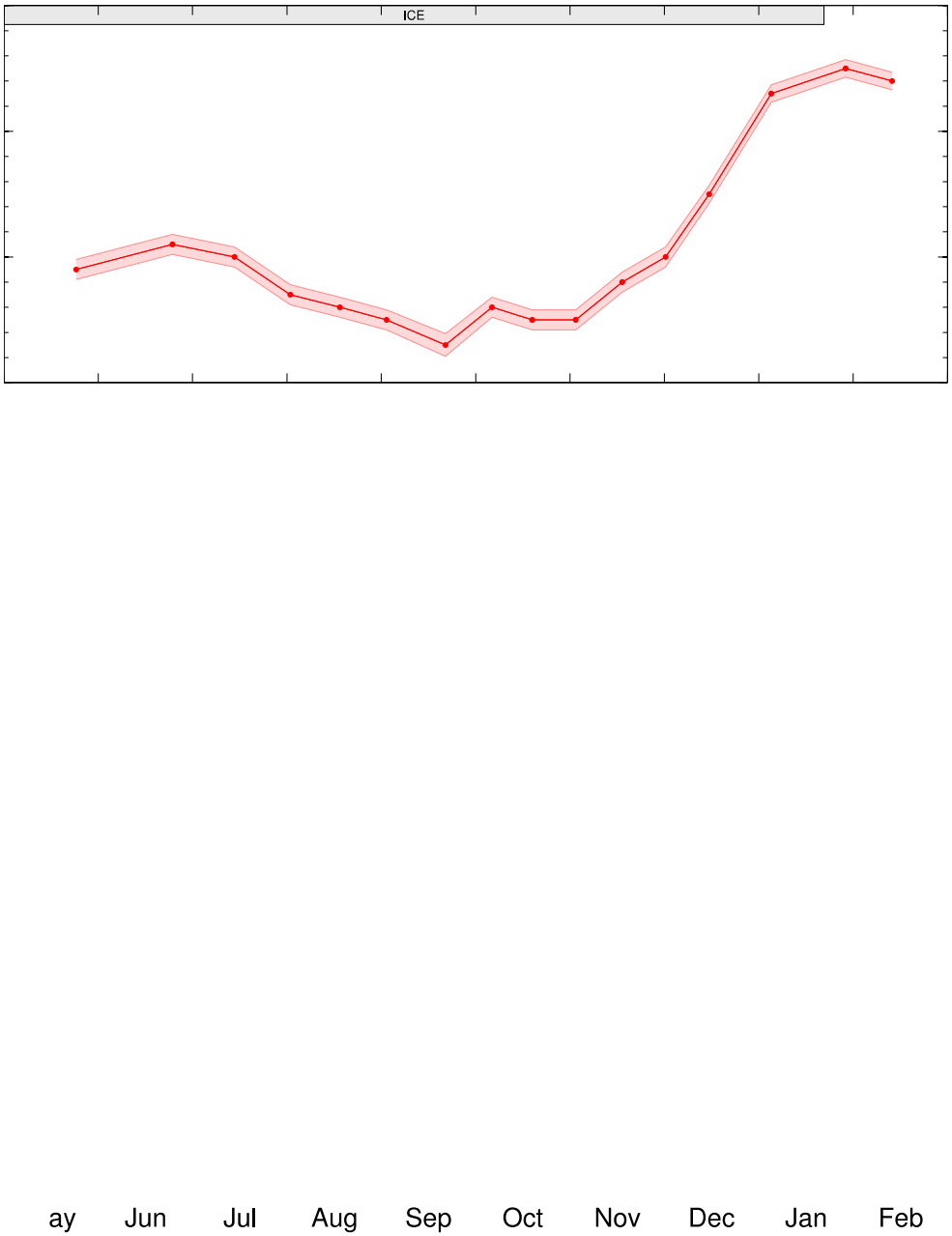

Figure 3.9. Seasonal cycle of (a) pH_{sws} (at in situ temperature) at Site 1 between May 2010 and February 2011 with (b) the aragonite saturation state (Ω_{ar}) and (c) seawater pCO_2 and the mean atmospheric pCO_2 (dashed line; 373.4 µatm). The shaded areas represent one standard deviation of propagated uncertainties.

3.4 Discussion

3.4.1 Net community production

Increased NCP in spring, that appears to be linked to greater light availability and the commencement of sea-ice melt, caused a rapid reduction in DIC (Figure 3.7). NCP was estimated from the total ΔDIC^{c}_{bio} and ΔDIC^{n}_{bio} (Equations 3.8 and 3.9; Table 3.5). In the productive months of November–February, the carbon based estimate of NCP (NCP_C) yielded a value of 1.8 ± 0.4 mol C m^{-2}, similar to the nitrate based estimate (NCP_N) of 1.6 ± 0.1 mol C m^{-2} with low values in other months. The total amount of carbon exported off the shelf due to the biological production in November-February is unknown. However due to the shallow nature of the study site, it is likely that much of this organically fixed carbon was later remineralized back into the water column (Gibson & Trull, 1999).

Despite the good agreement between the NCP_C and NCP_N estimates, it is worth considering potential biases in each. Inaccuracies associated with the estimate of local sea-ice concentrations may result in the sea-ice scaled NCP_C term being under (or over) estimated due to variations in DIC caused by air-sea gas exchange. Uncertainties in the NCP_N value may arise from the assumption of Redfield C/N utilization ratios, as ratios throughout the productive season varied in a manner that may reflect iron availability (Takeda, 1998) and/or species composition (Sambrotto et al., 2003). Although, when considered over the length of the productive season, nutrient utilization ratios within the surface waters of the Antarctic have been shown to mostly follow the classic Redfield model (Hoppema & Goeyens, 1999). Short-term variations in N/P utilization ratios have previously been associated with diatom growth in coastal Prydz Bay (Gibson, 1998) and in the Ross Sea (Arrigo et al., 1999; Sweeney et al., 2000). Gibson et al. (1997) also observed that different phytoplankton species in the study region were dominant at different times of the summer and that phytoplankton assemblages and the biomass present exhibited significant inter-annual variability. Gibson et al. (1997) suggested that this variability is a function of such environmental parameters as seasonal and inter-annual changes in light availability (sea-ice extent), water temperature and salinity, and nutrient availability. Considering that such inter-annual variations in biological productivity exist, it is necessary to

consider how these changes might influence the carbon cycle and therefore acidification trends over decadal time scales.

3.4.2 Decadal change in carbonate chemistry

The observed variability in the seasonal drawdown of DIC in spring and summer in high-latitude waters, driven largely by biological productivity, necessitates the use of winter-time observations when establishing trends in the long-term changes of carbonate chemistry. The mean winter *n*DIC concentrations (Figure 3.10a) between 1994 and 2010 show that the 2010 value (2224 ± 3 μmol kg^{-1} (1 s.d.; n=7)) is 34 μmol kg^{-1} higher than the 1994 winter value (2190 ± 5 μmol kg^{-1} (1 s.d.; n = 6; 11 July 1994 to 4 November 1994)). The anthropogenic component of this change can be estimated by recalculating winter-time carbonate system parameters, allowing for increases in atmospheric CO_2 over the 16-year period and assuming the surface waters tracked the atmospheric increase. By using 1994 TA values and increasing the calculated seawater pCO_2 by the observed atmospheric increase (~28 μatm) an estimated increase in winter-time DIC of 12 μmol kg^{-1} from 1994 to 2010 would be expected. This however, leaves an increase in *n*DIC of 22 μmol kg^{-1} above that expected from atmospheric uptake alone.

The seasonal cycle of pH_{sws} in1994 was similar to the cycle observed in 2010, with lower values in winter and early-spring and higher values in summer. The mean winter value of pH_{sws} in 2010 (8.00 ± 0.01 (1 s.d.; n = 7)) was 0.11 lower than the mean winter value in 1994 (8.11 ± 0.02 (1 s.d.; n = 6)) (Figure 3.10b). The expected decrease in pH_{sws} from 1994 values, if the surface ocean uptake tracks the atmospheric CO_2 increase, is 0.04, indicating that ocean CO_2 uptake is not the only process affecting carbon cycle dynamics on the shelf environment and driving observed changes in pH_{sws} from 1994 to 2010. Temperature variations between the two years cannot explain the observed differences in pH as seawater temperature was near freezing during both winters.

Due to the paucity of winter-time physical oceanographic observations in Prydz Bay and deep convective mixing over the continental shelf, previous inferences about the variability of winter-time Shelf Water properties have been restricted to summertime observations of remnant winter water from the temperature minimum layer in the oceanic domain (Smith et al., 1984). More recently, physical oceanographic

properties in June and November have been observed in the surface water (<20 m) near Davis by using Elephant seals equipped with CTD instruments. During these

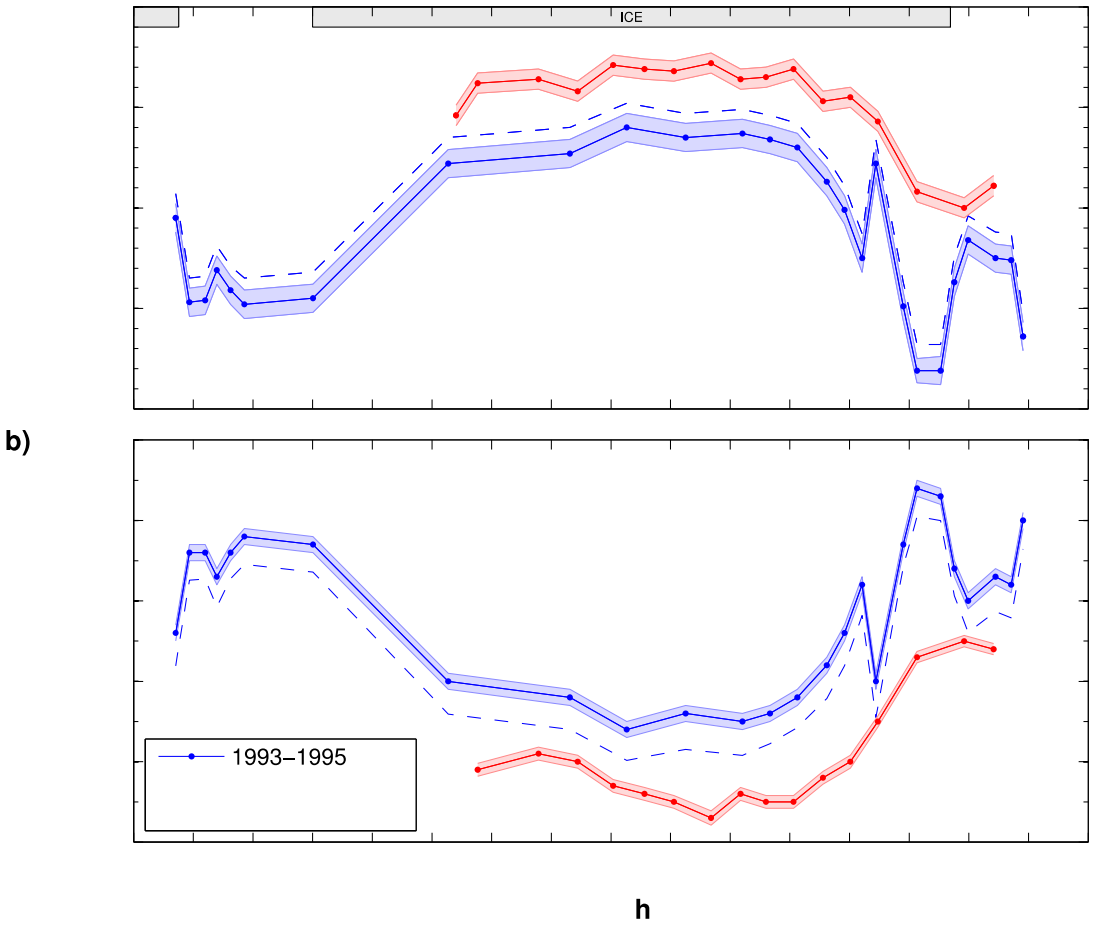

Figure 3.10. Seasonal cycles at Site 1 between May 2010 and February 2011 (red line), and December 1993 and February 1995 (blue line) (Gibson & Trull, 1999) of (a) salinity normalized (S = 34.32) DIC (*n*DIC) and (b) pH_{sws} (at in situ temperature). The dashed lines show the predicted response of both *n*DIC and pH_{sws} from 1994 values to 2010, assuming that ocean acidification (OA) was the only process controlling carbonate chemistry in Prydz Bay. The shaded areas represent one standard deviation of measurement accuracy and propagated uncertainties.

months, salinity values ranged from 33.40 to 34.40 (G. Williams, personal communication). The mean winter-time salinity value of 34.61 ± 0.08 (1 s.d.; n = 7) at Site 1 in 2010 was 0.58 higher than the mean winter value observed in 1994 (34.03 ± 0.07 (1 s.d.; n = 6)). Whilst the values observed at Site 1 in 2010 are outside of the range of values reported by using the Elephant seal data, it is clear that large variations in winter-time salinity exist in the coastal waters of Prydz Bay. Despite the observed variability in salinity regimes, the comparison of *n*DIC values between the two years removes the effects of freshwater flux on DIC concentrations.

Intrusions of Modified Circumpolar Deep Water (mCDW) onto the shelf in the eastern sector of Prydz Bay have also been observed using Elephant seal data (G. Williams, personal communication). Observations in 2005 of mCDW properties near the shelf-break in Prydz Bay (Princess Elizabeth Trough, 2005; http://cdiac.ornl.gov/oceans/glodap), suggest that the higher salinity, DIC and nutrient concentrations and lower pH values associated with such intrusions could help to explain some of the observed variability in chemical and physical oceanographic properties on the shelf.

Table 3.7. Drivers of decadal change in winter-time *n*DIC concentrations (μmol kg^{-1}) at Site 1 between 1994 and 2010.

	Total	**Ocean acidification**	**Biological production**	**Unknown**
$\Delta n\mathrm{DIC}_{1994-2010}$	34	12	17	5

A comparison of *n*N concentrations between 1994 and 2010 shows that mean winter nitrate values were 2.6 μmol kg^{-1} higher in 2010. This is outside the analytical error (0.3 μmol kg^{-1}), but of uncertain significance given the sparse sampling and overall trends of winter nitrate in each period (Figure 3.8b). Nonetheless, if this was the result of lower biological productivity prior to 2010 and assuming C/N remineralization occurred in Redfield proportions, a corresponding increase of ~17 μmol kg^{-1} in DIC relative to 1994 values would be observed. Adding this with the 12 μmol kg^{-1}, for equilibration with the anthropogenic increase of atmospheric CO_2, accounts for all but 5 μmol kg^{-1} of the observed increase in *n*DIC since 1994 (Table 3.7). This suggests that atmospheric CO_2 uptake and variations in the cycling of carbon and nutrients between 1994 and 2010 account for most of the observed change in DIC and pH.

3.5 Conclusion

These observations show the relative seasonal influences of biological production, ice formation and melt, and air-sea CO_2 flux in 2010, combined to drive changes in dissolved inorganic carbon (DIC) at a coastal site in Prydz Bay, East Antarctica. The largest changes in DIC were caused by phytoplankton growth beneath the sea ice in spring and summer, which resulted in low seawater pCO_2 values and a net CO_2 uptake of 0.54 ± 0.11 mol C m^{-2} year^{-1}. Comparison to previous work reveals that natural variability in carbon cycle dynamics over decadal time scales caused pH changes that

were nearly twice as large as those expected from anthropogenic CO_2 alone. This highlights the difficulties in establishing trends in the ocean carbon dioxide system in dynamic, high latitude, coastal locations with sparse temporal and spatial carbon cycle observations.

Acknowledgments

This research was supported by an Australian Postgraduate Award, CSIRO Oceans and Atmosphere scholarship, Lynchpin Ocean Project scholarship (to N. P. Roden), the Australian Climate Change Science Program and the Australian Commonwealth Cooperative Research Centre Program, and an Australian Antarctic Science grant (project no. 3134: vulnerability of Antarctic marine benthos to increased temperature and ocean acidification associated with climate change – Byrne, M., King, C., and Virtue, P.). Petra Heil from the Antarctic Climate and Ecosystems CRC provided sea-ice measurements. We thank Kate Berry for carbon analysis from CSIRO and Patti Virtue for comments and feedback on various drafts of this manuscript. Melanie Ho and Doctor Ben O'Leary provided valuable help with field sampling and the Australian Antarctic Division and the Australian Bureau of Meteorology are acknowledged for logistical support in the field.

4 Manipulating seawater pH under sea ice: carbonate chemistry of an in-situ Antarctic free ocean CO_2 enrichment experiment

Abstract

The first Antarctic free-ocean CO_2 enrichment (antFOCE) experiment was conducted at a coastal site near Casey station in East Antarctica to study the response of benthic communities to ocean acidification. This was achieved through the manipulation of seawater carbonate chemistry in experimental chambers from December 2014 to February 2015. Changes in dissolved CO_2 system parameters showed how the experimental setup successfully maintained a mean pH offset within the experimental chambers of -0.38 ± 0.07 pH units, relative to ambient values, for approximately 6 weeks of the 8-week experimental period. Diel and seasonal fluctuations in ambient pH were duplicated in experimental chambers, located on the seafloor (13 m depth) under sea ice, where the seawater pH was manipulated to match values expected in the surface mixed layer by the end of this century under the Intergovernmental Panel on Climate Change Representative Concentration Pathway 8.5 greenhouse gas concentration trajectory. The mean pH, saturation state of aragonite and the fugacity of CO_2 values in the experimental chambers were 7.680 ± 0.085, 0.62 ± 0.15 and 914 ± 160 µatm, respectively. This experiment demonstrates the feasibility of FOCE systems, even under extreme conditions such as those experienced under sea ice in Antarctica.

4.1 Introduction

Anthropogenic carbon dioxide (CO_2) has been accumulating in the oceans, lowering the pH of seawater (Feely et al., 2004; Orr et al., 2005), causing ocean acidification. Since the start of the Industrial Revolution the oceans have absorbed approximately 28% of CO_2 emissions to the atmosphere (Sabine et al., 2004; Le Quéré et al., 2015), causing a decrease in surface seawater pH of 0.1 units (Orr et al., 2005). Under the United Nations Intergovernmental Panel on Climate Change (IPCC) greenhouse gas concentration trajectories, surface ocean pH is predicted to decline by a further 0.2 to 0.4 units by 2100 (Pörtner et al., 2014). This decline in ocean pH is predicted to have serious consequences for marine ecosystems (Orr et al., 2005), from direct effects on physiology, metabolism, and calcification rates; to indirect effects on food webs, species interactions (Kroeker et al., 2013) and phytoplankton community composition (Neven et al., 2011; Trimborn et al., 2013).

One of the key challenges for ocean acidification research is to understand how the physiological effects of lower pH on individual species translates into ecosystem effects (Gattuso et al., 2011). The relative paucity of knowledge of the effects of ocean acidification, particularly on polar marine organisms and ecosystems, in comparison to other latitudes (Fabry et al., 2009), highlights the need for further experimental efforts in these regions. This is especially relevant given that the Southern Ocean is considered to be particularly sensitive to changes in carbonate chemistry, due primarily to its low buffer capacity (Sabine et al., 2004), which results in greater ocean acidification per unit CO_2 increase than temperate and tropical waters (Revelle & Suess, 1957). Field perturbation experiments at the community level will help bridge the gap in scaling from physiological studies on individual species to ecosystem effects (Pörtner et al., 2014).

Free-ocean CO_2 enrichment (FOCE) systems were developed to address the need for studies on the effects of ocean acidification on biological communities in-situ, over long time scales (from weeks to months) (Gattuso et al., 2014), whilst allowing for the natural variation in other environmental parameters. Originally developed at the Monterey Bay Aquarium Research Institute (MBARI) (Walz et al., 2008; Kirkwood et al., 2011), FOCE systems allow for the precise control of pH (by CO_2 enrichment) within in-situ experimental chambers as an offset from natural background pH values

(hereafter ambient pH) on intact benthic communities. They provide a crucial link between organism level studies and scaling up to ecosystem effects by allowing the indirect effects of species interactions and changes in food webs to be examined (Gattuso et al., 2014). MBARI is now compiling FOCE technology and expertise into an open source package called xFOCE (www.xfoce.org), which this chapter will contribute to. These efforts are being made so as to reduce the time investment and technological development required for future FOCE experiments and to establish a broader community that contributes expertise and technical support.

From 19 December 2014 to 27 February 2015, a consortium of Australian, MBARI and Plymouth Marine Laboratory researchers conducted the first Antarctic FOCE (antFOCE) experiment to investigate the impacts of higher atmospheric CO_2 concentrations and lower seawater pH on Antarctic benthic communities. We used a pH perturbation of -0.4 pH units from ambient values. This equates to the expected decrease in surface ocean mixed-layer pH under the IPCC's Representative Concentration Pathway (RCP) 8.5 greenhouse gas concentration trajectory for the year 2100, which equates to atmospheric CO_2 levels of approximately 936 ppm (IPCC, 2013). By maintaining a pH offset of -0.4 and allowing for natural pH variation, the pH in the experimental chambers would vary according to diel and seasonal processes that influence pH in the natural environment. This assumes that these processes themselves will not change under future ocean acidification scenarios, which will be discussed later in Section 4.4.1. This chapter describes the technical aspects and performance of the antFOCE system and reports on the changes in carbonate chemistry that were observed during the experiment, alongside high-resolution measurements of ambient pH in O'Brien Bay, near Casey station in East Antarctica (Figures 1.2 and 4.1).

4.2 Data and methods

The antFOCE system consisted of two experimental chambers (chambers A and B) and two replicate control chambers (chambers C and D) that enclosed sections of benthos, and two open control plots (no chambers, plots E and F) in ~13 metres of water depth beneath sea ice. The pH within the experimental chambers was manipulated (~0.4 pH units below ambient values) by the incremental addition/adjustment of CO_2 enriched seawater (ESW) during a two-week

'acclimatization' phase and an eight-week 'experimental' phase. This was controlled and monitored by a surface sensor array and a series of switchable taps and pumps that allowed seawater to be sampled from the surface (Figure 4.2). Specific details regarding each of these components will be discussed in the following sections.

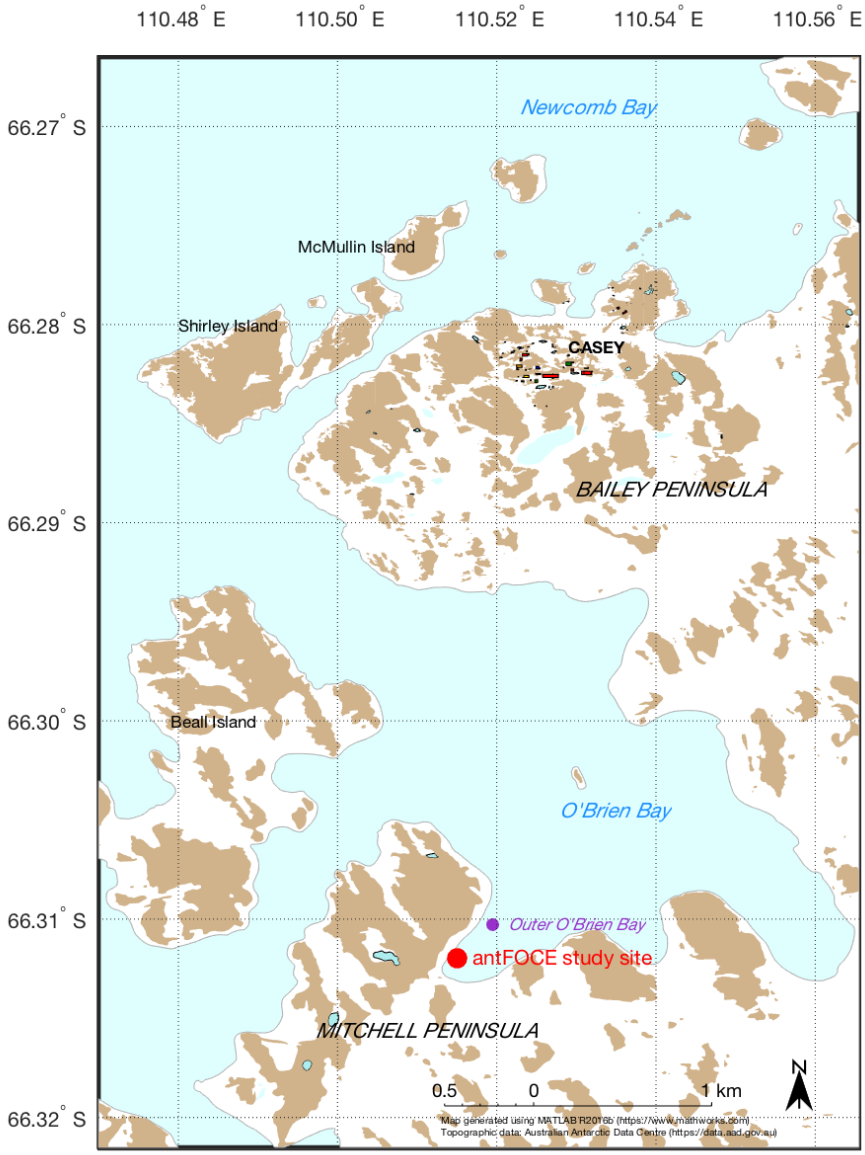

Figure 4.1 Map of the Mitchell and Bailey Peninsulas in the Windmill Islands of East Antarctica, showing the location of Casey station and the O'Brien Bay study sites.

4.2.1 Experimental setting

The antFOCE system was deployed in December 2014 after divers had surveyed the site for suitable areas to locate the seabed experimental setup. The site was selected

based on the following criteria: 1) accessibility from shore, 2) shallow water depth (for convenient diver access), 3) a mixed habitat of soft sediment and small boulders that supported a diverse and abundant invertebrate community and 4) a site that was not contaminated by activities from Casey station. The chambers were placed on patches of sediment at least 10 cm deep and at least 9 m^2 in extent so that sediment/water interactions could be monitored. Divers deployed the underwater components over a period of several weeks while the surface system was transported to the site and assembled. The site was located in a small sheltered embayment within the larger O'Brien Bay (Figure 4.1). The site was covered by fast ice for the duration of the experiment, which was 260 cm thick at the start and approximately 200 cm thick by the end of the experiment. The benthic habitat was a mixture of boulders, cobbles and patches of sediment and was dominated by invertebrates, with no macroalgae present due to the multi-year sea ice reducing light availability. The sediment was covered with a layer of microphytobenthos, which consisted primarily of diatoms (Thompson et al., 2007).

4.2.2 CO_2 enriched seawater

Seawater from near the seabed experimental setup was pumped to the surface and saturated with CO_2 in a pressurized cylinder (internal measurements 1520 mm long x diameter 240 mm, internal volume 69 L) housed in a shipping container with the generator. A mass flow controller (Alicat M series) was used to measure the amount of CO_2 being used, which was supplied from a bank of 69 CO_2 cylinders (food grade F size cylinder, holding 22 kg of CO_2) stored on site adjacent to the generator van. The ESW cylinder contained a misting showerhead at the top and was filled with plastic bio-balls (OVI-Flow ball 2 Biologic Media) to increase the surface area available for diffusion. The ESW, which had an approximate pH of 5.5, was introduced to the seabed experimental setup via a pump and hose system, as discussed below.

4.2.3 Seabed experimental setup

The four chambers were constructed from clear polycarbonate material that measured 2000 mm length x 500 mm width x 500 mm height, with three hinged lids on the top of the chamber and an open bottom. On the outlet end of the chamber there was a 10 mm stainless steel mesh screen. A 280 mm wide rubber skirt flap was attached to the

base of the chamber to help seal the sides. The chamber was attached to a 40 m long cylindrical equilibration duct (Plastcorp Mine flex stainless with steel wire; 500 mm diameter) via a stainless steel collar. The duct consisted of 4 x 10 m long sections joined with stainless steel collars. The inlet end of the duct was attached to 3.5 m of PVC storm water pipe, known as the thruster tube. Each thruster tube consisted of two sections of PVC pipe (250 mm diameter) joined with a collar. The ESW was introduced to the start of the pipe just behind the open end used for the intake of surrounding seawater, which was fitted with a cylindrical section of 10 mm stainless steel mesh (370 mm long, 250 mm diameter) to prevent the ingress of fish and large invertebrates. In the second section, a thruster (Navigator 65-5501) drew water into the pipe past a flow meter (General Oceanics digital lower flow) and into the duct and then eventually through the chamber. Water flow through the system was unidirectional and maintained at 3 cm s^{-1}.

4.2.4 Pump system and hoses

Peristaltic pumps were used to: 1) pump ambient seawater from near the chambers to the ESW unit (1 x Albin peristaltic ALP17 56 RPM fixed), 2) pump ESW down to the thruster tubes (2 x Albin peristaltic ALP17 29-6 RPM variable output speed) and 3) pump water from the chambers to the sensor panel (3 x Albin peristaltic ALP17 29 RPM fixed). These pumps were contained in a large insulated plastic box (Techni Ice 1100 L), which was heated internally with a diesel-burning heater (Webasto WEB902023480B). Pressure rated hoses were used to suck up water to use to make ESW (PVC Plutone clear/wire suction internal diam. 19 mm) and to the sensor panel from the chambers (PVC Plutone clear/wire suction 16 mm) as well as carry ESW to the thruster tubes (Barfell Diver air internal diam. 10 mm). The hoses were wrapped in a double coil of heat trace and all wrapped by a layer of insulation (FR Armaflex) contained within a canvas wrapping to prevent seawater freezing in the sub-zero air temperatures. The umbilical of the hoses also contained a 240V power cable that crossed the surface of the sea ice to a large metal sea-ice buoy, which sat in a 900 mm hole in the sea ice. The umbilical and cables passed through the centre of the buoy, into the water, and out to the seabed experimental setup. Power to the entire antFOCE system was supplied from a Cummins C22 D5 (X series) generator, housed on-site in a shipping container. An adjacent 400 L tank of diesel fuel was connected to the generator and regularly refilled from 200 L drums transported to the site.

4.2.5 Sensor array

Water was continuously pumped from the outlet end of three of the benthic chambers (both experimental chambers and one control, manually alternating between chamber C and D) to the surface where it was pumped through the sensor array. To obtain measurements, valves were used to enable water to flow sequentially from each chamber over the sensors for 10-minute periods. Water from chambers not being passed over the sensors went into an overflow disposal line. The sensor array consisted of a dissolved oxygen optode (Aanderaa, model 3835), thermosalinograph (Seabird SBE 45 MicroTSG) and for redundancy, two pH electrodes (Seabird SBE 18 and Honeywell Durafet). Water from the chambers was sampled for biogeochemical measurements (Section 4.2.7) using a valve on the water line leading into the sensor array. An additional pH electrode (Seabird SBE 18) was moved between chambers as a means to compare pH measurements in-situ with those from the surface sensor panel.

4.2.6 Control of pH

The pH of the experimental chambers was controlled by varying the amount of ESW pumped into the thruster tubes to achieve the -0.4 pH offset. The pH was measured by the Honeywell Durafet sensor and the flow rate of the ESW was adjusted slowly by a feedback control loop to ensure stability. Due to the surface sensor system cycling through each chamber every 10 minutes, and the seawater itself taking ~10 minutes to be pumped from the chamber to the surface, a delay of 30 minutes between estimates of pH offset was introduced. Adjustments to pH in the experimental chambers would then take another 10 minutes to propagate back down the ESW line and a further 22 minutes to flow through the equilibration ducting and into the chambers, introducing a total delay of ~1 hour in adjusting the pH within the chamber.

4.2.7 Biogeochemical measurements

Seawater samples of 250-mL, used for the analysis of DIC and TA, were collected from the surface sampling system and from a Niskin bottle at various locations within the study site. 100-µL of a saturated $HgCl_2$ solution was added to these samples to halt biological activity. DIC was determined using a Single Operator Multiparameter Metabolic Analyser following the procedure in Dickson et al. (2007), and TA was determined by open-cell potentiometric titration using a 0.1 M hydrochloric acid

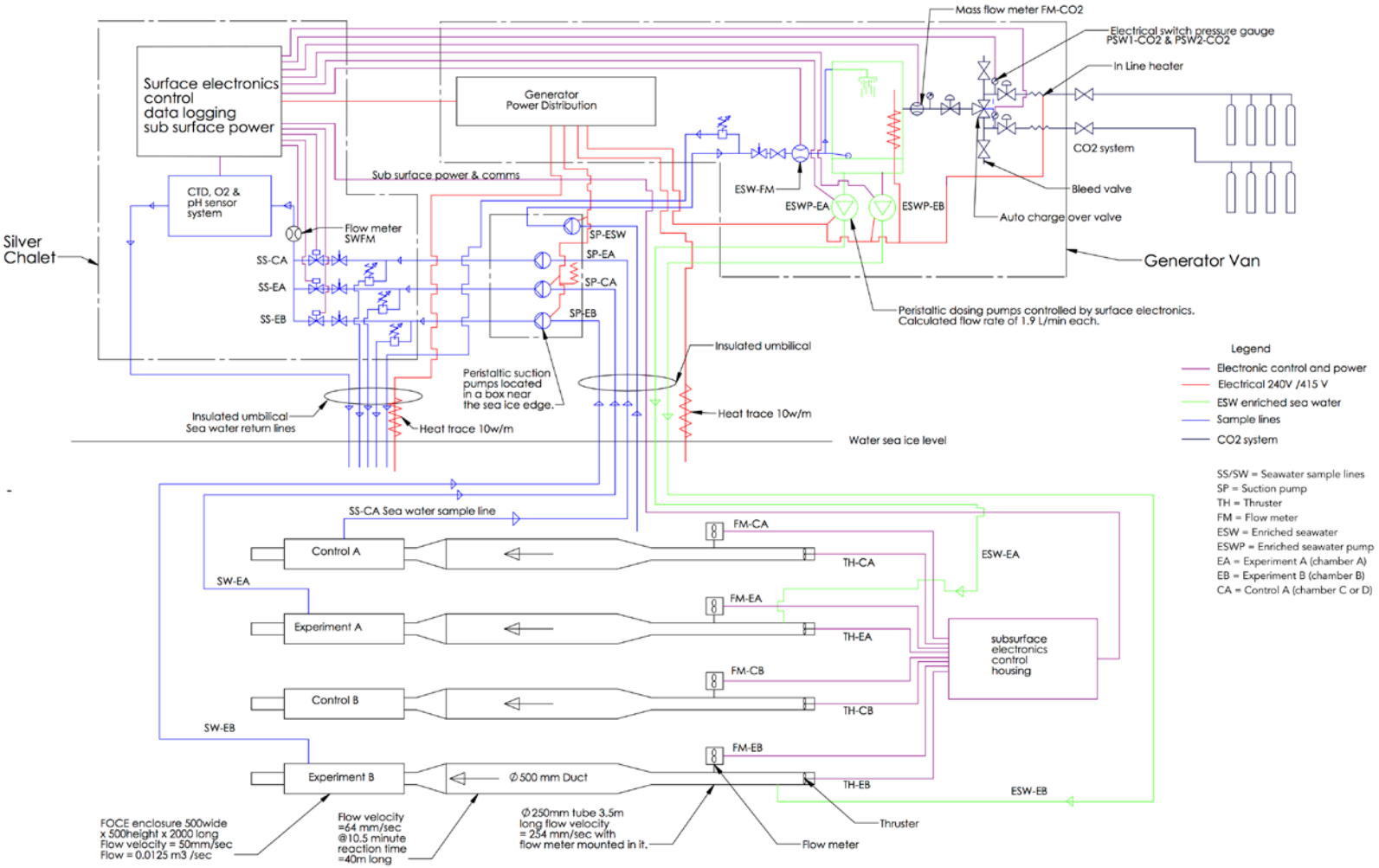

Figure 4.2 Schematic of the antFOCE system (generated by the Australian Antarctic Division's Science Technical Support group).

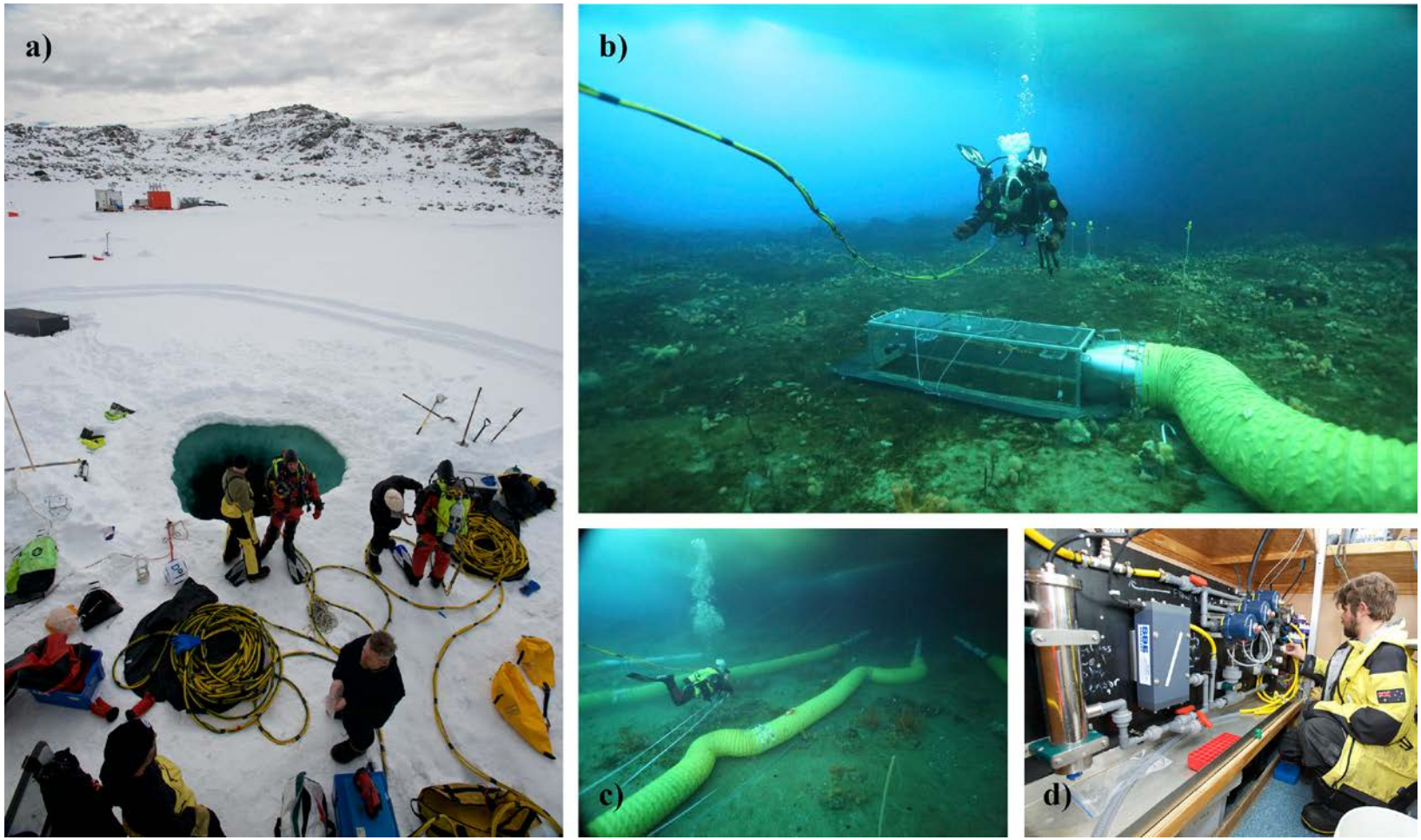

Figure 4.3 Photos of a) personnel preparing for a dive at the antFOCE field site, with the 'Silver Chalet', containing the surface sensor array, visible in the background next to the orange shipping container used to house the generator and CO_2 enriched seawater cylinder (Photo: N. Roden), b) a diver tending to one of the experimental chambers (Photo: AAD), c) the equilibration ducting with white thruster tubes attached (Photo: AAD), and d) the surface sensor array inside the Silver Chalet (Photo: N. Roden).

titrant (Dickson et al., 2007). Routine analysis of Certified Reference Material (batch 137) from Scripps Institution of Oceanography were used to verify the measurement accuracy and precision for DIC and TA analyses, which were better than ± 1.0 µmol kg^{-1} and ± 1.3 µmol kg^{-1}, respectively. Nutrient concentrations of nitrate (NO_3^-), nitrite (NO_2^-), phosphate (HPO_4^{2-}) and silicic acid (H_4SiO_4) were determined using standard colorimetic methods (Hansen & Koroleff, 2007), adapted for flow injection analysis on a SEAL AutoAnalyzer 3 HR, and yielded a measurement accuracy and precision of ± 0.4 µmol kg^{-1}, ± 0.01 µmol kg^{-1}, ± 0.06 µmol kg^{-1} and 3 µmol kg^{-1}, respectively.

pH electrodes in the antFOCE system were calibrated using calculated pH_{sws} values (accuracy and precision ± 0.005 pH units, based on propagated uncertainties of measured parameters), that were determined approximately every three days. The pH_{sws} values were calculated using discrete measurements of total dissolved inorganic carbon (DIC), total alkalinity (TA) and nutrients using the standard set of carbonate system equations with the CO2SYS program (van Heuven et al., 2011) and the dissociation constants of Roy et al. (1993). Due to minimal drift in the Honeywell Durafet sensor (stability better than 0.005 pH units over weeks to months; Martz et al., 2010), a mean offset correction was applied based on all calibration samples. Significant sensor drift occurred in the Seabird SBE 18 electrodes, which required an alternative calibration procedure, whereby it was assumed that the sensor drift was linearly proportional in time. However, this procedure did not significantly improve the data quality. It was determined that the drift was random in nature and unable to be corrected. As such, only the Honeywell Durafet data are considered here.

Two SeapHOx units (Martz et al., 2010; Bresnahan et al., 2014) were deployed on the seafloor in O'Brien Bay to measure ambient pH, dissolved oxygen, temperature and salinity at 1-hour intervals from 16 December 2014 to 28 February 2015. The units were located in 13 metres of water: one adjacent to the thruster tubes of the antFOCE system (experiment site), used to characterize the ambient seawater conditions, and the other ~300 metres further towards the mouth of O'Brien Bay (outer O'Brien Bay; Figure 4.1) to asses variability within the bay. Honeywell Durafet pH sensors inside the SeapHOx units were calibrated using the approach described previously, by collecting samples with a Niskin bottle. Oxygen optodes (Aanderaa, model 3835) were calibrated at the Commonwealth, Scientific and Industrial Research Organisation (CSIRO) Ocean Carbon Laboratory in Hobart, Tasmania, before and

after deployments using Winkler titrations. The calibration data were used to fit the optode response to a Stern-Volmer equation (Uchida et al., 2008), and yielded an accuracy and precision of ± 2 µmol kg^{-1}. Data from the oxygen optode in the surface sensor array were affected by air bubbles trapped inside its housing and are not considered any further in this study. The oxygen concentration at saturation was determined from atmospheric pressure, seawater temperature and salinity measurements (García & Gordon, 1992, 1993). Temperature and salinity were measured using two SBE 37-SI MicroCAT conductivity and temperature recorders that were calibrated at the CSIRO Oceanographic Calibration Facility in Hobart, Tasmania, and yielded an accuracy and precision of ± 0.002°C and 0.004, respectively.

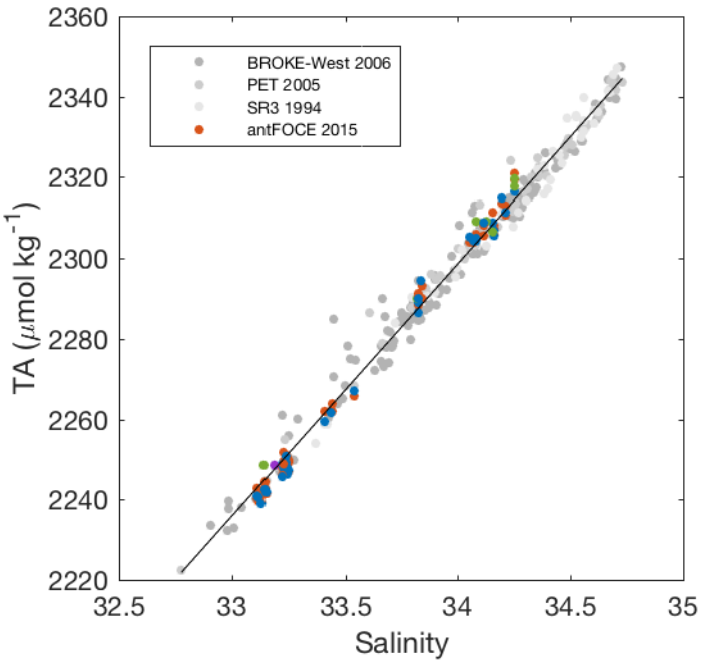

Figure 4.4 The salinity and TA relationship of waters south of 60°S and shallower than 500 m from BROKE-West in 2006, the Princess Elizabeth Trough in 2005 (PET) and from the WOCE SR3 transect, measured in 1994 (data available from GLODAPv2) along with values measured in this study (coloured dots; red = experimental chambers, blue = control chambers, green = ambient seawater, purple = outer O'Brien Bay). A linear regression yielded the following equation, $y = (62.8 \pm 0.4)x + (163 \pm 13)$ (n = 340, $r^2 = 0.99$, standard error = 4 µmol kg^{-1}).

TA data from this study were combined with data from previous studies in the Southern Ocean that used the same measurement techniques, and a linear regression

of salinity versus TA was calculated. This relationship (Figure 4.4) was used to calculate TA from high-resolution salinity measurements. Data used to calculate the regression were from samples shallower than 500 m and south of 60°S and included measurements from the CO_2/World Ocean Circulation Experiment (WOCE) hydrographic sections of the nearby Princess Elizabeth Trough in 2005, measurements from the southern end of the 1994 WOCE SR3 transect along 140°E, and measurements from the Baseline Research on Oceanography, Krill and the Environment – West (BROKE-West) study in 2006 (Roden et al., 2016). The correlation between the parameters in Figure 4.4 ($y = (62.8 \pm 0.4)x + (163 \pm 13)$; n = 340, $r^2 = 0.99$, standard error = 4 μmol kg^{-1}) shows that much of the TA variability was caused by freshwater fluxes and indicates that net calcification/dissolution of carbonate minerals in the water column was not a significant contributor to the TA variability, as discussed later in Section 4.3.1. The saturation state of aragonite (Ω_{ar}) (Mucci, 1983) and the fugacity of CO_2 (fCO_2) were calculated from high-resolution measurements of pH_{sws}, calculated TA, and the mean phosphate and silicic acid concentrations measured throughout the experimental period of 1.8 ± 0.2 μmol kg^{-1} and 50 ± 9 μmol kg^{-1}, respectively. Propagating the uncertainties associated with these measured and calculated input parameters, we estimate an uncertainty of ± 0.01 for Ω_{ar} and ± 8 μatm for fCO_2.

4.3 Results

4.3.1 System performance

The weekly values of biogeochemical parameters in the antFOCE system, measured from 19 December 2014 to 27 February 2015, are summarized in Tables 4.1, 4.2 and 4.3 and illustrated in Figure 4.5. The antFOCE deployment period is divided into two separate phases, a two-week acclimatization phase and an eight-week experimental phase. During the acclimatization phase, the pH of the experimental chambers was slowly lowered by incrementally increasing the amount of ESW being fed into the chambers until the target pH reduction of 0.4 from the control chambers was reached. During the eight-week experimental phase, a mean pH offset of -0.383 ± 0.066 and -0.382 ± 0.065 was achieved for chambers A and B, respectively. This resulted in mean undersaturated Ω_{ar} values of 0.62 ± 0.15 and 0.62 ± 0.13 (Table 4.2) and mean fCO_2 values of 914 ± 159 μatm and 911 ± 150 μatm (Table 4.3) for both experimental

chambers. The control chambers during the experimental phase had a mean Ω_{ar} of 1.39 ± 0.11 (1 s.d.). The mean fCO_2 value of the control chambers were 354 ± 42 µatm (1 s.d.), which, like fCO_2 values in the ambient environment, were undersaturated with respect to the mean atmospheric fCO_2 value of 379 ± 3 µatm (1 s.d.).

A comparison of measured TA values in the experimental and control chambers showed no detectable increases in TA as a result of $CaCO_3$ dissolution (Figure 4.4), despite the experimental chambers having undersaturated Ω_{ar} values. This was initially determined by normalising (*n*) the sum of TA and nitrate (TA+N) concentrations to the mean salinity of 33.645 observed during the antFOCE deployment period. This accounts for changes in these parameters as a result of freshwater input/removal and assumes that TA, nutrients and salinity change in proportion to each other. Summing the concentrations of TA and nitrate accounts for changes in TA associated with the uptake or release of dissolved nitrate during photosynthesis or respiration (Brewer & Goldman, 1976). Consequently, both the experimental and control chambers had similar mean *n*TA+*n*N values of 2302 ± 3 µmol kg^{-1} (1 s.d.; n = 57) and 2301 ± 3 µmol kg^{-1} (1 s.d.; n = 28), respectively. This result is not unexpected given the short residence time of water within the chambers of ~66 seconds. If we assume a maximum dissolution rate (Archer et al., 1989), porosity and carbonate content within the sediments (<10% by volume), the expected flux of alkalinity due to $CaCO_3$ dissolution equates to only 0.0009 µmol L^{-1}, which would be undetectable given the given the accuracy and precision of the TA measurements themselves (± 1.3 µmol kg^{-1}).

During the acclimatization and experimental phases, the system experienced a series of power outages and stoppages due to equipment failure. The failure of the onsite power generator, which was thought to be due to a faulty oil pressure sensor, caused the majority of these outages except for two occasions, where the failure of individual thrusters resulted in system stoppages. Divers replaced the damaged thrusters and the system was restarted within 24 hours. During these system stoppages, CO_2 system parameters within the experimental chambers would slowly revert back to ambient conditions until the system could be restarted again. Because measuring the pH of the chambers relied on an external power supply, we were unable to characterize the biogeochemical conditions within the chambers during these system stoppages.

Therefore, the results we report here represent the conditions within the antFOCE chambers from when the system was actually running. Upon restarting the experimental system the pH would gradually be brought back to the desired offset. Depending on how long the system had been down for, this would usually be achieved over a 2-4 hour period. Over the 14 day acclimatization period, 8.55 days were lost due to system stoppages, and over the 56 day experimental period 12.19 days were lost due to system stoppages (downtime), as indicated by the grey bars on Figure 4.5 and summarized in Tables 4.1, 4.2 and 4.3.

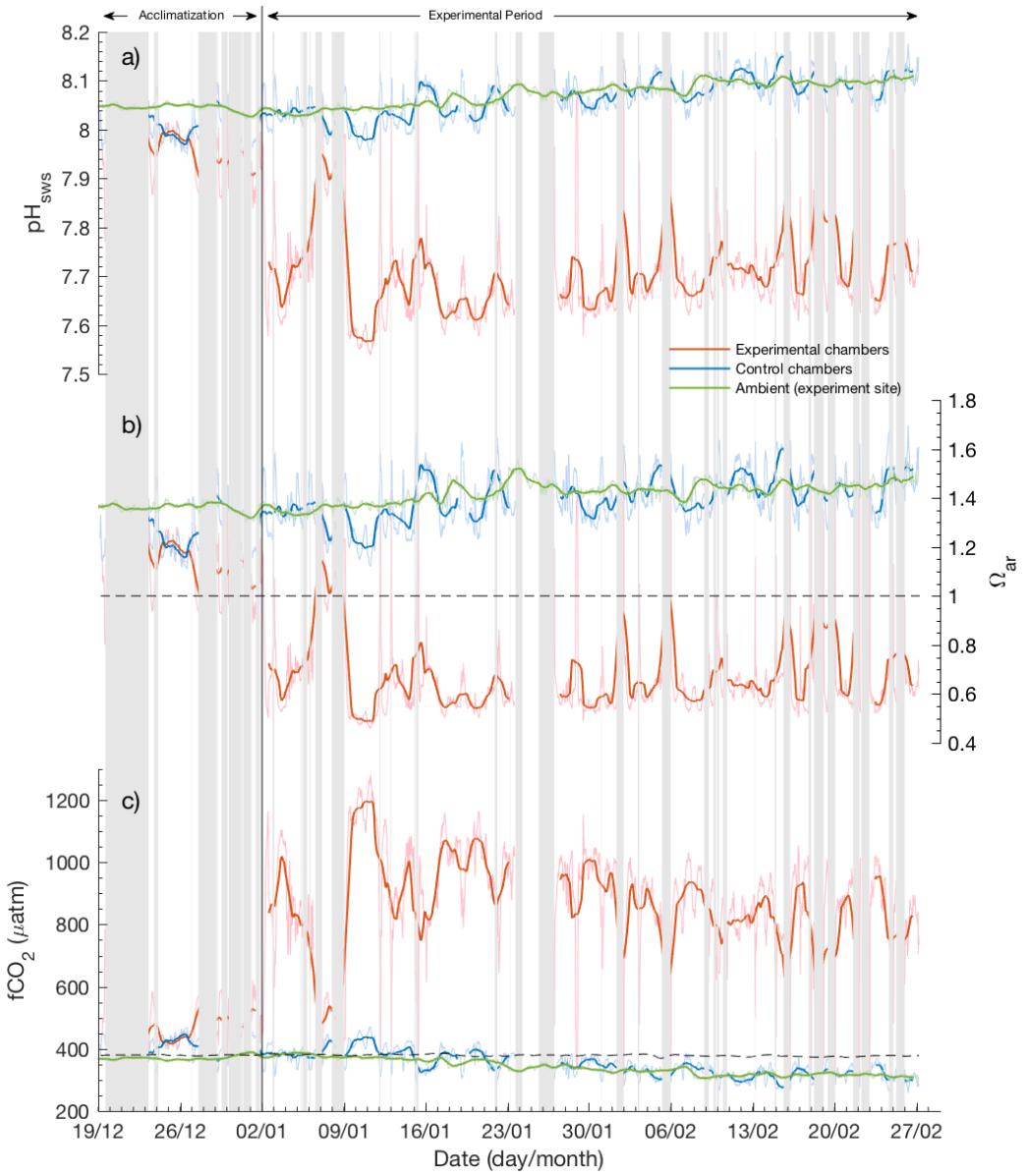

Figure 4.5 a) Measured pH_{sws}, b) calculated saturation state or aragonite (Ω_{ar}) and c) calculated fugacity of CO_2 (fCO_2) (µatm) of seawater with atmospheric fCO_2 (dashed line) of ambient (green line; experiment site), experimental chambers (red line; mean of chambers A and B) and control chambers (blue line; chambers C and D combined) during the antFOCE acclimatization and experimental periods. Lighter coloured lines show high-resolution measurements, with darker coloured lines showing 24-hour low-pass (moving average) filtered data. The grey bars represent periods of experimental system downtime.

Table 4.1 Weekly summary of mean pH_{sws} values (± 1 s.d.) during the acclimatization (19 December 2014 – 2 January 2015) and experimental (2 January 2015 – 27 February 2015) periods of the antFOCE experiment with the total number of downtime days (system stoppages) for each corresponding week and period.

	Ambient (experiment site)	**Control chambers**	**$Offset_{cont-amb}$**	**Experimental chamber (A)**	**$Offset_{exp-cont}$ chamber (A)**	**Experimental chamber (B)**	**$Offset_{exp-cont}$ chamber (B)**	**Downtime (*total days*)**
Acclimatization period								
Week 1	8.047 ± 0.005	7.991 ± 0.019	-0.059 ± 0.020	7.972 ± 0.060	-0.020 ± 0.058	7.974 ± 0.053	-0.017 ± 0.053	*4.15*
Week 2	8.042 ± 0.010	7.998 ± 0.037	-0.049 ± 0.037	7.941 ± 0.057	-0.059 ± 0.067	7.938 ± 0.051	-0.058 ± 0.056	*4.40*
Mean	8.045 ± 0.008	7.994 ± 0.029	-0.054 ± 0.030	7.957 ± 0.060	-0.038 ± 0.065	7.958 ± 0.055	-0.036 ± 0.058	*8.55*
Experimental period								
Week 1	8.037 ± 0.008	8.029 ± 0.032	-0.006 ± 0.035	7.742 ± 0.110	-0.290 ± 0.113	7.746 ± 0.105	-0.285 ± 0.109	*2.26*
Week 2	8.046 ± 0.006	8.017 ± 0.041	-0.029 ± 0.040	7.638 ± 0.091	-0.381 ± 0.057	7.648 ± 0.088	-0.370 ± 0.056	*0.44*
Week 3	8.058 ± 0.011	8.048 ± 0.031	-0.010 ± 0.031	7.653 ± 0.050	-0.395 ± 0.028	7.648 ± 0.050	-0.400 ± 0.027	*0.22*
Week 4	8.077 ± 0.010	8.060 ± 0.026	-0.015 ± 0.028	7.672 ± 0.096	-0.391 ± 0.074	7.681 ± 0.097	-0.382 ± 0.076	*2.03*
Week 5	8.084 ± 0.007	8.075 ± 0.030	-0.009 ± 0.031	7.677 ± 0.063	-0.402 ± 0.025	7.675 ± 0.051	-0.400 ± 0.026	*1.49*
Week 6	8.095 ± 0.015	8.093 ± 0.033	-0.003 ± 0.032	7.699 ± 0.062	-0.392 ± 0.054	7.694 ± 0.051	-0.399 ± 0.032	*1.10*
Week 7	8.096 ± 0.008	8.092 ± 0.035	-0.004 ± 0.032	7.694 ± 0.081	-0.405 ± 0.034	7.695 ± 0.073	-0.401 ± 0.041	*2.32*
Week 8	8.101 ± 0.008	8.093 ± 0.032	-0.009 ± 0.030	7.694 ± 0.072	-0.402 ± 0.042	7.691 ± 0.060	-0.404 ± 0.033	*2.33*
Mean	8.074 ± 0.025	8.061 ± 0.044	-0.011 ± 0.034	7.680 ± 0.085	-0.383 ± 0.066	7.681 ± 0.078	-0.382 ± 0.065	*12.19*

Table 4.2 Weekly summary of mean aragonite saturation state (Ω_{ar}) values (± 1 s.d.) during the acclimatization (19 December 2014 – 2 January 2015) and experimental (2 January 2015 – 27 February 2015) periods of the antFOCE experiment with the total number of downtime days (system stoppages) for each corresponding week and period.

	Ambient (experiment site)	**Control chambers**	**Offset$_{cont-amb}$**	**Experimental chamber (A)**	**Offset$_{exp-cont}$ chamber (A)**	**Experimental chamber (B)**	**Offset$_{exp-cont}$ chamber (B)**	**Downtime (*total days*)**
Acclimatization period								
Week 1	1.36 ± 0.01	1.21 ± 0.05	-0.16 ± 0.05	1.17 ± 0.14	-0.04 ± 0.13	1.17 ± 0.11	-0.04 ± 0.10	*4.15*
Week 2	1.36 ± 0.02	1.24 ± 0.10	-0.13 ± 0.10	1.10 ± 0.13	-0.14 ± 0.16	1.09 ± 0.12	-0.14 ± 0.13	*4.40*
Mean	1.36 ± 0.02	1.22 ± 0.08	-0.15 ± 0.08	1.14 ± 0.14	-0.09 ± 0.15	1.14 ± 0.12	-0.08 ± 0.13	*8.55*
Experimental period								
Week 1	1.35 ± 0.02	1.33 ± 0.09	-0.02 ± 0.10	0.74 ± 0.19	-0.60 ± 0.21	0.75 ± 0.18	-0.59 ± 0.2	*2.26*
Week 2	1.38 ± 0.02	1.30 ± 0.11	-0.08 ± 0.11	0.58 ± 0.15	-0.72 ± 0.09	0.60 ± 0.14	-0.70 ± 0.09	*0.44*
Week 3	1.42 ± 0.04	1.39 ± 0.09	-0.03 ± 0.09	0.60 ± 0.07	-0.79 ± 0.05	0.59 ± 0.07	-0.80 ± 0.05	*0.22*
Week 4	1.46 ± 0.04	1.39 ± 0.07	-0.04 ± 0.08	0.62 ± 0.18	-0.78 ± 0.14	0.63 ± 0.19	-0.77 ± 0.14	*2.03*
Week 5	1.43 ± 0.02	1.40 ± 0.09	-0.03 ± 0.09	0.60 ± 0.11	-0.81 ± 0.05	0.60 ± 0.08	-0.81 ± 0.05	*1.49*
Week 6	1.44 ± 0.03	1.43 ± 0.09	-0.01 ± 0.09	0.62 ± 0.11	-0.80 ± 0.11	0.61 ± 0.09	-0.82 ± 0.08	*1.10*
Week 7	1.44 ± 0.02	1.43 ± 0.10	-0.01 ± 0.10	0.62 ± 0.15	-0.82 ± 0.07	0.62 ± 0.13	-0.82 ± 0.09	*2.32*
Week 8	1.46 ± 0.03	1.44 ± 0.10	-0.03 ± 0.09	0.62 ± 0.14	-0.82 ± 0.10	0.61 ± 0.11	-0.83 ± 0.08	*2.33*
Mean	1.42 ± 0.05	1.39 ± 0.11	-0.03 ± 0.10	0.62 ± 0.15	-0.77 ± 0.13	0.62 ± 0.13	-0.77 ± 0.13	*12.19*

Table 4.3 Weekly summary of mean fugacity of carbon dioxide (fCO_2) (µatm) values (± 1 s.d.) during the acclimatization (19 December 2014 – 2 January 2015) and experimental (2 January 2015 – 27 February 2015) periods of the antFOCE experiment with the total number of downtime days (system stoppages) for each corresponding week and period.

	Ambient (experiment site)	**Control chambers**	**Offset$_{cont-amb}$**	**Experimental chamber (A)**	**Offset$_{exp-cont}$ chamber (A)**	**Experimental chamber (B)**	**Offset$_{exp-cont}$ chamber (B)**	**Downtime (*total days*)**
Acclimatization period								
Week 1	368 ± 4	425 ± 20	59 ± 20	450 ± 75	26 ± 74	446 ± 84	23 ± 87	*4.15*
Week 2	374 ± 9	419 ± 37	49 ± 38	485 ± 69	69 ± 80	487 ± 62	67 ± 66	*4.40*
Mean	371 ± 8	422 ± 29	55 ± 30	466 ± 74	46 ± 79	465 ± 77	43 ± 81	*8.55*
Experimental period								
Week 1	379 ± 7	387 ± 31	7 ± 34	810 ± 203	428 ± 202	801 ± 191	417 ± 190	*2.26*
Week 2	370 ± 6	400 ± 39	30 ± 39	1028 ± 189	631 ± 149	1003 ± 179	605 ± 141	*0.44*
Week 3	359 ± 10	369 ± 29	10 ± 29	979 ± 110	610 ± 85	990 ± 112	622 ± 86	*0.22*
Week 4	340 ± 9	354 ± 23	13 ± 24	938 ± 155	589 ± 127	919 ± 153	569 ± 128	*2.03*
Week 5	329 ± 6	338 ± 26	8 ± 26	908 ± 112	575 ± 74	908 ± 97	571 ± 69	*1.49*
Week 6	319 ± 13	321 ± 28	3 ± 26	855 ± 106	530 ± 93	861 ± 92	541 ± 66	*1.10*
Week 7	318 ± 7	321 ± 28	4 ± 26	868 ± 129	556 ± 79	865 ± 121	549 ± 86	*2.32*
Week 8	314 ± 7	321 ± 26	8 ± 24	868 ± 111	550 ± 75	872 ± 100	553 ± 67	*2.33*
Mean	341 ± 25	354 ± 42	11 ± 31	914 ± 159	564 ± 130	911 ± 150	559 ± 124	*12.19*

4.3.2 Ambient variability

The mean values of carbonate system parameters within the control chambers throughout the experimental period, when considered over weekly intervals, were largely the same as values observed in the ambient environment (Tables 4.1, 4.2 and 4.3). The control chambers however, showed significantly more diel variability compared to ambient values (Table 4.4). The mean diel change of pH_{sws} in the ambient environment was 0.020 ± 0.008 (1 s.d.), compared to 0.077 ± 0.027 (1 s.d.) for the control chambers. A comparison of changes in pH_{sws} and oxygen concentration within the ambient environment itself showed that pH and oxygen at the outer O'Brien Bay site was generally higher than the values observed near the experiment site. These changes are summarized in Tables 4.4 and 4.5 and illustrated in Figures 4.6 and 4.7. Sea-ice cover of different thickness and age characterized these two locations, with multi-year sea ice over the experimental site measuring 260 cm in thickness, and first-year ice over the outer O'Brien Bay site measuring 150 cm in thickness at the start of the season.

The measured ambient pH_{sws} at both sites generally increased during the deployment period with a seasonal range of 8.019 to 8.130 pH units at the experimental site and 8.045 to 8.192 units at the outer O'Brien Bay site (Figure 4.6a). Higher pH levels and an increase in short-term (diel) variability as the season progressed, characterized the outer site. This increase in diel variability (Figure 4.7b), compared to the experiment site (Figure 4.7a), is also observed in the dissolved oxygen concentration (Figure 4.7c and 4.7d), which had a seasonal range of 333 to 374 µmol kg^{-1} at the experiment site and 335 to 400 µmol kg^{-1} at the outer site. Oxygen concentration at both sites peaked in late-January (Figure 4.6b) just before a significant decrease in salinity was observed throughout the bay (Figure 4.6d).

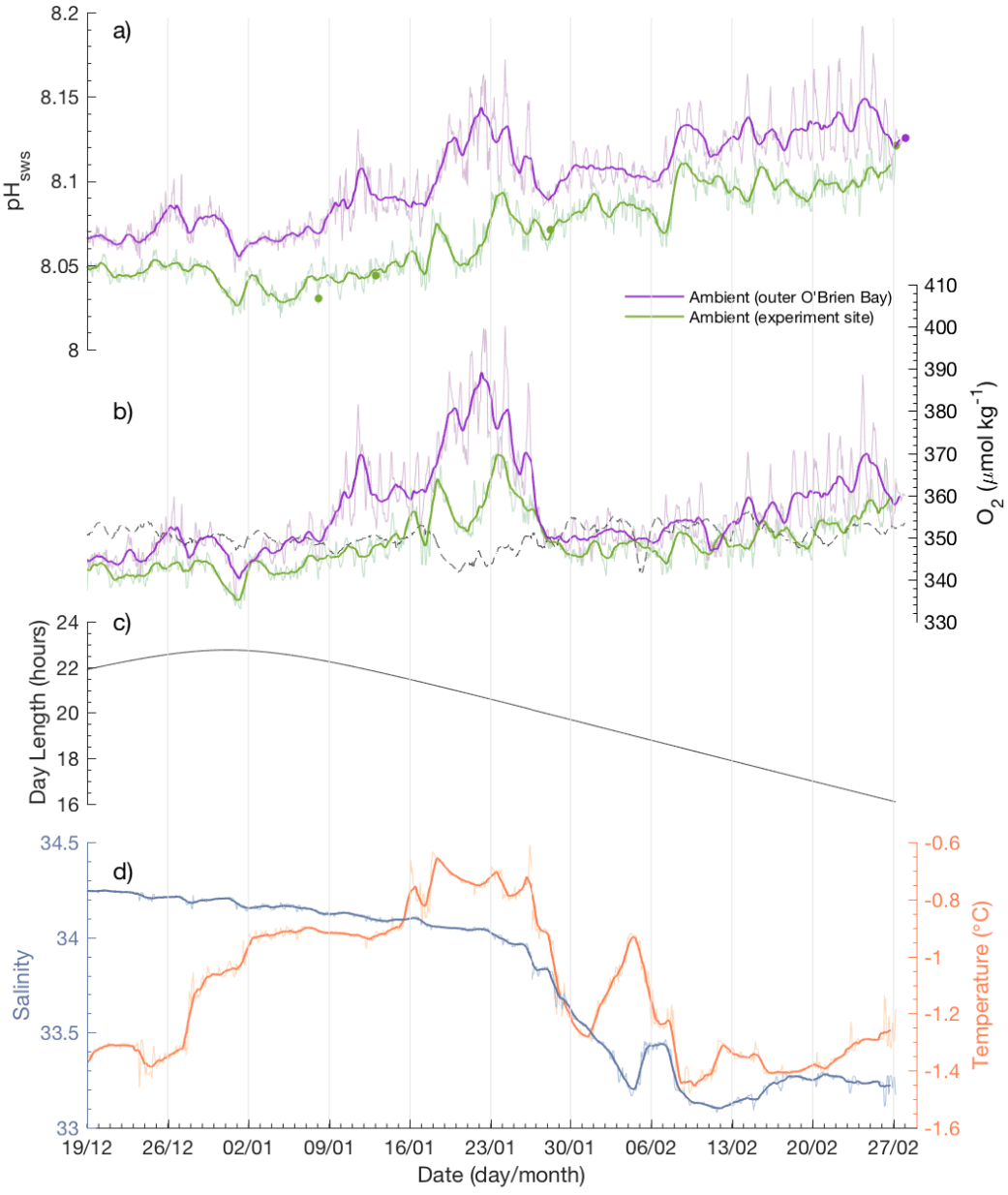

Figure 4.6 Ambient measurements between 19 December 2014 and 28 February 2015 of a) pH_{sws} (dots show calibration points) and b) dissolved oxygen (µmol kg^{-1}) with oxygen saturation (dashed line), c) day length (hours) and d) salinity and temperature (°C) from the experiment site. Lighter coloured lines show high-resolution measurements, with darker coloured line showing 24-hour low-pass (moving average) filtered data.

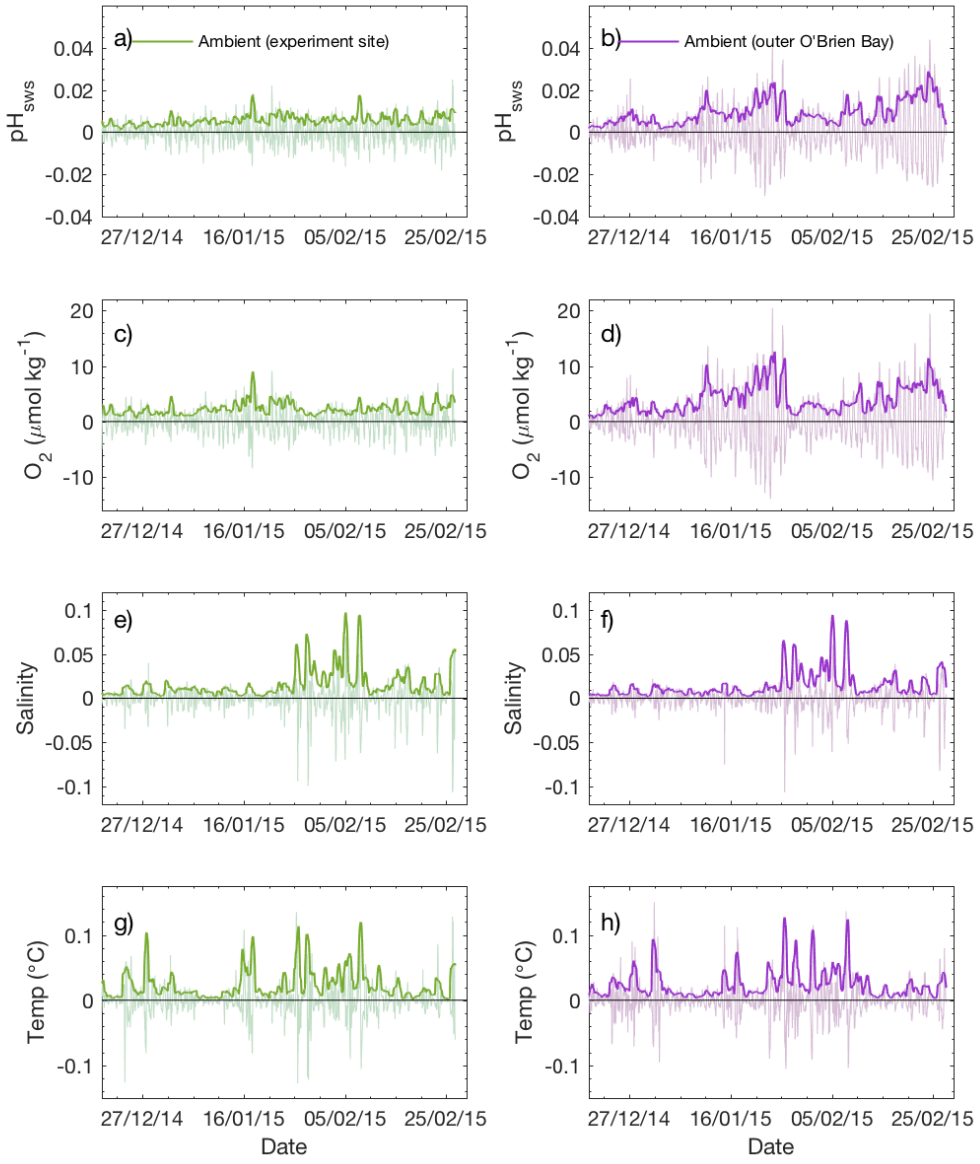

Figure 4.7 High-pass filtered pH_{sws} (a and b), dissolved oxygen (µmol kg^{-1}; c and d), salinity (e and f) and temperature (°C; g and h). The zero represents a moving 24-hour average value at any given time. Darker coloured lines are the s.d. of 24-hour moving average of the high-frequency data (lighter coloured lines).

Table 4.4 Summary of daily changes within O'Brien Bay (19 December 2014 – 27 February 2015) of seawater pH_{sws}, dissolved oxygen (µmol kg^{-1}), calculated dissolved inorganic carbon (µmol kg^{-1}), saturation state of aragonite (Ω_{ar}), fugacity of CO_2 (fCO_2) (µatm), salinity and temperature (°C).

	pH_{sws}	O_2 (µmol kg^{-1})	DIC (µmol kg^{-1})	Ω_{ar}	fCO_2 (µatm)	Salinity	Temp (°C)
Ambient (experiment site)							
Minimum range	0.008	3	3	0.02	8	0.007	0.008
Maximum range	0.049	23	22	0.16	44	0.226	0.301
Mean range (± 1 s.d.)	0.020 ± 0.008	8 ± 3	9 ± 4	0.06 ± 0.02	18 ± 7	0.050 ± 0.048	0.076 ± 0.069
Ambient (outer O'Brien Bay)							
Minimum range	0.007	4	2	0.02	6	0.004	0.012
Maximum range	0.073	33	28	0.24	52	0.221	0.343
Mean range (± 1 s.d.)	0.029 ± 0.016	13 ± 7	11 ± 6	0.09 ± 0.05	23 ± 12	0.046 ± 0.045	0.082 ± 0.067
Control chambers							
Minimum range	0.014	-	5	0.04	10	-	-
Maximum range	0.127	-	47	0.37	115	-	-
Mean range (± 1 s.d.)	0.077 ± 0.027	-	28 ± 10	0.22 ± 0.08	69 ± 25	-	-
Experimental chamber (A)							
Minimum range	0.039	-	12	0.04	43	-	-
Maximum range	0.535	-	167	1.13	891	-	-
Mean range (± 1 s.d.)	0.242 ± 0.17	-	73 ± 52	0.46 ± 0.36	390 ± 246	-	-
Experimental chamber (B)							
Minimum range	0.046	-	14	0.07	49	-	-
Maximum range	0.545	-	167	1.1	835	-	-
Mean range (± 1 s.d.)	0.231 ± 0.16	-	69 ± 49	0.43 ± 0.34	382 ± 233	-	-

Table 4.5 Summary of ambient seasonal values within O'Brien Bay (19 December 2014 – 27 February 2015) of seawater pH_{sws}, dissolved oxygen (µmol kg^{-1}), calculated dissolved inorganic carbon (µmol kg^{-1}), saturation state of aragonite (Ω_{ar}), fugacity of CO_2 (fCO_2) (µatm), salinity and temperature (°C).

	pH_{sws}	O_2 (µmol kg^{-1})	DIC (µmol kg^{-1})	Ω_{ar}	fCO_2 (µatm)	Salinity	Temp (°C)
Ambient (experiment site)							
Minimum	8.019	333	2105	1.30	291	33.079	-1.479
Maximum	8.130	374	2206	1.55	397	34.257	-0.609
Range	0.112	41	100	0.25	106	1.178	0.870
Mean (± 1 s.d.)	8.068 ± 0.025	348 ± 7	2166 ± 32	1.41 ± 0.05	348 ± 26	33.785 ± 0.430	-1.120 ± 0.242
Ambient (outer O'Brien Bay)							
Minimum	8.045	335	2089	1.37	249	33.088	-1.466
Maximum	8.192	400	2196	1.79	371	34.256	-0.639
Range	0.146	65	107	0.42	122	1.168	0.827
Mean (± 1 s.d.)	8.100 ± 0.028	356 ± 11	2153 ± 32	1.51 ± 0.07	320 ± 25	33.776 ± 0.432	-1.112 ± 0.243

4.4 Discussion

4.4.1 Manipulation of carbonate chemistry

The antFOCE system, in line with the xFOCE goals, reduced pH and maintained a pH offset in the experimental chambers that closely tracked the variation observed in the control chambers (Figure 4.8). This offset does not include periods where power and equipment failures resulted in system outages. As a result, the diel variability in the experimental chambers was often larger than the seasonal variability observed at other Antarctic coastal sites (e.g. Gibson & Trull, 1999; Roden et al., 2013; Legge et al., 2015). In a global context this diel variability was not as extreme as the short-term pH variability (days to weeks) observed in many other coastal ecosystems, including kelp forests (range: 0.544), estuaries (range: 0.992), upwelling systems (range: 0.467) and CO_2 vents (range: 1.43) (Hofmann et al., 2011).

Although these system outages will provide challenges in interpreting the biological responses in the experimental chambers, it is possible that these large pH fluctuations could provide unexpected insights into the resilience of Antarctic benthic communities to rapid changes in environmental conditions. Particularly as future pH variability is expected to increase as a result of the reduced buffer capacity of seawater as more CO_2 is absorbed from the atmosphere. The effects of this reduced buffer capacity were not immediately observed in the experimental chambers because the pH values were engineered to track the natural variability inside the control chambers. Understanding how diel and seasonal changes in dissolved CO_2 parameters will manifest themselves in response to future ocean acidification is of great interest to the biogeochemistry community. FOCE technology, therefore, could provide a useful tool for investigating these future changes.

The pH of the control chambers had greater variability than that measured in the ambient environment. A similar observation was made by Cox et al. (2016) in the European FOCE experiment conducted on a seagrass meadow, where the median diel pH variation was 75% greater in the control chambers compared to the ambient environment. The mean diel pH variation in our control chambers was as much as 285% greater (Table 4.4). This variation could have been due to the influence of the chambers themselves on the enclosed biological communities, or alternatively, biological activity or gas exchange (bubbles) within the sample lines may have

contributed to the observed changes. It is unlikely that other physical processes within the sample lines, such as warming, could be responsible for such variations in pH, as temperature changes caused by the heat trace in the sample lines (~3°C of warming) for example, were accounted for when adjusting measured pH values to in-situ conditions. The small volume of air that was occasionally observed in the sample hoses may have contaminated seawater sampled from the chambers, although this volume of air was very small when compared to the volume of water being sampled. Furthermore, a comparison of calculated pH_{sws} from samples of DIC, TA and nutrients, simultaneously collected from the surface sampling system and from inside one of the control chambers with a Niskin bottle, agreed to within 0.001 pH units. This indicates that the carbonate chemistry of seawater as it was pumped from the chambers to the surface sensor array did not change significantly and suggests that much of the difference between the ambient pH and the pH measured in the antFOCE chambers was caused by greater variability in biological production inside the chambers themselves.

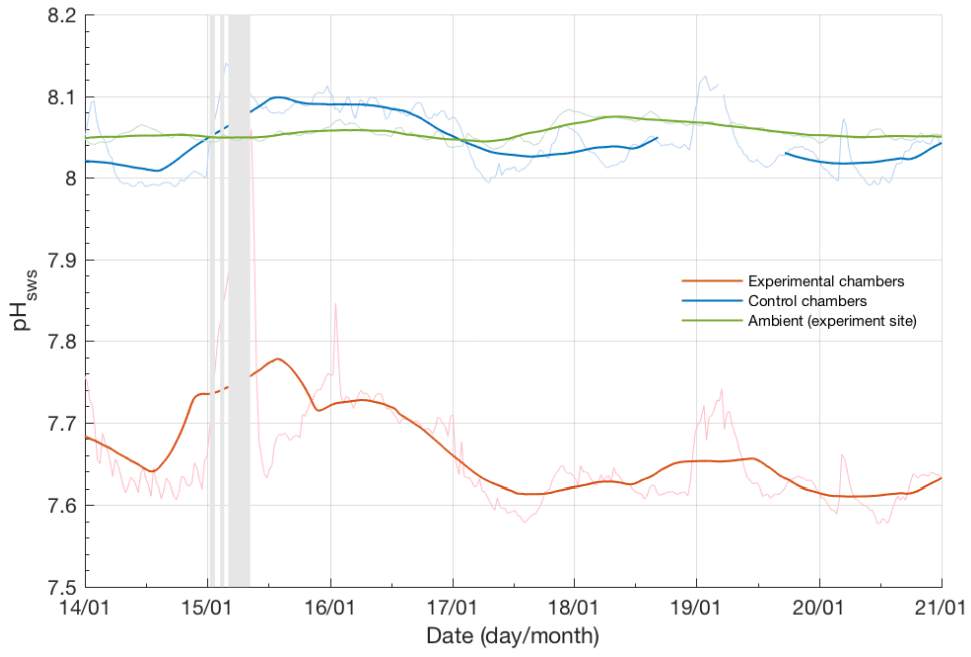

Figure 4.8 Measured pH_{sws} over 7 days (14 January 2015 – 21 January 2015) of ambient (green line; experiment site), experimental chambers (red line; mean of chambers A and B) and control chambers (blue line; chambers C and D combined) during the antFOCE experimental period. Lighter coloured lines show high-resolution measurements, with darker coloured lines showing 24-hour low-pass (moving average) filtered data. The grey bars represent periods of experimental system downtime.

Power outages causing system shutdowns, were the main technical problems in the antFOCE system. These were attributable, post experiment, to a faulty oil pressure sensor in the power generator. These outages resulted in increased variability in pH experienced in the experimental chambers, with numerous (Table 4.1) periods where pH reverted back to ambient or between the desired offset and ambient. Implementing power redundancies (e.g. battery backup) into future system designs could reduce the impact of power outages on experimental integrity.

During periods when the antFOCE system was functioning normally, conditions in the experimental chambers represented a significant departure from conditions likely to be experienced over a full annual cycle (e.g. Gibson & Trull, 1999; Roden et al., 2013; Legge et al., 2015; Kapsenberg et al., 2015). A seasonal cycle of carbonate chemistry in coastal Antarctica typically features pH values elevated by primary production in summer and lower values during winter driven by net heterotrophy. At McMurdo station in the Ross Sea for example, coastal pH ranges from 7.93 in June to 8.24 in January, with Ω_{ar} in January ranging from 1.79 to 2.03, while in June it reaches 1.03 (Kapsenberg et al., 2015). At Davis station, East Antarctica, as discussed in Chapter 3, carbonate system parameters were measured between May and February, and the natural seasonal cycle of pH was found to vary from a low of 7.99 in September to 8.20 in January, while Ω_{ar} varied from 1.19 to 1.92 seasonally (Roden et al., 2013).

This seasonal cycle is an important consideration for future FOCE experiments in polar regions, as experimental treatments based on an offset from summer conditions alone may not fully capture the extremes in carbonate chemistry that organisms will be exposed to under future atmospheric CO_2 scenarios. For example, a -0.4 pH offset from ambient conditions maintained over a full year could result in pH levels as low as 7.53 in late winter. This is particularly relevant for organisms, such as pteropods, that have life cycles across multiple seasons (Bednaršek et al., 2012), Antarctic invertebrates with sensitive larval stages (Peck et al., 2004; Peck, 2005), or organisms with extremely slow development times (Peck et al., 2007). Laboratory based ocean acidification experiments have shown adverse affects to the larval stages of Antarctic invertebrates at pH levels of 7.6 – 7.8 (Byrne et al., 2013; Gonzalez-Bernat et al., 2013; Yu et al., 2013), which suggests that the timing of key life stages in relation to

future changes in the seasonal cycle of carbonate chemistry will be important for an organism's survivability.

4.4.2 Short-term ambient variability

A comparison of ambient pH and dissolved oxygen concentration at two separate locations within O'Brien Bay demonstrates the spatially variable nature of carbonate chemistry within Antarctic coastal systems. This variability was most likely driven by different rates of biological productivity that was influenced by the different sea-ice regimes over each site. Thicker multi-year sea ice over the experiment site for example, would have reduced the amount of light available for photosynthetic communities in the local area, compared to the thinner first-year ice over the outer O'Brien Bay site. Differences in stratification or freshwater input are unlikely to be responsible, as a comparison of temperature and salinity at each site showed no significant differences. The outer site had an increased diel variability (Figure 4.7), particularly later in the season, and generally elevated pH and dissolved oxygen values throughout the season compared to the experiment site (Figure 4.6). The dissolved oxygen concentration was, on average, 8 µmol kg^{-1} higher and the calculated DIC concentration ~13 µmol kg^{-1} lower at the outer site (Table 4.5). Dividing this difference in oxygen concentration by 1.4 allows this value to be expressed in terms of organic carbon production, or DIC uptake (Laws, 1991; Bender et al., 1999). For a photosynthetic oxygen production of 8 µmol kg^{-1}, an approximate decrease of 6 µmol kg^{-1} of DIC would be expected. This explains the majority of the offset observed between the two sites when the uncertainty of calculated DIC concentrations (± 4 µmol kg^{-1}) is considered.

4.5 Conclusion

This is the first in-situ experiment in a polar region to successfully simulate predictions of ocean acidification conditions in a controlled experiment and demonstrates the feasibility of FOCE systems, even under extreme conditions such as those experienced under sea ice in Antarctica. The antFOCE in-situ system overcomes many of the problems associated with mesocosm or laboratory based experiments including a lack of full community representation, disturbance to microbial communities, hydrodynamic isolation, food limitation or control, unnatural light, and lack of natural variation in carbonate system parameters. The use of a

FOCE system also alleviates extreme fluctuations associated with natural analogues such as CO_2 vents (Hall-Spencer et al., 2008; Basso et al., 2015), where carbonate system parameters, as a result of variable rates of CO_2 venting, can vary rapidly over a short period of time (hours to days).

The antFOCE system was not without its technical challenges. Equipment failure and problems with maintaining a reliable power supply to a remote location compromised the experimental integrity. These problems can largely be avoided in future FOCE designs through the implementation of power system redundancies, although these will increase the expense and complexity of the overall system. Aspects of the system that worked well include the use of the Honeywell Durafet pH sensors, which proved to be a reliable way to monitor pH in both the experimental sensor array and in the ambient environment. The monitoring of ambient conditions revealed local variations in pH and dissolved oxygen concentration that were most likely caused by differences in biological productivity. Understanding local variability and the natural range of exposures that organisms are already subjected to could help improve future FOCE experiments and provide a deeper understanding of the effects of ocean acidification.

Acknowledgments

NR was supported by an Australian Postgraduate Award and a CSIRO Oceans and Atmosphere scholarship. The antFOCE project was funded by the Antarctic Gateway Partnership and supported by the Australian Antarctic Division, the Institute for Marine and Antarctic Studies, CSIRO Oceans and Atmosphere, the Monterey Bay Aquarium Research Institute and Plymouth Marine Laboratory. NR participated in fieldwork, managed the carbonate chemistry laboratory measurements and analysis, helped with SeapHOx deployment and data processing and was the primary author of this Chapter. NR would like to thank the dedicated team of commercial and scientific divers, engineers, and science technical support staff who contributed to the development and deployment of the antFOCE system. He would also like to thank Kate Berry and Erik van Ooijen for carbon analysis and technical support in the field as well as the personnel at Casey station for their logistical support throughout the field season.

5 Conclusion

The biogeochemical dynamics in the seasonal sea ice zone (SIZ) of East Antarctica were investigated across different spatial and temporal scales. The SIZ was found to be a weak net source of CO_2 to the atmosphere of 0.07 ± 0.13 mol C m^{-2} during the ice-free period (November to February), which is lower than the zonally averaged climatology between 58-78°S of 0.14 ± 0.07 mol C m^{-2} $year^{-1}$ (Takahashi et al., 2009; Wanninkhof et al., 2013; Lenton et al., 2013). Waters over the shelf and north of the Southern Antarctic Circumpolar Current Front were sites of oceanic CO_2 uptake. This uptake was driven by strong biological productivity as observed from net community production estimates that were as high as 6.4 mol C m^{-2}. Although micronutrients were not measured, it is likely that this strong biological productivity over the shelf was sustained through their supply from a combination of sea-ice melt and oceanic sediment interactions. The largest CO_2 uptake was observed at a coastal location near Davis station, the magnitude of which, is commensurate with other coastal and shelf based estimates in East Antarctica and along the west Antarctic Peninsula. Further offshore, in the western sector of the study area, the warmer waters of the eastern extension of the Weddell Gyre dominated surface water biogeochemical dynamics, reducing gas solubility and causing CO_2 outgassing.

The timing of sea-ice formation and melt was an important control on the carbon cycle dynamics of the region. Wintertime under-ice estimates of fCO_2 indicated that the majority of the surface waters in the study region were supersaturated with respect to the atmosphere. Winter sea-ice cover and summer biological productivity, particularly over the shelf, reduced the flux of CO_2 from the ocean. The relatively brief ice-free period during summer appears to allow sufficient gas exchange, over annual timescales, for the surface waters of the region to track the atmospheric increase in CO_2. Although seasonal observations from Davis station, 16 years apart, suggest that decadal variability in biological productivity can also influence dissolved CO_2 system parameters beyond the changes expected from atmospheric uptake alone.

To determine the future impacts of ocean acidification on benthic communities in the Antarctic environment, the first Antarctic free-ocean CO_2 enrichment (antFOCE) experiment was conducted on the sea floor under multiyear sea ice near Casey station,

East Antarctica. The results show that it is possible to accurately change the carbonate chemistry of seawater in-situ to create predicted future ocean acidification conditions and demonstrates the feasibility of using FOCE systems in the Antarctic environment. Future iterations of FOCE technology should include redundancies for power supply and eventually introduce expected future stressors into the experimental design, such as temperature and freshening. The observed spatial variability of seawater chemistry in the local environment near Casey, and in the broader SIZ of East Antarctica, suggests that certain types of marine habitat may serve as summertime refugia from future ocean changes. Particularly those areas with elevated biological production (Shadwick et al., 2013). FOCE technology could provide a useful tool for testing this hypothesis, particularly when the natural variability in dissolved CO_2 system parameters of a study site has been fully characterised.

Currently, the capacity of the ocean in the SIZ to sequester CO_2 from the atmosphere to the ocean interior is strongly influenced by the presence of sea ice. However, because the observed changes to the East Antarctic sea ice are complex and are comprised of mixed signals on regional to local scales, making predictions about the future CO_2 source/sink nature of the SIZ is difficult. This is highlighted by the large variability in the drivers and timing of carbon cycling dynamics in this region. The future CO_2 uptake or outgassing in the study area will most likely depend on the response of the solubility and biological pumps to changes in sea-ice seasonality and the enhanced ventilation of carbon- and nutrient-rich deep water driven by strengthening winds over the Southern Ocean.

References

Álvarez, M., Ríos, A.F. & Rosón, G., 2002. Spatio-temporal variability of air–sea fluxes of carbon dioxide and oxygen in the Bransfield and Gerlache Straits during Austral summer 1995–96. *Deep Sea Research Part II: Topical Studies in Oceanography*, 49(4–5), pp.643–662.

Ambrose, D. & Lawrenson, I.J., 1972. The vapour pressure of water. *The Journal of Chemical Thermodynamics*, 4(5), pp.755–761.

Archer, D., Emerson, S. & Reimers, C., 1989. Dissolution of calcite in deep-sea sediments: pH and O_2 microelectrode results. *Geochimica et Cosmochimica Acta*, 53(11), pp.2831–2845.

Arrhenius, S., 1896. XXXI. On the influence of carbonic acid in the air upon the temperature of the ground. *Philosophical Magazine Series 5*, 41(251), pp.237–276.

Arrigo, K.R., van Dijken, G. & Long, M., 2008. Coastal Southern Ocean: A strong anthropogenic CO_2 sink. *Geophysical Research Letters*, 35, p.L21602.

Arrigo, K.R., van Dijken, G.L. & Bushinsky, S., 2008. Primary production in the Southern Ocean, 1997-2006. *Journal of Geophysical Research*, 113.

Arrigo, K.R., Robinson, D.H., Worthen, D.L., Dunbar, R.B., DiTullio, G.R., VanWoert, M. & Lizotte, M.P., 1999. Phytoplankton community structure and the drawdown of nutrients and CO_2 in the Southern Ocean. *Science*, 283, pp.365–367.

Arrigo, K.R., Worthen, D., Schnell, A. & Lizotte, M.P., 1998. Primary production in Southern Ocean waters. *Journal of Geophysical Research*, 103(C8), pp.15587–15600.

Atlas, R., Hoffman, R.N., Ardizzone, J., Leidner, S.M., Jusem, J.C., Smith, D.K. & Gombos, D., 2011. A Cross-calibrated, Multiplatform Ocean Surface Wind Velocity Product for Meteorological and Oceanographic Applications. *Bulletin of the American Meteorological Society*, 92(2), pp.157–174.

de Baar, H.J.W., de Jong, J.T.M., Bakker, D.C.E., Löscher, B.M., Veth, C., Bathmann, U. & Smetacek, V., 1995. Importance of iron for plankton blooms and carbon dioxide drawdown in the Southern Ocean. *Nature*, 373(6513), pp.412–415.

Bakker, D.C.E. et al., 2014. An update to the Surface Ocean CO_2 Atlas (SOCAT version 2). *Earth System Science Data*, 6(1), pp.69–90.

Bakker, D.C.E., de Baar, H.J.W. & Bathmann, U.V., 1997. Changes of carbon dioxide in surface waters during spring in the Southern Ocean. *Deep Sea Research Part II: Topical Studies in Oceanography*, 44(1–2), pp.91–127.

Bakker, D.C.E., Hoppema, M., Schröder, M., Geibert, W. & de Baar, H.J.W., 2008. A rapid transition from ice covered CO_2–rich waters to a biologically mediated CO_2 sink in the eastern Weddell Gyre. *Biogeosciences*, 5(5), pp.1373–1386.

Basso, L., Hendriks, I.E., Rodríguez-Navarro, A.B., Gambi, M.C. & Duarte, C.M., 2015. Extreme pH Conditions at a Natural CO_2 Vent System (Italy) Affect Growth, and Survival of Juvenile Pen Shells (Pinna nobilis). *Estuaries and Coasts*, 38(6), pp.1986–1999.

Bates, N.R., 2006. Air-sea CO_2 fluxes and the continental shelf pump of carbon in the Chukchi Sea adjacent to the Arctic Ocean. *Journal of Geophysical Research*, 111(C10013).

Bates, N.R., Hansell, D.A., Carlson, C.A. & Gordon, L.I., 1998. Distribution of CO_2 species, estimates of net community production, and air-sea CO_2 exchange in the Ross Sea polynya. *Journal of Geophysical Research: Oceans*, 103(C2), pp.2883–2896.

Bates, N.R., Moran, B.S., Hansell, D.A. & Mathis, J.T., 2006. An increasing CO_2 sink in the Arctic Ocean due to sea-ice loss. *Geophysical Research Letters*, 33(23).

Bednaršek, N., Tarling, G.A., Bakker, D.C.E., Fielding, S., Jones, E.M., Venables, H.J., Ward, P., Kuzirian, A., Lézé, B., Feely, R.A. & Murphy, E.J., 2012. Extensive dissolution of live pteropods in the Southern Ocean. *Nature Geoscience*, 5(12), pp.881–885.

Bednaršek, N., Tarling, G.A., Fielding, S. & Bakker, D.C.E., 2012. Population

dynamics and biogeochemical significance of Limacina helicina antarctica in the Scotia Sea (Southern Ocean). *Deep Sea Research Part II: Topical Studies in Oceanography*, 59, pp.105–116.

Bellerby, R.G.J., Hoppema, M., Fahrbach, E., de Baar, H.J.W. & Stoll, M.H.C., 2004. Interannual controls on Weddell Sea surface water fCO_2 during the autumn–winter transition phase. *Deep Sea Research Part I: Oceanographic Research Papers*, 51(6), pp.793–808.

Bender, M., Orchardo, J., Dickson, M.-L., Barber, R. & Lindley, S., 1999. In vitro O_2 fluxes compared with ^{14}C production and other rate terms during the JGOFS Equatorial Pacific experiment. *Deep Sea Research Part I: Oceanographic Research Papers*, 46(4), pp.637–654.

Bender, M.L., Dickson, M.-L. & Orchardo, J., 2000. Net and gross production in the Ross Sea as determined by incubation experiments and dissolved O2 studies. *Deep Sea Research Part II: Topical Studies in Oceanography*, 47(15–16), pp.3141–3158.

Borges, A. & Gypens, N., 2010. Carbonate chemistry in the coastal zone responds more strongly to eutrophication than to ocean acidification. *Limnology and Oceanography*, 55(1).

Borges, A.V., Tilbrook, B., Metzl, N., Lenton, A. & Delille, B., 2008. Inter-annual variability of the carbon dioxide oceanic sink south of Tasmania. *Biogeosciences*, 5(1), pp.141–155.

Boyd, P.W. & Mackie, D., 2008. Comment on "The Southern Ocean biological response to aeolian iron deposition." *Science (New York, N.Y.)*, 319(5860), p.159.

Bresnahan, P.J., Martz, T.R., Takeshita, Y., Johnson, K.S. & LaShomb, M., 2014. Best practices for autonomous measurement of seawater pH with the Honeywell Durafet. *Methods in Oceanography*, 9, pp.44–60.

Brewer, P.G. & Goldman, J.C., 1976. Alkalinity changes generated by phytoplankton growth. *Limnology and Oceanography*, 21(1), pp.108–117.

Broecker, W.S. & Peng, T.-H., 1982. *Tracers in the Sea*, Palisades, NY: Lamont-

Doherty Geological Observatory.

Brown, P.J., Jullion, L., Landschützer, P., Bakker, D.C.E., Naveira Garabato, A.C., Meredith, M.P., Torres-Valdés, S., Watson, A., Hoppema, M., Loose, B., Jones, E.M., Telszewski, M., Jones, S.D. & Wanninkhof, R., 2015. Carbon dynamics of the Weddell Gyre, Southern Ocean. *Global Biogeochemical Cycles*, 29(3), pp.288–306.

Brzezinski, M.A., 1985. The Si:C:N ratio of marine diatoms: interspecific variability and the effect of some environmental variables. *Journal of Phycology*, 21(3), pp.347–357.

Byrne, M., Ho, M.A., Koleits, L., Price, C., King, C.K., Virtue, P., Tilbrook, B. & Lamare, M., 2013. Vulnerability of the calcifying larval stage of the Antarctic sea urchin *Sterechinus neumayeri* to near-future ocean acidification and warming. *Global Change Biology*, 19(7), pp.2264–2275.

Cai, W.-J. & Wang, Y., 1998. The chemistry, fluxes, and sources of carbon dioxide in the estuarine waters of the Satilla and Altamaha Rivers, Georgia. *Limnology and Oceanography*, 43(4), pp.657–668.

Carrillo, C.J., Smith, R.C. & Karl, D.M., 2004. Processes regulating oxygen and carbon dioxide in surface waters west of the Antarctic Peninsula. *Marine Chemistry*, 84(3–4), pp.161–179.

Cassar, N., Bender, M.L., Barnett, B.A., Fan, S., Moxim, W.J., Levy, H. & Tilbrook, B., 2007. The Southern Ocean biological response to aeolian iron deposition. *Science (New York, N.Y.)*, 317(5841), pp.1067–70.

Cassar, N., DiFiore, P.J., Barnett, B.A., Bender, M.L., Bowie, A.R., Tilbrook, B., Petrou, K., Westwood, K.J., Wright, S.W. & Lefevre, D., 2011. The influence of iron and light on net community production in the Subantarctic and Polar Frontal Zones. *Biogeosciences*, 8(2), pp.227–237.

Cassar, N., Nevison, C.D. & Manizza, M., 2014. Correcting oceanic O_2/Ar-net community production estimates for vertical mixing using N_2O observations. *Geophysical Research Letters*, 41(24), pp.8961–8970.

Castro-Morales, K., Cassar, N., Shoosmith, D.R. & Kaiser, J., 2013. Biological production in the Bellingshausen Sea from oxygen-to-argon ratios and oxygen triple isotopes. *Biogeosciences*, 10(4), pp.2273–2291.

Cavalieri, D.J., Parkinson, C.L., Gloersen, P. & Zwally, H., 2015. Sea ice concentration from Nimbus-7 SMMR and DMSP SSM/I-SSMIS passive microwave data, Version 1. *NASA National Snow and Ice Data Centre Distributed Active Archive Center*. Available at: http://dx.doi.org/10.5067/8GQ8LZQVL0VL [Accessed June 3, 2015].

Charrassin, J.-B. et al., 2008. Southern Ocean frontal structure and sea-ice formation rates revealed by elephant seals. *Proceedings of the National Academy of Sciences of the United States of America*, 105(33), pp.11634–9.

Chierici, M. & Fransson, A., 2009. Calcium carbonate saturation in the surface water of the Arctic Ocean: undersaturation in freshwater influenced shelves. *Biogeosciences*, (6), pp.2421–2432.

Copin-Montegut, C., 1988. A new formula for the effect of temperature on the partial pressure of CO_2 in seawater. *Marine Chemistry*, 25(1), pp.29–37.

Le Corre, P. & Minas, H.J., 1983. Distribution et évolution des éléments nutritifs dans le secteur indien de l'Océan Antarctique en fin de période estivale. *Oceanologica Acta*, 6(4), pp.365–381.

Cox, T.E., Gazeau, F., Alliouane, S., Hendriks, I.E., Mahacek, P., Le Fur, A. & Gattuso, J.-P., 2016. Effects of in situ CO_2 enrichment on structural characteristics, photosynthesis, and growth of the Mediterranean seagrass Posidonia oceanica. *Biogeosciences*, 13(7), pp.2179–2194.

Culberson, C.H., Knapp, G., Stalcup, M.C., Williams, R.T. & Zemlyak, F., 1991. *A Comparison of methods for the determination of dissolved oxygen in seawater*, Woods Hole, MA: WOCE Hydrographic Programme Office, Woods Hole Oceanographic Institution.

Davidson, A.T. & Marchant, H.J., 1992. Protist abundance and carbon concentration during a Phaeocystis-dominated bloom at an Antarctic coastal site. *Polar Biology*, 12(3–4).

Davidson, A.T., Scott, F.J., Nash, G. V., Wright, S.W. & Raymond, B., 2010. Physical and biological control of protistan community composition, distribution and abundance in the seasonal ice zone of the Southern Ocean between 30 and 80°E. *Deep Sea Research Part II: Topical Studies in Oceanography*, 57(9–10), pp.828–848.

Delille, B., Jourdain, B., Borges, A. V., Tison, J.-L. & Delille, D., 2007. Biogas (CO_2, O_2, dimethylsulfide) dynamics in spring Antarctic fast ice. *Limnology and Oceanography*, 4(52), pp.1367–1379.

Dickson, A.G. & Afghan, J.D., 2003. Reference materials for oceanic CO_2 analysis: a method for the certification of total alkalinity. *Marine Chemistry*, (80), pp.185–197.

Dickson, A.G. & Millero, F.J., 1987. A comparison of the equilibrium constants for the dissociation of carbonic acid in seawater media. *Deep Sea Research Part A. Oceanographic Research Papers*, 34(10), pp.1733–1743.

Dickson, A.G., Sabine, C.L. & Christian, J.R. eds., 2007. *Guide to best practices for ocean CO2 measurements* PICES Spec., Sidney, BC, Canada: North Pacific Marine Science Organisation.

Dieckmann, G.S., Nehrke, G., Papadimitriou, S., Göttlicher, J., Steininger, R., Kennedy, H., Wolf-Gladrow, D. & Thomas, D.N., 2008. Calcium carbonate as ikaite crystals in Antarctic sea ice. *Geophysical Research Letters*, 35(8), p.L08501.

Dlugokencky, E. & Tans, P.P., 2016. Recent global monthly mean CO_2. *NOAA/ESRL*. Available at: http://www.esrl.noaa.gov/gmd/ccgg/trends/global.html [Accessed November 5, 2016].

Dlugokencky, E.J., Lang, P.M., Masarie, K.A., Crotwell, A.M. & Crotwell, M.J., 2015. Atmospheric carbon dioxide dry air mole fractions from the NOAA ESRL Carbon Cycle Cooperative Global Air Sampling Network, 1968-2014, Version: 2015-08-03, Path: //aftp.cmdl.noaa.gov/data/trace_gases/co.

Dore, J.E., Houlihan, T., Hebel, D. V., Tien, G., Tupas, L. & Karl, D.M., 1996. Freezing as a method of sample preservation for the analysis of dissolved

inorganic nutrients in seawater. *Marine Chemistry*, 53(3–4), pp.173–185.

Etheridge, D.M., Steele, L.P., Langenfelds, R.L., Francey, R.J., Barnola, J.-M. & Morgan, V.I., 1996. Natural and anthropogenic changes in atmospheric CO2 over the last 1000 years from air in Antarctic ice and firn. *Journal of Geophysical Research: Atmospheres*, 101(D2), pp.4115–4128.

Eveleth, R., Timmermans, M.-L. & Cassar, N., 2014. Physical and biological controls on oxygen saturation variability in the upper Arctic Ocean. *Journal of Geophysical Research: Oceans*, 119(11), pp.7420–7432.

Fabry, V.J., McClintock, J.B. & Mathis, J.T., 2009. Ocean acidification at high latitudes: the bellwether. *Oceanography*.

Feely, R.A., Sabine, C.L., Hernandez-Ayon, J.M., Ianson, D. & Hales, B., 2008. Evidence for upwelling of corrosive “acidified” water onto the continental shelf. *Science*, 320(5882), pp.1490–1492.

Feely, R.A., Sabine, C.L., Lee, K. & Berelson, W., 2004. Impact of anthropogenic CO_2 on the $CaCO_3$ system in the oceans. *Science*, 305(5682), pp.362–366.

Foldvik, A. & Gammelsrød, T., 1988. Notes on Southern Ocean hydrography, sea-ice and bottom water formation. *Palaeogeography, Palaeoclimatology, Palaeoecology*, 67(1–2), pp.3–17.

Gao, Z., Chen, L. & Gao, Y., 2008. Air-sea carbon fluxes and their controlling factors in Prydz Bay in the Antarctic. *Acta Oceanologica Sinica*, 27(3), pp.136–146.

García, H.E. & Gordon, L.I., 1993. Erratum: Oxygen solubility in seawater: Better fitting equations. *Limnology and Oceanography*, 38(3), p.656.

García, H.E. & Gordon, L.I., 1992. Oxygen solubility in seawater: Better fitting equations. *Limnology and Oceanography*, 37(6), pp.1307–1312.

Gattuso, J.-P., Bijma, J., Gehlen, M., Riebesell, U. & Turley, C., 2011. Ocean acidification: knowns, unknowns, and perspectives. In J.-P. Gattuso & L. Hansson, eds. *Ocean Acidification*. Oxford UK: Oxford University Press, pp. 291–311.

Gattuso, J.-P., Kirkwood, W., Barry, J.P., Cox, E., Gazeau, F., Hansson, L., Hendriks, I., Kline, D.I., Mahacek, P., Martin, S., McElhany, P., Peltzer, E.T., Reeve, J., Roberts, D., Saderne, V., Tait, K., Widdicombe, S. & Brewer, P.G., 2014. Free-ocean CO_2 enrichment (FOCE) systems: present status and future developments. *Biogeosciences*, 11(15), pp.4057–4075.

Geibert, W., Assmy, P., Bakker, D.C.E., Hanfland, C., Hoppema, M., Pichevin, L.E., Schröder, M., Schwarz, J.N., Stimac, I., Usbeck, R. & Webb, A., 2010. High productivity in an ice melting hot spot at the eastern boundary of the Weddell Gyre. *Global Biogeochemical Cycles*, 24(3).

Gibson, J.A.E., 1998. Carbon flow through inshore marine environments of the Vestfold Hills, East Antarctica. *ANARE Reports*, 139, pp.1–222.

Gibson, J.A.E., Swadling, K.M. & Burton, H.R., 1997. Interannual variations in dominant phytoplankton species and biomass near Davis station, East Antarctica. *NIPR Symposium on Polar Biology Proceedings*, 10, pp.77–89.

Gibson, J.A.E. & Trull, T.W., 1999. Annual cycle of fCO_2 under sea-ice and in open water in Prydz Bay, East Antarctica. *Marine Chemistry*, 66(3–4), pp.187–200.

Gibson, J.A.E., Trull, T.W., Nichols, P.D., Summons, R.E. & McMinn, A., 1999. Sedimentation of ^{13}C-rich organic matter from Antarctic sea-ice algae: a potential indicator of past sea-ice extent. *Geology*, 27(4), pp.331–334.

Gill, A.E., 1973. Circulation and bottom water production in the Weddell Sea. *Deep Sea Research*, 20(2), pp.111–140.

Gonzalez-Bernat, M.J., Lamare, M. & Barker, M., 2013. Effects of reduced seawater pH on fertilisation, embryogenesis and larval development in the Antarctic seastar *Odontaster validus*. *Polar Biology*, 36(2), pp.235–247.

Goyet, C. & Poisson, A., 1989. New determination of carbonic acid dissociation constants in seawater as a function of temperature and salinity. *Deep Sea Research Part A. Oceanographic Research Papers*, 36(11), pp.1635–1654.

Gruber, N. & Sarmiento, J.L., 2002. Large-scale biogeochemical-physical interactions in elemental cycles. In A. R. Robinson, J. J. McCarthy, & B. J. Rothschild, eds.

The Sea. New York, NY, USA: John Wiley & Sons, pp. 337–399.

Hall-Spencer, J.M., Rodolfo-Metalpa, R., Martin, S., Ransome, E., Fine, M., Turner, S.M., Rowley, S.J., Tedesco, D. & Buia, M.-C., 2008. Volcanic carbon dioxide vents show ecosystem effects of ocean acidification. *Nature*, 454(7200), pp.96–99.

Hansen, H.P. & Koroleff, F., 2007. Determination of nutrients. In K. Grasshoff, K. Kremling, & M. Ehrhardt, eds. *Methods of Seawater Analysis*. Weinheim, Germany: Wiley-VCH Verlag GmbH, pp. 159–228.

Hansson, I., 1973. A new set of acidity constants for carbonic acid and boric acid in sea water. *Deep Sea Research and Oceanographic Abstracts*, 20(5), pp.461–478.

Hauri, C., Doney, S.C., Takahashi, T., Erickson, M., Jiang, G. & Ducklow, H.W., 2015. Two decades of inorganic carbon dynamics along the Western Antarctic Peninsula. *Biogeosciences*, 12(9), pp.6929–6969.

van Heuven, S., Pierrot, D., Rae, J.W.B., Lewis, E. & Wallace, D.W.R., 2011. MATLAB Program Developed for CO_2 System Calculations. *ORNL/CDIAC-105, Carbon Dioxide Information Analysis Center, Oak Ridge National Laboratory US Department of Energy*.

van Heuven, S.M.A.., Hoppema, M., Jones, E.M. & de Baar, H.J.W., 2014. Rapid invasion of anthropogenic CO_2 into the deep circulation of the Weddell Gyre. *Philosophical transactions. Series A, Mathematical, physical, and engineering sciences*, 372(2019), p.20130056.

Heywood, K.J., Sparrow, M.D., Brown, J. & Dickson, R.R., 1999. Frontal structure and Antarctic Bottom Water flow through the Princess Elizabeth Trough, Antarctica. *Deep Sea Research Part I: Oceanographic Research Papers*, 46(7), pp.1181–1200.

Hobbs, W.R., Massom, R., Stammerjohn, S., Reid, P., Williams, G. & Meier, W., 2016. A review of recent changes in Southern Ocean sea ice, their drivers and forcings. *Global and Planetary Change*, 143, pp.228–250.

Hofmann, G.E., Smith, J.E., Johnson, K.S., Send, U., Levin, L.A., Micheli, F., Paytan,

A., Price, N.N., Peterson, B., Takeshita, Y., Matson, P.G., Crook, E.D., Kroeker, K.J., Gambi, M.C., Rivest, E.B., Frieder, C.A., Yu, P.C. & Martz, T.R., 2011. High-frequency dynamics of ocean pH: a multi-ecosystem comparison. W.-C. Chin, ed. *PloS ONE*, 6(12), p.e28983.

Honjo, S., 2004. Particle export and the biological pump in the Southern Ocean. *Antarctic Science*, 16(4), pp.501–516.

Hoppema, M. & Goeyens, L., 1999. Redfield behavior of carbon, nitrogen, and phosphorus depletions in Antarctic surface water. *Limnology and Oceanography*, 44(1), pp.220–224.

Houghton, R.A., 2007. Balancing the Global Carbon Budget. *Annual Review of Earth and Planetary Sciences*, 35(1), pp.313–347.

Howard, S.L., Hyatt, J. & Padman, L., 2004. Mixing in the pycnocline over the western Antarctic Peninsula shelf during Southern Ocean GLOBEC. *Deep Sea Research Part II: Topical Studies in Oceanography*, 51(17–19), pp.1965–1979.

Hunt, B.P.V., Pakhomov, E.A., Hosie, G.W., Siegel, V., Ward, P. & Bernard, K., 2008. Pteropods in Southern Ocean ecosystems. *Progress in Oceanography*, 78(3), pp.193–221.

Hutchins, D.A. & Bruland, K.W., 1998. Iron-limited diatom growth and Si:N uptake ratios in a coastal upwelling regime. *Nature*, 393(6685), pp.561–564.

IPCC, 2013. *Climate Change 2013: The Physical Science Basis. Contribution of Working Group I to the Fifth Assessment Report of the Intergovernmental Panel on Climate Change* T. F. Stocker et al., eds., Cambridge, United Kingdom and New York, NY, USA.: Cambridge University Press.

Ishii, M., Inoue, H.Y., Matsueda, H. & Tanoue, E., 1998. Close coupling between seasonal biological production and dynamics of dissolved inorganic carbon in the Indian Ocean sector and the western Pacific Ocean sector of the Antarctic Ocean. *Deep Sea Research I*, 45, pp.1187–1209.

Jarvis, T., Kelly, N., Kawaguchi, S., van Wijk, E. & Nicol, S., 2010. Acoustic characterisation of the broad-scale distribution and abundance of Antarctic krill

(Euphausia superba) off East Antarctica (30-80°E) in January-March 2006. *Deep Sea Research Part II: Topical Studies in Oceanography*, 57(9–10), pp.916–933.

Jennings, J.C., Gordon, L.I. & Nelson, D.M., 1984. Nutrient depletion indicates high primary productivity in the Weddell Sea. *Nature*, 309(5963), pp.51–54.

Johnson, G.C., 2008. Quantifying Antarctic Bottom Water and North Atlantic Deep Water volumes. *Journal of Geophysical Research*, 113(C5), p.C05027.

Johnson, K.M., Körtzinger, A., Mintrop, L., Duinker, J.C. & Wallace, D.W.R., 1999. Coulometric total carbon dioxide analysis for marine studies: measurement and internal consistency of underway TCO_2 concentrations. *Marine Chemistry*, 67(1–2), pp.123–144.

Jones, E.M., Bakker, D.C.E., Venables, H.J. & Hardman-Mountford, N.J., 2015. Seasonal cycle of CO_2 from the sea ice edge to island blooms in the Scotia Sea, Southern Ocean. *Marine Chemistry*, 177, pp.490–500.

Kaiser, J., Reuer, M.K., Barnett, B. & Bender, M.L., 2005. Marine productivity estimates from continuous O_2/Ar ratio measurements by membrane inlet mass spectrometry. *Geophysical Research Letters*, 32(19), p.L19605.

Kapsenberg, L., Kelley, A.L., Shaw, E.C., Martz, T.R. & Hofmann, G.E., 2015. Near-shore Antarctic pH variability has implications for the design of ocean acidification experiments. *Scientific Reports*, 5, p.9638.

Kara, A.B., Rochford, P.A. & Hurlburt, H.E., 2003. Mixed layer depth variability over the global ocean. *Journal of Geophysical Research*, 108(C3), p.3079.

Kawaguchi, S., Nicol, S., Virtue, P., Davenport, S.R., Casper, R., Swadling, K.M. & Hosie, G.W., 2010. Krill demography and large-scale distribution in the Western Indian Ocean sector of the Southern Ocean (CCAMLR Division 58.4.2) in Austral summer of 2006. *Deep Sea Research Part II: Topical Studies in Oceanography*, 57(9–10), pp.934–947.

Khatiwala, S., Primeau, F. & Hall, T., 2009. Reconstruction of the history of anthropogenic CO_2 concentrations in the ocean. *Nature*, 462(7271), pp.346–9.

Kirkwood, W.J., Peltzer, E.T., Walz, P., Headley, K., Herlien, B., Kecy, C., Maughan,

T., O'Reilly, T., Salamy, K.A., Shane, F., Scholfield, J. & Brewer, P.G., 2011. Cabled instrument technologies for ocean acidification research — FOCE (free ocean CO_2 enrichment). In *2011 IEEE Symposium on Underwater Technology and Workshop on Scientific Use of Submarine Cables and Related Technologies*. IEEE, pp. 1–8.

Körtzinger, A., Mintrop, L., Wallace, D.W.., Johnson, K.M., Neill, C., Tilbrook, B., Towler, P., Inoue, H.Y., Ishii, M., Shaffer, G., Torres Saavedra, R.F., Ohtaki, E., Yamashita, E., Poisson, A., Brunet, C., Schauer, B., Goyet, C. & Eischeid, G., 2000. The international at-sea intercomparison of fCO_2 systems during the R/V Meteor Cruise 36/1 in the North Atlantic Ocean. *Marine Chemistry*, 72(2–4), pp.171–192.

Kroeker, K.J., Kordas, R.L., Crim, R., Hendriks, I.E., Ramajo, L., Singh, G.S., Duarte, C.M. & Gattuso, J.-P., 2013. Impacts of ocean acidification on marine organisms: quantifying sensitivities and interaction with warming. *Global Change Biology*, 19(6), pp.1884–1896.

Landschützer, P., Gruber, N., Haumann, F.A., Rödenbeck, C., Bakker, D.C.E., van Heuven, S., Hoppema, M., Metzl, N., Sweeney, C., Takahashi, T., Tilbrook, B. & Wanninkhof, R., 2015. The reinvigoration of the Southern Ocean carbon sink. *Science (New York, N.Y.)*, 349(6253), pp.1221–4.

Lannuzel, D., van der Merwe, P.C., Townsend, A.T. & Bowie, A.R., 2014. Size fractionation of iron, manganese and aluminium in Antarctic fast ice reveals a lithogenic origin and low iron solubility. *Marine Chemistry*, 161, pp.47–56.

Laws, E.A., 1991. Photosynthetic quotients, new production and net community production in the open ocean. *Deep Sea Research Part A. Oceanographic Research Papers*, 38(1), pp.143–167.

Legge, O.J., Bakker, D.C.E., Johnson, M.T., Meredith, M.P., Venables, H.J., Brown, P.J. & Lee, G.A., 2015. The seasonal cycle of ocean-atmosphere CO_2 flux in Ryder Bay, West Antarctic Peninsula. *Geophysical Research Letters*, 42(8), pp.2934–2942.

Lenton, A., Codron, F., Bopp, L., Metzl, N., Cadule, P., Tagliabue, A. & Le Sommer,

J., 2009. Stratospheric ozone depletion reduces ocean carbon uptake and enhances ocean acidification. *Geophysical Research Letters*, 36(12), p.L12606.

Lenton, A., Tilbrook, B., Law, R.M., Bakker, D., Doney, S.C., Gruber, N., Ishii, M., Hoppema, M., Lovenduski, N.S., Matear, R.J., McNeil, B.I., Metzl, N., Mikaloff Fletcher, S.E., Monteiro, P.M.S., Rödenbeck, C., Sweeney, C. & Takahashi, T., 2013. Sea–air CO_2 fluxes in the Southern Ocean for the period 1990–2009. *Biogeosciences*, 10(6), pp.4037–4054.

Li, X., Holland, D.M., Gerber, E.P. & Yoo, C., 2014. Impacts of the north and tropical Atlantic Ocean on the Antarctic Peninsula and sea ice. *Nature*, 505(7484), pp.538–42.

Loose, B., McGillis, W.R., Schlosser, P., Perovich, D. & Takahashi, T., 2009. Effects of freezing, growth, and ice cover on gas transport processes in laboratory seawater experiments. *Geophysical Research Letters*, 36(5), p.L05603.

Lueker, T.J., Dickson, A.G. & Keeling, C.D., 2000. Ocean pCO_2 calculated from dissolved inorganic carbon, alkalinity, and equations for K1 and K2: validation based on laboratory measurements of CO_2 in gas and seawater at equilibrium. *Marine Chemistry*, 70(1–3), pp.105–119.

Marshall, J. & Speer, K., 2012. Closure of the meridional overturning circulation through Southern Ocean upwelling. *Nature Geoscience*, 5(3), pp.171–180.

Martz, T.R., Connery, J.G. & Johnson, K.S., 2010. Testing the Honeywell Durafet for seawater pH applications. *Limnology and Oceanography: Methods*, 8, pp.172–184.

Massom, R., Reid, P., Stammerjohn, S., Raymond, B., Fraser, A. & Ushio, S., 2013. Change and variability in East antarctic sea ice seasonality, 1979/80-2009/10. *PloS one*, 8(5), p.e64756.

McNeil, B.I. & Matear, R.J., 2008. Southern Ocean acidification: A tipping point at 450-ppm atmospheric CO_2. *Proceedings of the National Academy of Sciences*, 105(48), pp.18860–18864.

McNeil, B.I., Tilbrook, B. & Matear, R.J., 2001. The accumulation and uptake of

anthropogenic CO_2 in the Southern Ocean, south of Australia between 1968 and 1996. *Journal of Geophysical Research*, 106(C12), pp.31432–31445.

Mehrbach, C., Culberson, C.H., Hawley, J.E. & Pytkowicz, R.M., 1973. Measurement of the apparent dissociation constants of carbonic acid in seawater at atmospheric pressure. *Limnology and Oceanography*, 18(6), pp.897–907.

Meijers, A.J.S., 2014. The Southern Ocean in the Coupled Model Intercomparison Project phase 5. *Philosophical transactions of the Royal Society A*, 372(2019), p.20130296.

Meijers, A.J.S., Klocker, A., Bindoff, N.L., Williams, G.D. & Marsland, S.J., 2010. The circulation and water masses of the Antarctic shelf and continental slope between 30 and 80°E. *Deep Sea Research Part II: Topical Studies in Oceanography*, 57(9–10), pp.723–737.

Middleton, J.H. & Humphries, S.E., 1989. Thermohaline structure and mixing in the region of Prydz Bay, Antarctica. *Deep Sea Research*, 36(8), pp.1255–1266.

Miller, L.A., Papakyriakou, T.N., Collins, R.E., Deming, J.W., Ehn, J.K., Macdonald, R.W., Mucci, A., Owens, O., Raudsepp, M. & Sutherland, N., 2011. Carbon dynamics in sea ice: A winter flux time series. *Journal of Geophysical Research*, 116(C2), p.C02028.

Millero, F.J., 2010. Carbonate constants for estuarine waters. *Marine and Freshwater Research*, 61(2), pp.139–142.

Millero, F.J., Graham, T.B., Huang, F., Bustos-Serrano, H. & Pierrot, D., 2006. Dissociation constants of carbonic acid in seawater as a function of salinity and temperature. *Marine Chemistry*, 100(1–2), pp.80–94.

Millero, F.J. & Leung, W.H., 1976. Thermodynamics of seawater at one atmosphere. *Am. J. Sci.; (United States)*, 276:9.

Millero, F.J., Pierrot, D., Lee, K., Wanninkhof, R.H., Feely, R., Sabine, C.L., Key, R.M. & Takahashi, T., 2002. Dissociation constants for carbonic acid determined from field measurements. *Deep Sea Research Part I: Oceanographic Research Papers*, 49(10), pp.1705–1723.

Mojica Prieto, F.J. & Millero, F.J., 2002. The values of pK1 + pK2 for the dissociation of carbonic acid in seawater. *Geochimica et Cosmochimica Acta*, 66(14), pp.2529–2540.

Mucci, A., 1983. The solubility of calcite and aragonite in seawater at various salinities, temperatures, and one atmosphere total pressure. *American Journal of Science*, 283(7), pp.780–799.

Mucci, A., Lansard, B. & Miller, L.A., 2010. CO_2 fluxes across the air-sea interface in the southeastern Beaufort Sea: Ice-free period. *Journal of Geophysical Research*, 115(C04003).

Naegler, T., Ciais, P., Rodgers, K. & Levin, I., 2006. Excess radiocarbon constraints on air-sea gas exchange and the uptake of CO_2 by the oceans. *Geophysical Research Letters*, 33(L11802).

Neven, I.A., Stefels, J., van Heuven, S.M.A.C. & Elzenga, J.T.M., 2011. High plasticity in inorganic carbon uptake by Southern Ocean phytoplankton in response to ambient CO2. *Deep Sea Research Part II: Topical Studies in Oceanography*, 58(25), pp.2636–2646.

Nomura, D., Granskog, M.A., Assmy, P., Simizu, D. & Hashida, G., 2013. Arctic and Antarctic sea ice acts as a sink for atmospheric CO_2 during periods of snowmelt and surface flooding. *Journal of Geophysical Research: Oceans*, 118(12), pp.6511–6524.

Nomura, D., Yoshikawa-Inoue, H., Kobayashi, S., Nakaoka, S., Nakata, K. & Hashida, G., 2014. Winter to summer evolution of pCO_2 in surface water and air–sea CO_2 flux in the seasonal ice zone of the Southern Ocean. *Biogeosciences*, 11, pp.5749–5761.

Nunes Vaz, R.A. & Lennon, G.W., 1996. Physical oceanography of the Prydz Bay region of Antarctic waters. *Deep Sea Research Part I: Oceanographic Research Papers*, 43(5), pp.603–641.

Ohshima, K.I., Fukamachi, Y., Williams, G.D., Nihashi, S., Roquet, F., Kitade, Y., Tamura, T., Hirano, D., Herraiz-Borreguero, L., Field, I., Hindell, M., Aoki, S. & Wakatsuchi, M., 2013. Antarctic Bottom Water production by intense sea-ice

formation in the Cape Darnley polynya. *Nature Geoscience*, 6(3), pp.235–240.

Orr, J.C. et al., 2005. Anthropogenic ocean acidification over the twenty-first century and its impact on calcifying organisms. *Nature*, 437(7059), pp.681–686.

Orsi, A.H., Johnson, G.C. & Bullister, J.L., 1999. Circulation, mixing, and production of Antarctic Bottom Water. *Progress in Oceanography*, 43(1), pp.55–109.

Orsi, A.H., Whitworth, T. & Nowlin, W.D., 1995. On the meridional extent and fronts of the Antarctic Circumpolar Current. *Deep Sea Research Part I: Oceanographic Research Papers*, 42(5), pp.641–673.

Pardo, P.C., Pérez, F.F., Khatiwala, S. & Ríos, A.F., 2014. Anthropogenic CO_2 estimates in the Southern Ocean: Storage partitioning in the different water masses. *Progress in Oceanography*, 120, pp.230–242.

Park, Y.-H., Charriaud, E. & Fieux, M., 1998. Thermohaline structure of the Antarctic Surface Water/Winter Water in the Indian sector of the Southern Ocean. *Journal of Marine Systems*, 17(1–4), pp.5–23.

Pasquer, B., Mongin, M., Johnston, N. & Wright, S., 2010. Distribution of particulate organic matter (POM) in the Southern Ocean during BROKE-West (30°E - 80°E). *Deep Sea Research Part II: Topical Studies in Oceanography*, 57(9–10), pp.779–793.

Peck, L.S., 2005. Prospects for surviving climate change in Antarctic aquatic species. *Frontiers in zoology*, 2(8).

Peck, L.S., Powell, D.K. & Tyler, P.A., 2007. Very slow development in two Antarctic bivalve molluscs, the infaunal clam *Laternula elliptica* and the scallop *Adamussium colbecki*. *Marine Biology*, 150(6), pp.1191–1197.

Peck, L.S., Webb, K.E. & Bailey, D.M., 2004. Extreme sensitivity of biological function to temperature in Antarctic marine species. *Functional Ecology*, 18(5), pp.625–630.

Peng, T.-H., Takahashi, T., Broecker, W.S. & Olafsson, J., 1987. Seasonal variability of carbon dioxide, nutrients and oxygen in the northern North Atlantic surface water: observations and a model. *Tellus B*, 39B(5), pp.439–458.

Perrin, R.A., Lu, P. & Marchant, H.J., 1987. Seasonal variation in marine phytoplankton and ice algae at a shallow Antarctic coastal site. *Hydrobiologia*, (146), pp.33–46.

Pierrot, D., Neill, C., Sullivan, K., Castle, R., Wanninkhof, R.H., Lüger, H., Johannessen, T., Olsen, A., Feely, R.A. & Cosca, C.E., 2009. Recommendations for autonomous underway pCO_2 measuring systems and data-reduction routines. *Deep Sea Research Part II: Topical Studies in Oceanography*, 56(8–10), pp.512–522.

Pörtner, H.-O., Karl, D.M., Boyd, P.W., Cheung, W., Lluch-Cota, S., Nojiri, Y., Schmidt, D.N., Zavialov, P.O., Alheit, J. & Aristegui, J., 2014. Ocean systems. In C. B. Field et al., eds. *Climate Change 2014: Impacts, Adaption, and Vulnerability Part A: Global and Sectoral Aspects Contribution of Working Group II to the Fifth Assessment Report of the Intergovernmental Panel on Climate Change*. Cambridge, United Kingdom and New York, NY, USA.: Cambridge University Press, pp. 411–484.

Post, A.L., Meijers, A.J.S., Fraser, A.D., Meiners, K.M., Ayers, J., Bindoff, N.L., Griffiths, H.J., Van de Putte, A.P., O'Brien, P.E., Swadling, K.M. & Raymond, B., 2014. Environmental Setting. In C. De Boyer et al., eds. *Biogeographic Atlas of the Southern Ocean*. Cambridge: Scientific Committee on Antarctic Research, pp. 46–64.

Post, A.L., O'Brien, P.E., Beaman, R.J., Riddle, M.J. & De Santis, L., 2010. Physical controls on deep water coral communities on the George V Land slope, East Antarctica. *Antarctic Science*, 22(4), pp.371–378.

Le Quéré, C. et al., 2015. Global Carbon Budget 2015. *Earth System Science Data*, 7(2), pp.349–396.

Le Quéré, C., Rödenbeck, C., Buitenhuis, E.T., Conway, T.J., Langenfelds, R., Gomez, A., Labuschagne, C., Ramonet, M., Nakazawa, T., Metzl, N., Gillett, N. & Heimann, M., 2007. Saturation of the southern ocean CO_2 sink due to recent climate change. *Science (New York, N.Y.)*, 316(5832), pp.1735–8.

Raven, J., Caldeira, K., Elderfield, H., Hoegh-Guldberg, O., Liss, P., Riebesell, U.,

Shepherd, J., Turley, C. & Watson, A., 2005. Ocean acidification due to increasing atmospheric carbon dioxide. *The Royal Society policy document 12/05. Clyvedon Press. Cardiff, UK.*

Redfield, A.C., Ketchum, B.H. & Richards, F.A., 1963. The influence of organisms on the composition of seawater. In M. N. Hill, ed. *The Sea*. New York: Wiley Interscience, pp. 26–79.

Reuer, M.K., Barnett, B.A., Bender, M.L., Falkowski, P.G. & Hendricks, M.B., 2007. New estimates of Southern Ocean biological production rates from O_2/Ar ratios and the triple isotope composition of O_2. *Deep Sea Research Part I: Oceanographic Research Papers*, 54(6), pp.951–974.

Revelle, R. & Suess, H.E., 1957. Carbon dioxide exchange between atmosphere and ocean and the question of an increase of atmospheric CO_2 during the past decades. *Tellus*, 9(1), pp.18–27.

Rintoul, S., Hughes, C. & Olbers, D., 2001. The Antarctic Circumpolar Current System. In G. Siedler, J. Church, & J. Gould, eds. *Ocean circulation and climate.* New York: Academic Press, pp. 271–302.

Robinson, C., Archer, S. & Williams, P., 1999. Microbial dynamics in coastal waters of East Antarctica: plankton production and respiration. *Marine Ecology Progress Series*, 180, pp.23–36.

Roden, N.P., Shadwick, E.H., Tilbrook, B. & Trull, T.W., 2013. Annual cycle of carbonate chemistry and decadal change in coastal Prydz Bay, East Antarctica. *Marine Chemistry*, 155, pp.135–147.

Roden, N.P., Tilbrook, B., Trull, T.W., Virtue, P. & Williams, G.D., 2016. Carbon cycling dynamics in the seasonal sea-ice zone of East Antarctica. *Journal of Geophysical Research: Oceans*, 121(12), pp.8749–8769.

Rosenberg, M. & Gorton, R., 2006. BROKE-West Survey, Marine Science Cruise AU603 - Oceanographic Field Measurements and Analysis. Technical Report. Available at: http://data.aad.gov.au/aadc/metadata/metadata_redirect.cfm?md=/AMD/AU/BROKE-West_CTD_au0603.

Roy, R.N., Roy, L.N., Vogel, K.M., Porter-Moore, C., Pearson, T., Good, C.E., Millero, F.J. & Campbell, D.M., 1993. The dissociation constants of carbonic acid in seawater at salinities 5 to 45 and temperatures 0 to 45°C. *Marine Chemistry*, 44(2–4), pp.249–267.

Rubin, S.I., Takahashi, T., Chipman, D.W. & Goddard, J.G., 1998. Primary productivity and nutrient utilization ratios in the Pacific sector of the Southern Ocean based on seasonal changes in seawater chemistry - A comparative study. *Deep Sea Research Part I: Oceanographic Research Papers*, 45(8), p.24.

Sabine, C.L., Feely, R.A., Gruber, N., Key, R.M., Lee, K., Bullister, J.L., Wanninkhof, R., Wong, C.S., Wallace, D.W.R., Tilbrook, B., Millero, F.J., Peng, T.-H., Kozyr, A., Ono, T. & Rios, A.F., 2004. The oceanic sink for anthropogenic CO2. *Science (New York, N.Y.)*, 305(5682), pp.367–71.

Sallée, J.-B., Matear, R.J., Rintoul, S.R. & Lenton, A., 2012. Localized subduction of anthropogenic carbon dioxide in the Southern Hemisphere oceans. *Nature Geoscience*, 5(8), pp.579–584.

Sambrotto, R.N., Matsuda, A., Vaillancourt, R., Brown, M., Langdon, C., Jacobs, S.S. & Measures, C., 2003. Summer plankton production and nutrient consumption patterns in the Mertz Glacier Region of East Antarctica. *Deep Sea Research Part II: Topical Studies in Oceanography*, 50(8–9), pp.1393–1414.

Schallenberg, C., van der Merwe, P., Chever, F., Cullen, J.T., Lannuzel, D. & Bowie, A.R., 2016. Dissolved iron and iron(II) distributions beneath the pack ice in the East Antarctic (120°E) during the winter/spring transition. *Deep Sea Research Part II: Topical Studies in Oceanography*, 131, pp.96–110.

Schwarz, J.N., Raymond, B., Williams, G.D., Pasquer, B., Marsland, S.J. & Gorton, R.J., 2010. Biophysical coupling in remotely-sensed wind stress, sea surface temperature, sea ice and chlorophyll concentrations in the South Indian Ocean. *Deep Sea Research Part II: Topical Studies in Oceanography*, 57(9–10), pp.701–722.

Sedwick, P.N. & DiTullio, G.R., 1997. Regulation of algal blooms in Antarctic Shelf Waters by the release of iron from melting sea ice. *Geophysical Research Letters*,

24(20), pp.2515–2518.

Semiletov, I., Makshtas, A. & Akasofu, S.I., 2004. Atmospheric CO_2 balance: The role of Arctic sea ice. *Geophysical Research Letters*, 31(L05121).

Semiletov, I.P., Pipko, I.I., Repina, I. & Shakhova, N.E., 2007. Carbonate chemistry dynamics and carbon dioxide fluxes across the atmosphere-ice-water interfaces in the Arctic Ocean: Pacific sector of the Arctic. *Journal of Marine Systems*, 66(1–4), pp.204–226.

Shadwick, E.H., Thomas, H., Chierici, M., Else, B., Fransson, A., Michel, C., Miller, L.A., Mucci, A., Niemi, A., Papakyriakou, T.N. & Tremblay, J.É., 2011. Seasonal variability of the inorganic carbon system in the Amundsen Gulf region of the southeastern Beaufort Sea. *Limnology and Oceanography*, 56(1), pp.303–322.

Shadwick, E.H., Tilbrook, B. & Williams, G.D., 2014. Carbonate chemistry in the Mertz Polynya (East Antarctica): Biological and physical modification of dense water outflows and the export of anthropogenic CO_2. *Journal of Geophysical Research: Oceans*, 119(1), pp.1–14.

Shadwick, E.H., Trull, T.W., Thomas, H. & Gibson, J.A.E., 2013. Vulnerability of Polar Oceans to Anthropogenic Acidification: Comparison of Arctic and Antarctic Seasonal Cycles. *Scientific Reports*, 3.

Smith, N., Zhaoqian, D. & Kerry, K., 1984. Water masses and circulation in the region of Prydz Bay, Antarctica. *Deep Sea Research. Part A*, 31(9), pp.1121–1147.

Smith, W.O. & Nelson, D.M., 1986. Importance of ice edge phytoplankton production in the Southern Ocean. *Bioscience*, 36, pp.251–257.

Sokolov, S. & Rintoul, S.R., 2007. On the relationship between fronts of the Antarctic Circumpolar Current and surface chlorophyll concentrations in the Southern Ocean. *Journal of Geophysical Research*, 112(C7), p.C07030.

Stammerjohn, S.E., Martinson, D.G., Smith, R.C., Yuan, X. & Rind, D., 2008. Trends in Antarctic annual sea ice retreat and advance and their relation to El Niño-

Southern Oscillation and Southern Annular Mode variability. *Journal of Geophysical Research: Oceans*, 113(C03S90).

Steele, L.P., Krummel, P.B. & Langenfelds, R.L., 2007. Atmospheric CO_2 concentration from sites in the CSIRO Atmospheric Research GASLAB air sampling network (August 2007 version). In *Trends: A Compendium of Data on Global Change*. Carbon Dioxide Information Analysis Center, Oak Ridge National Laboratory.

Sweeney, C., Gloor, E., Jacobson, A.R., Key, R.M., McKinley, G., Sarmiento, J.L. & Wanninkhof, R.H., 2007. Constraining global air-sea gas exchange for CO_2 with recent bomb ^{14}C measurements. *Global Biogeochemical Cycles*, 21(2).

Sweeney, C., Hansell, D.A., Carlson, C.A., Codispoti, L.A., Gordon, L.I., Marra, J., Millero, F.J., Smith, W.O. & Takahashi, T., 2000. Biogeochemical regimes, net community production and carbon export in the Ross Sea, Antarctica. *Deep Sea Research Part II: Topical Studies in Oceanography*, 47(15–16), pp.3369–3394.

Takahashi, T. et al., 2009. Climatological mean and decadal change in surface ocean pCO_2, and net sea-air CO_2 flux over the global oceans. *Deep Sea Research Part II: Topical Studies in Oceanography*, 56(8–10), pp.554–577.

Takahashi, T., Sweeney, C., Hales, B., Chipman, D., Newberger, T., Goddard, J., Iannuzzi, R. & Sutherland, S., 2012. The Changing Carbon Cycle in the Southern Ocean. *Oceanography*, 25(3), pp.26–37.

Takeda, S., 1998. Influence of iron availability on nutrient consumption ratio of diatoms in oceanic waters. *Nature*, 393(6687), pp.774–777.

Thompson, B.A.W., Goldsworthy, P.M., Riddle, M.J., Snape, I. & Stark, J.S., 2007. Contamination effects by a “conventional” and a “biodegradable” lubricant oil on infaunal recruitment to Antarctic sediments: A field experiment. *Journal of Experimental Marine Biology and Ecology*, 340(2), pp.213–226.

Thompson, D.W.J., Solomon, S., Kushner, P.J., England, M.H., Grise, K.M. & Karoly, D.J., 2011. Signatures of the Antarctic ozone hole in Southern Hemisphere surface climate change. *Nature Geoscience*, 4(11), pp.741–749.

Touratier, F., Azouzi, L. & Goyet, C., 2007. CFC-11, $\Delta^{14}C$ and ^{3}H tracers as a means to assess anthropogenic CO_2 concentrations in the ocean. *Tellus B*, 59(2), pp.318–325.

Touratier, F. & Goyet, C., 2004. Definition, properties, and Atlantic Ocean distribution of the new tracer TrOCA. *Journal of Marine Systems*, 46(1–4), pp.169–179.

Trimborn, S., Brenneis, T., Sweet, E. & Rost, B., 2013. Sensitivity of Antarctic phytoplankton species to ocean acidification: Growth, carbon acquisition, and species interaction. *Limnology and Oceanography*, 58(3), pp.997–1007.

Uchida, H., Kawano, T., Kaneko, I., Fukasawa, M., Uchida, H., Kawano, T., Kaneko, I. & Fukasawa, M., 2008. In Situ Calibration of Optode-Based Oxygen Sensors. *Journal of Atmospheric and Oceanic Technology*, 25(12), pp.2271–2281.

Venables, H.J., Clarke, A. & Meredith, M.P., 2013. Wintertime controls on summer stratification and productivity at the western Antarctic Peninsula. *Limnology and Oceanography*, 58(3), pp.1035–1047.

Virtue, P., Kawaguchi, S., McIvor, J., Nicol, S., Wotherspoon, S., Brown, M., Casper, R., Davenport, S., Finley, L., Foster, J., Yoshida, T. & Yoshiki, T., 2010. Krill growth and condition in Western Indian Ocean sector of the Southern Ocean 30-80°E in austral summer 2006. *Deep Sea Research Part II: Topical Studies in Oceanography*, 57(9–10), pp.948–955.

Volk, T. & Hoffert, M.I., 1985. Ocean carbon pumps: Analysis of relative strengths and efficiencies in ocean-driven atmospheric CO_2 changes. In E. T. Sundquist & W. S. Broecker, eds. *The Carbon Cycle and Atmospheric CO2: Natural Variations, Archean to Present*. American Geophysical Union, pp. 99–110.

Walz, P.M., Kirkwood, W.J., Peltzer, E.T., Hester, K.C. & Brewer, P.G., 2008. Creating Controlled CO_2 Perturbation Experiments on the Seafloor - Development of FOCE Techniques. In *OCEANS 2008 - MTS/IEEE Kobe Techno-Ocean*. IEEE, pp. 1–4.

Wanninkhof, R., 2014. Relationship between wind speed and gas exchange over the ocean revisited. *Limnology and Oceanography: Methods*, 12(6), pp.351–362.

Wanninkhof, R.H., 1992. Relationship between wind speed and gas exchange. *Journal of Geophysical Research*, 97(C5), pp.7373–7382.

Wanninkhof, R.H., Lewis, E., Feely, R.A. & Millero, F.J., 1999. The optimal carbonate dissociation constants for determining surface water pCO_2 from alkalinity and total inorganic carbon. *Marine Chemistry*, 65(3–4), pp.291–301.

Wanninkhof, R.H., Park, G.-H., Takahashi, T., Sweeney, C., Feely, R., Nojiri, Y., Gruber, N., Doney, S.C., McKinley, G.A., Lenton, A., Le Quéré, C., Heinze, C., Schwinger, J., Graven, H. & Khatiwala, S., 2013. Global ocean carbon uptake: magnitude, variability and trends. *Biogeosciences*, 10(3), pp.1983–2000.

Watson, A.J. et al., 2009. Tracking the variable North Atlantic sink for atmospheric CO_2. *Science (New York, N.Y.)*, 326(5958), pp.1391–3.

Weiss, R.F., 1974. Carbon dioxide in water and seawater: the solubility of a non-ideal gas. *Marine Chemistry*, 2(3), pp.203–215.

Westwood, K.J., Griffiths, B.F., Meiners, K.M. & Williams, G.D., 2010. Primary productivity off the Antarctic coast from 30°–80°E; BROKE-West survey, 2006. *Deep Sea Research Part II: Topical Studies in Oceanography*, 57(9–10), pp.794–814.

Whitworth, T., Orsi, A.H., Kim, S.-J., Nowlin, W.D. & Locarnini, R.A., 1998. *Ocean, Ice, and Atmosphere: Interactions at the Antarctic Continental Margin* S. S. Jacobs & R. F. Weiss, eds., Washington, D. C.: American Geophysical Union.

Williams, G.D., Herraiz-Borreguero, L., Roquet, F., Tamura, T., Ohshima, K.I., Fukamachi, Y., Fraser, A.D., Gao, L., Chen, H., McMahon, C.R., Harcourt, R. & Hindell, M., 2016. The suppression of Antarctic bottom water formation by melting ice shelves in Prydz Bay. *Nature Communications*, 7, p.12577.

Williams, G.D., Nicol, S., Aoki, S., Meijers, A.J.S., Bindoff, N.L., Iijima, Y., Marsland, S.J. & Klocker, A., 2010. Surface oceanography of BROKE-West, along the Antarctic margin of the south-west Indian Ocean (30-80°E). *Deep Sea Research Part II: Topical Studies in Oceanography*, 57(9–10), pp.738–757.

Worby, A.P., Geiger, C.A., Paget, M.J., Van Woert, M.L., Ackley, S.F. & DeLiberty,

T.L., 2008. Thickness distribution of Antarctic sea ice. *Journal of Geophysical Research*, 113(C5), p.C05S92.

Worby, A.P., Massom, R.A., Allison, I., Lytle, V.I. & Heil, P., 1998. East Antarctic sea ice: a review of its structure, properties and drift. In M. O. Jeffries, ed. *Antarctic sea ice: physical processes, interactions and variability. Antarctic Research Series 74*. American Geophysical Union, pp. 41–67.

Wright, S.W., van den Enden, R.L., Pearce, I., Davidson, A.T., Scott, F.J. & Westwood, K.J., 2010. Phytoplankton community structure and stocks in the Southern Ocean (30–80°E) determined by CHEMTAX analysis of HPLC pigment signatures. *Deep Sea Research Part II: Topical Studies in Oceanography*, 57(9–10), pp.758–778.

Yager, P.L., Wallace, D.W.R., Johnson, K.M., Smith, W.O., Minnett, P.J. & Deming, J.W., 1995. The Northeast Water Polynya as an atmospheric CO_2 sink: A seasonal rectification hypothesis. *Journal of Geophysical Research*, 100(C3), p.4389.

Yu, P.C., Sewell, M.A., Matson, P.G., Rivest, E.B., Kapsenberg, L. & Hofmann, G.E., 2013. Growth Attenuation with Developmental Schedule Progression in Embryos and Early Larvae of *Sterechinus neumayeri* Raised under Elevated CO_2 H. Browman, ed. *PLoS ONE*, 8(1), p.e52448.

Zeebe, R.E. & Wolf-Gladrow, D., 2005. *CO_2 in seawater: equilibrium, kinetics, isotopes*, Elsevier.

Zemmelink, H.J., Delille, B., Tison, J.L., Hintsa, E.J., Houghton, L. & Dacey, J.W.H., 2006. CO_2 deposition over the multi-year ice of the western Weddell Sea. *Geophysical Research Letters*, 33(13), p.L13606.